Master's thesis

NTNU
Norwegian University of Science and Technology
Faculty of Engineering
Department of Mechanical and Industrial Engineering

Bjørn Torjus Nygard Lerberg

A novel prototyping technique for non-imaging optics

Specular lens surfaces from 3D printed molds

Master's thesis in Engineering and ICT
Supervisor: Håkon Jarand Dugstad Johnsen
Co-supervisor: Erik Andreassen
June 2023

NTNU
Norwegian University of
Science and Technology

Bjørn Torjus Nygard Lerberg

A novel prototyping technique for non-imaging optics

Specular lens surfaces from 3D printed molds

Master's thesis in Engineering and ICT
Supervisor: Håkon Jarand Dugstad Johnsen
Co-supervisor: Erik Andreassen
June 2023

Norwegian University of Science and Technology
Faculty of Engineering
Department of Mechanical and Industrial Engineering

NTNU
Norwegian University of
Science and Technology

Abstract

This study explores an innovative approach to directly 3D printing non-imaging optical prototypes. By utilizing commercially available 3D-printing technology and simple tools, the research presents a press-forming procedure capable of producing well-performing free-form lenses. The procedure utilizes simple, but clever 3D-printing techniques to press-form heated PMMA into a desired shape. The lenses are evaluated through multiple tests, designed to evaluate their optical performance. A professionally 3D printed lens in Accura ClearVue material serves as a benchmark for existing market solutions. This novel approach has been motivated by a concept designed to improve the efficiency of solar troughs. The lenses in this study feature a complex geometry, possessing manufacturing challenges beyond those associated with traditional aspherical lenses. The outcome of the research could provide valuable insights into cost-effective prototypes for non-imaging optics. The press-formed prototypes are found to significantly outperform the 3D printed benchmark in a purpose-built test jig, utilizing image analysis to compare the performance of the different lenses.

Sammendrag

Denne studien undersøker et innovativt alternativ til å direkte 3D-printe non-imaging optiske prototyper. Ved å benytte kommersielt tilgjengelig 3D-printeteknologier og enkle verktøy, presenterer studien en kreativ press-forming prosess. Kapabel til å produsere velfungerende fri-form linser. Prosedyren benytter enkle, men smarte teknikker innen 3D-printing for å press-forme en PMMA plate til en linse. De produserte linsene blir evaluert gjennom flere tester ment til å bedømme den optiske ytelsen. En profesjonelt 3D-printet linse i materialet Accura ClearVue blir brukt som et referansepunkt for eksisterende løsninger i markedet. Motivasjonen bak å undersøke press-forming stammer fra konseptet Etendue Rotating. Et konsept utviklet for å øke effektiviteten til solar troughs, en type termisk solkonsentrator. Linsene som blir produsert innehar en avansert geometri, utfordrende å produsere sammenlignet med konvensjonelle asfæriske linser. Studien demonstrerer en kostnadsbesparende metode for non-imaging optiske prototyper. I tillegg blir en formålsbygget fysisk test benyttet med bildeanalyse benytter for å evaluere den optiske oppførselene til linsene. Fra testen avdekkes det klart bedre ytelse hos de press-formede linsene sammenlignet med markedsreferansen.

Acknowledgments

I want to thank my supervisor, Håkon Jarand Dugstad Johnsen, who has provided great advice and motivation throughout the whole project, dedicating generous amounts of time and effort to this project. In addition, I want to thank the great people at the Department of Mechanical and Industrial Engineering for providing the facilities and resources utilized in the project. In addition, the co-supervisor of the project Erik Andreassen for providing insightful perspectives into the details of polymers. Thanks to the great people and volunteers at Omega Workshop for running a great workshop, providing a unique opportunity for the students at NTNU.

Thank you, to my great girlfriend Regine, for her love and patience through a busy semester.

Finally, I want to thank my family for always being supportive and helpful.

Table of Contents

List of Figures

List of Tables

Acronyms

AM Additive manufacturing. 14

CSP Concentrated Solar Power. 5, 9, 10

DLP Digital light processing. 13

FDM Fused Deposition Modeling. 13

FWHM Full width at half maximum. 21

LFS Low Force Stereolithography. 13

PV Photovoltaic. 10

RMS Root mean square. 9

SLA Stereolithography. 9, 13

Å Ångstrøm. 1, 9, 25

1 Introduction

3D printing has revolutionized the realm of design and engineering, dramatically reducing the time and effort from concept to prototype. The increasing availability and commercialization of the technology have made rapid prototyping accessible not only for established companies but also for individual enthusiasts. Despite certain limitations in terms of material and some design limitations, 3D printing has undeniably been at the forefront in a new era of design and engineering.

This thesis aims to explore how 3D printing and standard tools can be utilized for creating a free-form optical lens prototype. Specifically a lens configuration for increasing the concentration of solar thermal concentrators. The research conducts a comparative analysis between the manufactured lenses and a professionally manufactured alternative. A key aspect of this research involves investigating how press-forming a PMMA plate with 3D printed molds, can yield a well-performing optical prototype. Furthermore, the research investigates how this simple, yet innovative technique stands up to a professional alternative.

1.1 Background

This section introduces the scope of this project and the problem statement. Highlighting the motivation and background for why it's relevant to investigate press-forming of lenses with 3D printed molds. The section introduces non-imaging optics and the current state of 3D printed optics. Following this, the subsections introduce solar troughs- a specific type of thermal solar concentrator. In addition to Etendue rotating, a way of increasing the efficiency and temperature in solar troughs. Finally, a subsection justifying why investigating polymer prototypes is relevant, despite their non-viability in real-world thermal solar power applications.

The field of non-imaging optics is focused on control and manipulation of light from one surface to another without necessarily preserving the optical image of the light. Non-imaging optics is widely adopted in the Concentrated Solar Power (CSP) field. Due to its unique properties when it comes to redirecting and manipulating sunlight and, therefore its energy [1].

Though 3D-printing has come a long way the last decade, there are still challenges to overcome. One of the less adapted fields is optics. Traditionally glass optics are either shaped by pressing heated glass into a desired shape with a mold, or machined with special machining tools. This is an expensive and resource-demanding process. Therefore prototyping optics is challenging for both researchers and industry due to its costly and resource-demanding nature.

1.1.1 Solar troughs

A solar trough is a type of thermal solar concentrator where a parabolic mirror concentrates light onto an absorber tube. The absorber tube typically has a fluid that transports the energy to its destination of use. A key feature of these concentrators is their 2-dimensional curve, a very scaleable solution, but with less concentration compared to its 3-dimensional counterparts, this is further elaborated in subsection 1.1.2. A solar trough is illustrated in Figure 1a, observe the 2D curvature of the trough, meanwhile Figure 1b depicts a concentrator utilizing a 3D curved geometry of the mirrors. The trough systems are usually aligned with a north-south axis and rotated around one axis to track the sun throughout the day [2].

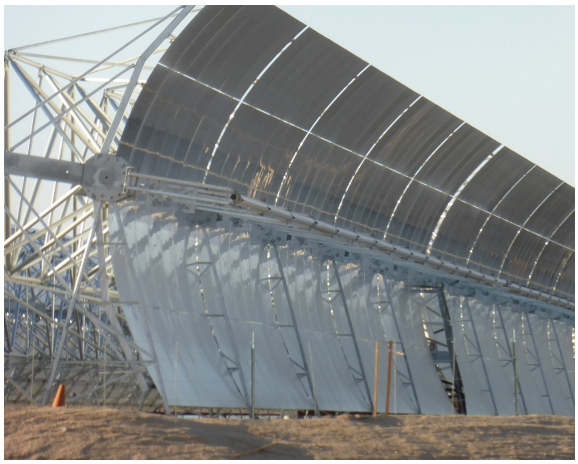

(a) Image: Parabolic trough at Harper Lake in California from Wikipedia, licensed under CC BY-SA 3.0 [3]

(b) Image: Stirling Energy Systems - Dish Stirling Engine by Derek Curry, licensed under CC BY-SA 2.0. [4]

Figure 1: 2D (1a) and 3D(1b) solar thermal concentrators

1.1.2 Etendue rotating

The motivation for researching simple prototyping techniques for advanced lenses stems from a concept developed for increasing the efficiency of solar troughs. Specifically, this concept improves the efficiency of the trough by increasing its concentration factor, consequently increasing the energy density of the system. As per the principles of thermodynamics, a higher energy density is favorable as it implies lower entropy, thereby potentially enhancing the efficiency of the system as a whole. The concept is called Etendue rotating. By utilizing advanced optical geometry, one can reach 3D concentration in an else 2D constricted environment like the solar trough. More specifically by Etendue rotating the light, one can achieve a 3-dimensional concentration factor [5]. The concept is illustrated in Figure 2, where a presentation of the light ray's path is illustrated. Following are the mathematical derivations to calculate the theoretical concentration limits.

Traditional solar troughs are limited to a 2D concentration limit. Meanwhile, a doubly curved 3D dimensional geometry reaches a higher concentration limit, respectively calculated by:

$$C_{\max,2D} = 1/sin\theta$$

$$C_{\max,3D} = 1/(sin\theta)^2$$

Where θ is the acceptance angle of the optics. In this project, the lenses are optimized for an acceptance angle of 1.5°. All acceptance and dispersion angles are given in radius angle in this research. Inputting the acceptance angle to the equations, the two corresponding limits would be:

$$C_{\max,2D} = 1/sin1.5^\circ \approx 38x$$

$$C_{\max,3D} = 1/(sin1.5^\circ)^2 \approx 1459x$$

With increased concentration, the light becomes more focused, resulting in a thinner focal line. Observe Figure 3 where the blue Etendue rotator lenses in Figure 3b concentrate light onto a thinner compared to the Traditional trough in Figure 3a. However, this increased concentration comes with the need for additional tracking. The lenses must be positioned according to the sun's changing elevation angle throughout the day, necessitating an additional tracking system in such setups.

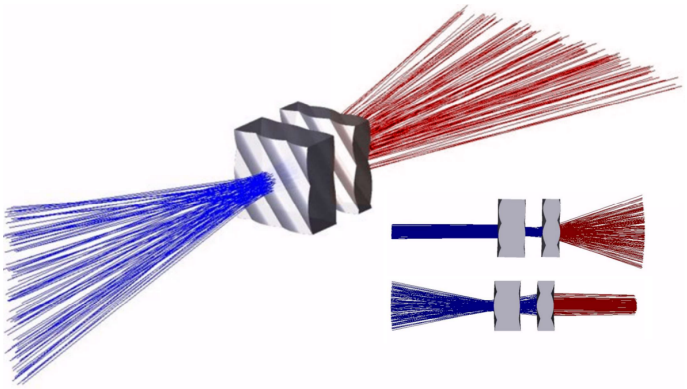

Figure 2: Figure adapted with permission from "Rethinking the Secondary Concentrator: A High-Concentration Retrofit for Linear Solar Collectors," by H. J. D. Johnsen and J. C. Miñano, presented at SolarPACES 2022

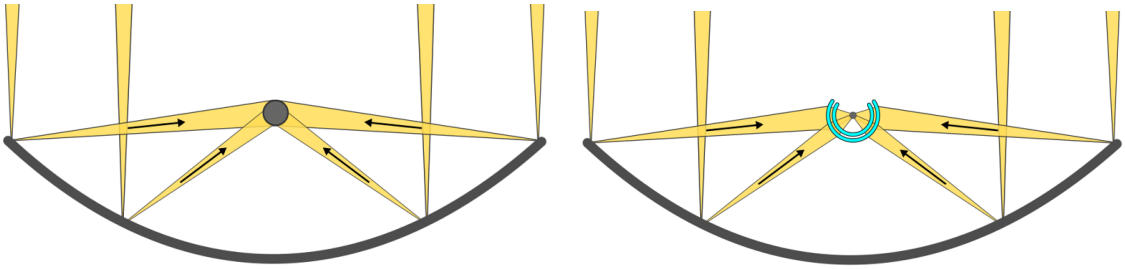

(a) Traditional trough

(b) Trough fitted with Etendue rotator lenses

Figure 3: Figure adapted with permission from "Rethinking the Secondary Concentrator: A High-Concentration Retrofit for Linear Solar Collectors," by H. J. D. Johnsen and J. C. Miñano, presented at SolarPACES 2022.

1.1.3 Etendue rotating model concept

This section presents the design of the etendue rotating lenses. The lense geometries stem from numerical optimization. The goal of this project is to create prototypes of these lenses and to check how well the prototypes perform compared to the virtual simulated model.

Observe how Figure 4a has a larger collector tube than the etendue Figure 4b. This is a result of the increased concentration the Etendue Rotating lenses perform. In a real-world scenario, these receiver tubes would have had some type of glass enclosure for isolation, which is not included in the Figures.

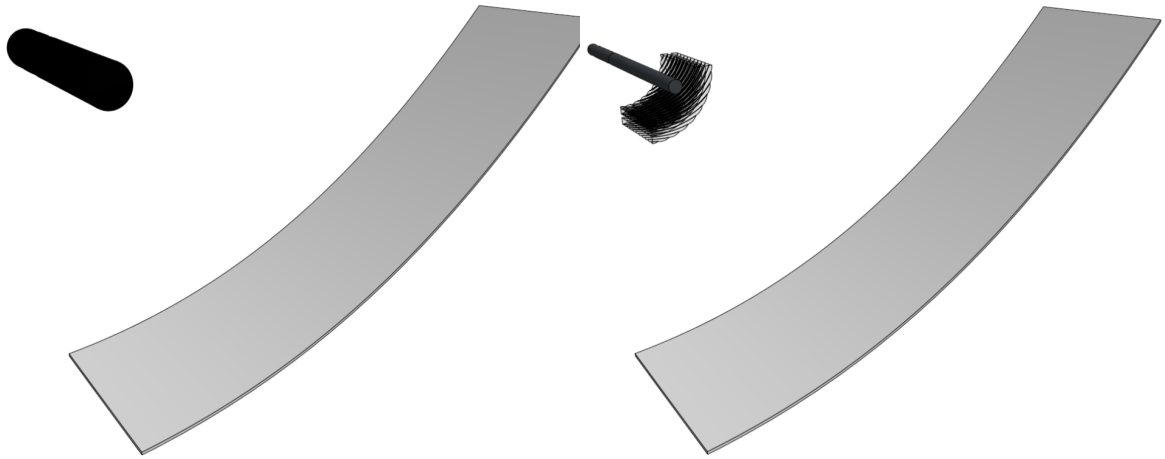

(a) Standard trough

(b) Trough fitted with Etendue rotator lenses

Figure 4: (not to scale) Sectioned 90°view of a standard trough and etendue rotator set up. Observe the smaller receiver tube in the Etendue configuration Figure 4b compared to 4a

Figure 5 demonstrates how light would be focused on a plane. This is relevant later in the study, but in a real-world application, this would have been a tube structure, and the light would have come from every direction around the lenses. The lenses interact uniformly with light around their length axis. In this Figure, the length axis is the depth of the image, traveling inwards.

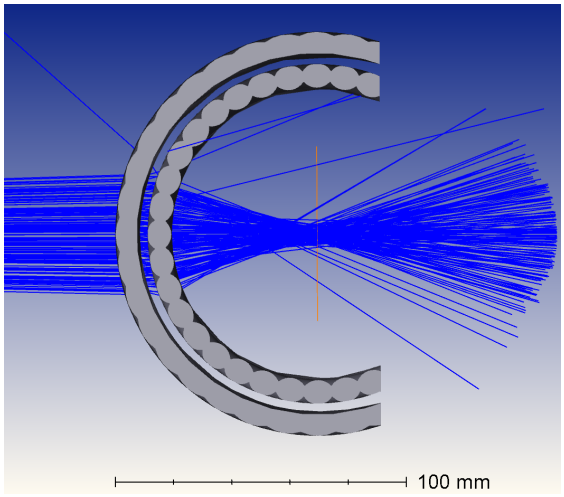

Figure 5: Unsectioned simulated Etendue rotator lenses interacting with light with 1.64° dispersion angle. The orange line represents a theoretical focal plane, which would have been a tube in an actual model.

1.1.4 Why polymers

This project explores the possibility of creating free-form non-imaging optical parts in a rapid prototyping context. Within this context, polymers offer several advantages over glass. Processing and shaping polymers require much less heat and force, therefore easing the manufacturing process. Though not as abrasion resistant, with lesser refractive index and more dispersion, making glass more effective regarding optical properties. These properties are counterweighed in terms of how simple the manufacturing process is for polymers compared to glass in a rapid prototyping context. Multiple iterations of free-form optics can be created with minor material costs and resources.

1.2 Problem description and project goal

This study aims to further explore the possibilities of rapid prototyping within the field of non-imaging optics. A fundamental challenge in prototyping optics lies in surface quality, specifically roughness. Additional factors are within the material itself, particularly in 3D printing, where most materials have considerable volume absorption and scattering. The aim of this project is to research alternative methods for manufacturing a free-form optical lens within a rapid prototyping environment. The study is motivated by a lens configuration designed to improve the efficiency of a specific type of solar concentrator. A key element is utilizing the least possible special equipment to manufacture the lenses.

1.3 Theory

In this section, the relevant theories of the project are presented. More specifically, we encompass relevant optical properties, behavior, and considerations of CSP systems, 3d printing technologies, prototyping techniques for optics, and some design and engineering processes. The aim is to equip the reader with a basic understanding of the relevant theory for the research. The theories are described briefly. As such, it is advantageous for readers to possess some basic understanding and familiarity with mechanical engineering and non-imaging optics fundamentals.

1.3.1 Relevant optical properties

This subsection outlines some relevant theories and fundamentals for this research.

Refraction occurs when light travels through different media. Light in the same way as sound changes speed when traveling through different media. The change in speed will consequently change the direction of light as long as the incident angle is not normal to the media. This is governed by Snell's Law which relates the incoming angle to the outgoing angle.

Dispersion, as mentioned the light travels at different speeds through different media. The same applies to the different frequencies of light. This means that depending on the dispersion of a material, the different wavelengths of light will refract slightly differently. Dispersion is the property of a material, and the behavior of light is a consequence.

Surface quality- roughness, waviness, form
To characterize the surface quality we specify three properties. All three depend on the size scale of the feature or wavelength. **Roughness** is a measure of small-scale irregularities on a surface. In the field of optics, one usually considers very small irregularities. In fact, the measured dimensions are so small, one often use an own measuring unit, namely Ångstrøm (Å), which corresponds to 0.1nm. With that in mind, we can specify the desired surface roughness. Generally, one desires roughness significantly lower than the wavelengths traveling through the system, which implies in the range of a few nanometers. Within commercial optics, a typical finish is 50Å RMS, while a precision finish is 20Å RMS and high-quality 5Å RMS[6]. A rough surface will result in light scattering and a matt surface. **Waviness** quantifies how well the surface texture resembles the theoretical model on a bigger scale[7]. A typical example of this would be the layer steps in a SLA print, which is typically in the µm scale of measure. **Form or Figure** is the overall shape of the specimen and represents surface quality on the largest scale. Figure 6 illustrates the three different properties, and how they combine.

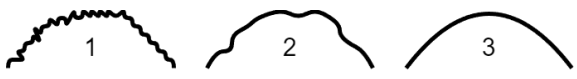

Figure 6: The three surface characteristics (exaggerated) (1) Roughness[µm, nm and Å], (2) Waviness[µm to mm] and (3) Form[mm]

.

Scattering is the phenomenon that occurs when light deviates from its intended path due to

irregularities or disruption. Factors influencing scattering come from surface roughness, surface irregularities, internal irregularities, structural variations like density, etc. We can divide scattering into two categories, **volume scattering** and **surface scattering** [8]. In the scope of this project, we will mainly focus on surface scattering. This is due to it being the only parameter we can control, with the exception of which material we choose. Meanwhile, the internal scattering is mainly given by the material, and production techniques earlier in the specimens life cycle.

Further into this study, two materials are presented, PMMA(commonly known as acrylic glass) and a transparent 3D-printable photopolymer resin. Comparing these two materials, we assume that the 3D-resin has a higher degree of volume absorption than the PMMA. This is attributed to the fact that the Resin needs to absorb light to initiate the polymerization process. Consequently, some elements in the resin will yield reduced transparency. Additionally, the refraction through the 3D printed material might be slightly different due to different degrees of polymerization through the material, inducing

Transparency and transmission Another consideration, when using polymers for optics is the transparancy of the material. Materials like PMMA show excellent optical transparency in the visible light spectrum and to some extent in the infrared, but can be somewhat limited outside this spectra [9]. Observing Figure 7 we can observe where PMMA and some other polymers have the best transmission.

In this project two materials have been used for prototyping lenses, the following transmission are given from their data sheets, both transmissions are from the same standard of testing(ASTM D-1003). The numbers are from a 0.5mm thick sample, the max thickness of the lenses in this research is 8mm. Suggesting the actual transmission would be slightly lower:

- Perspex PMMA: $> 92\%$(see appendix D)
- Accura Clearvue: 87.2%(see appendix C)

Spectrum irradiance and energy
The power from sunlight available for energy production varies on a multitude of factors. Among them are, latitude, smog and aerosol levels, time of day and so on. The solar constant $\approx 1.37kW/m^2$ [11] represents an analytical average for the amount of light that hits the atmosphere. Though the light hitting earth is usually less due to the mentioned factors. Consequently, standards of solar irradiance have been created, among them are the *AM1.5d* for direct sunlight hitting a surface [12]. For concentrating solar systems we use standards that only consider direct sunlight(like AM1.5d), without scattering from different sources. This is different than for Photovoltaic energy production, because scattered light will also create energy in the same way that direct rays does.[13] More specifically Concentrated Solar Power (CSP) usually utilizes optics that are engineered to harvest direct sunlight, by redirecting rays from a known source, like the sun. As a result, scattered light is unlikely to hit the desired target in a CSP system. Observe Figure 7b for an illustration of direct solar irradiance on Earth's surface.

Fresnels law describes how light(a form of electromagnetism) is reflected and transmitted when passing between two different media. It takes into account the angle of incidence and refraction index of the two media [14]. In practical use, we can assume that 4% of light is reflected when passing between one air/glass surface, at 0°incidence. This would imply that the 4 surfaces that light passes through in this research would lose at least 85% of the light. Therefore, for the Etendue rotating concept to be viable, the efficiency increase would have to be significant enough that this phenomenon would be compensated for.

In order to minimize this type of reflection, various coating techniques exists. One alternative is a thin coating with an optimized refraction index applied to the lens, yielding lower Fresnel reflections. Consequently, less light is reflected on the coating surface compared to the original material. Furthermore, when the light travels to the lens material, additional reflection occurs. To further mitigate Fresnel reflection, the coating thickness is dimensioned to create destructive interference. Consequently, reflected light from the lens and the coating will cancel each other out. Implying more light will travel through the lens due to the conservation of energy in the

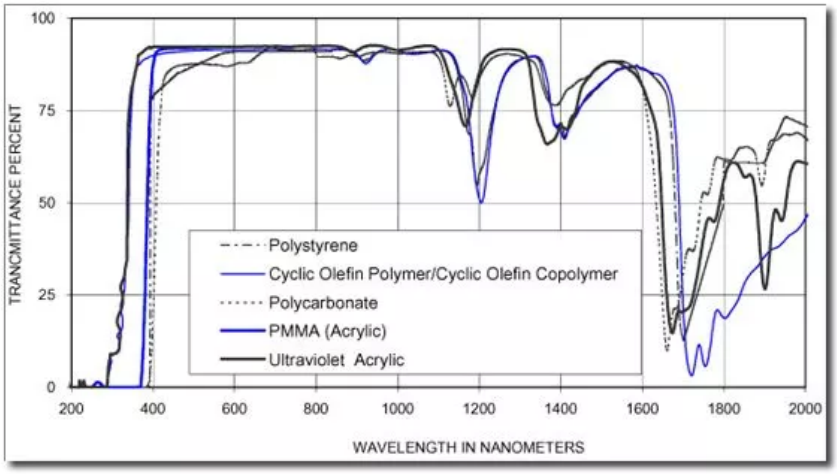

(a) Figure: Transmission spectrum for polymers from company GS Plastic Optics, used with permission. Source: https://www.gsoptics.com/transmission-curves/

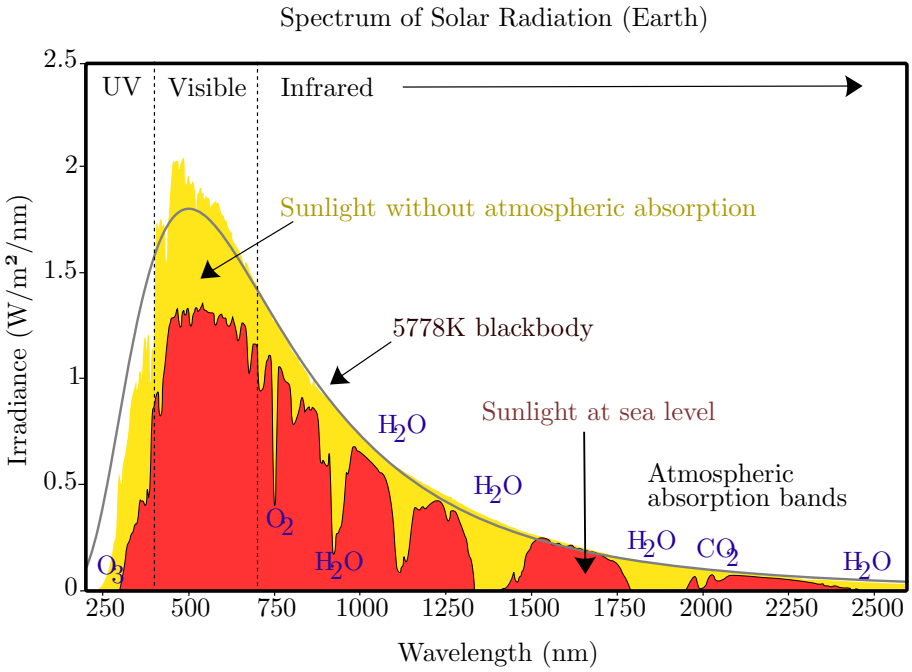

(b) Figure: Spectrum of Solar Radiation by Robert A. Rohde, CC BY-SA 3.0 https://creativecommons.org/licenses/by-sa/3.0, via Wikimedia Commons

Figure 7: Specimens in Figure 7a graph are 1-3mm thick, the data graph is meant to illustrate approximate values, and is not used quantitatively in this project [10]. Keep in mind the visible light spectrum is in the range of 380-750nm. Figure 7b presents direct sunlight at the top of earths atmosphere (in yellow), and at sea level (in red). Some wavelengths are absorbed by different gases in the atmosphere, noted in the diagram. These data will have some deviations depending on the location on earth.

system[15]. These coating techniques can also be adapted for polymers, one of such techniques is through vapor deposition[16].

Acceptance angle related to solar concentrator mirrors plays a crucial role in the concentrator system. This angle must account for irregularities in the mirror surface, that can scatter the incoming solar rays. The angular radius of the sun observed from Earth is 0.27°, and correspondingly the dispersion angle of sun rays is 0.27°. Once these rays are reflected off the mirror, their disperseion angle increases. Accordingly, the optics in this research is optimized with an

expected maximum dispersion angle, also known as the acceptance angle. This factor loosens the tolerances needed in manufacturing the lenses and in adjusting their position corresponding to the suns elevation angle throughout the day. Thereby accommodating potential inaccuracies in the solar tracking system.

Abberations, can be described as optical imaging defects. A ideal lens or concentrating mirror focuses all the light rays to a single focal point where all the rays pass through. In practical terms this is not possible, light rays will deviate from the focal point due to multiple factors, these deviations can be grouped into different types of aberrations. The main types of aberrations are: spherical aberration, coma, distortion and chromatic aberration. [17] In the scope of this project coma and distortion aren't considered relevant because the research focuses on non-imaging optics.

Spherical aberration occurs when light traveling at different angles before and after a lens, will focus at different distances from the lens, depending on where the light rays is intersecting the lens or mirror [18, pp.59-63]. Observing Figure 8, the distance between point B and C is a measure of the spherical aberrations of the lens, measured in distance. Chromatic aberration is a phenomenon occurring due to the dispersion property of materials. Different wavelengths of light will have slightly different refraction through a material, and therefore exit at slightly different angles.

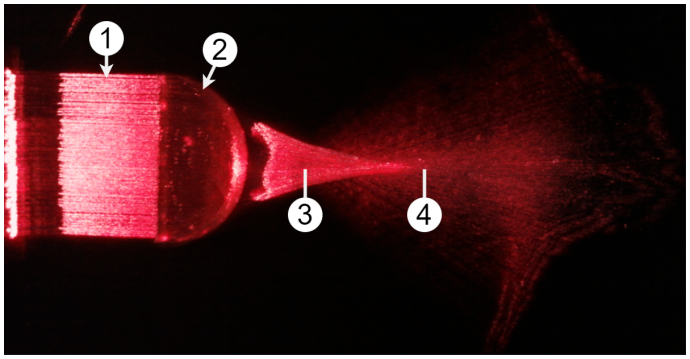

Figure 8: Image: Lens spherical aberration RL. originally create by Adam Gabrys https://commons.wikimedia.org/wiki/File:Lens_spherical_aberration_RL.jpg. Pointers and explanation added by B T. N. Lerberg, https://creativecommons.org/licenses/by-sa/3.0/legalcode. (1) Initial light rays. (2) Lens. (3) Rays far from the optical axis is focused closer to the lens. (4) Rays closer to the optical axis are focused further from the lens. The distance between (3) and (4) is a measure of spherical abberations.

The solar zenith angle refers to the angle of the sun in relation to a vertical line on the Earth's surface. This angle is 0° when the sun is directly overhead. In the scope of this project, we are researching a solar concentrator optimized for use at the equator, where the sun varies from an angle of 0° zenith to 23.5° zenith. This range allows for symmetric focusing areas in the lens geometry, which simplifies testing and prototyping. Its worth noting that the Etendue rotator concept isn't limited to the equator, the system can be optimized for a variety of latitudes.

1.3.2 Manufacturing tolerances

When a physical part is manufactured, the physical model will always have some deviations from the theoretical model. Surface roughness, already elaborated in Section 1.3.1, is a primary difference. A second key deviation is surface profile or form. Which can be described as the overall shape and structure of the geometry.

Variations in profile or surface slopes will result in angular differences between the light rays in the virtual and physical models. A third affecting factor is the positioning of each component in the system, implying the position between the receiver tube, lenses, and mirror relative to each other.

In non-imaging optics, we can quantify distance deviation as angle deviation. This implies a translational difference between the physical slopes and the virtual slopes can be interpreted as a

rotational deviation. Hence if a light ray strikes the surface at a different position than expected, we can examine the incident angle, and not the distance error [19]. A practical method to compare these deviations is therefore through a 2-dimensional plot of the cross-sections of the virtual and physical surfaces. In this research, this is achieved through 3D-scanning the physical part, comparing it with the virtual model in software, and presenting the difference through a 2-dimensional plot, with angle deviation.

1.3.3 3D printing

During this project, a couple of 3d printing technologies have been considered and utilized. This subsection gives a brief introduction to the different technologies and their key properties.

Stereolithography printing, a technique where layers of photopolymers are cured on top of each other to form a part. The UV light used to cure the layers on top of each other is directed from a diode or light source through some optics that guide the beam to its designated position[20]. The material usually starts as a liquid in a tray, and the UV light polymerizes it into a solid. Normally, the process involves a post-processing technique where it's exposed to additional UV light to fully cure. These are very precise printers, and one can assume that they are more precise than their popular counterpart Fused Deposition Modeling.

Low Force Stereolithography is a variation of SLA printing, the Formlabs 3 printer utilizes a flexible film in the bottom of the resin tray. This means that the forces exerted on the part during printing are reduced [21]. A flexible resin vat is not Formlabs specific, but the combination of the SLA Laser engine and their flexible vat is.

Fused deposition modeling The most common type of 3D printer. Utilizing a hot nozzle to melt and extrude a thermoplastic filament. The filament is fed through the nozzle from a spool, depositing layers on top of each other to form a structure on a build plate.

Digital light processing (DLP) Printing A type of SLA printer. Where a DLP device creates an image of the desired layer. In contrast to a laser- SLA printer, where a laser is scanned over the surface, to create the desired geometry.

Two-photon printing or two photon absorption. Most SLA printers use a linear focal point, meaning some material outside the focus point will be exposed to light. Consequently, yielding in polymerization outside the desired area. Two-photon printers use the two-photon absorption phenomenon to cure photopolymers. This process has a non-linear focal point. Consequently, no polymerization will happen outside the desired area. These printers are able to create sub-micrometer features and are usually not able to create structures as big as the desired geometry in this research [22].

Layer stepping, is a common characteristic of most 3D printing processes. Usually, layers are built on top of each other to create a structure. This process will normally yield layer lines in the structure. These lines are referred to as layer stepping.

1.3.4 Prototyping of glass

Typically optic lenses start out as a glass blank, then ground to the desired shape and polished. This is a tedious process requiring special tools. With limiting geometrical factors, typically one only manufactures simple aspherical lenses. Other manufacturing techniques are diamond turning, injection molding, and precision glass molding. These are all processes great for their purpose, but not really friendly for multiple design iterations or a rapid prototyping environment. [23]

The characteristics of glass, like its high melting point, brittleness, and challenging machining capabilities are typically not desirable in a rapid prototyping process. Some processes exists where one can create glass structures through additive manufacturing, but it's still in an early stage, and not widely adopted. An investigation demonstrating this technique is presented in Section 1.4.

1.3.5 Mechanical properties and production techniques

In this subsection, some important mechanical properties are presented, along with their influencing factors in this research.

PMMA In this research, Perspex CC, cast PMMA sheet have been utilized to create the lens geometries. The material has great transmission from the spec sheet 92% light transmission(ASTM D1003 3mm thickness). 10 year uv weathering guarantee. Vicat softening point 105℃ and refractive index 1.49(ISO489A))see Appendix: D).

Non isothermal molding A process that enables the manufacturing of glass without the need for post-processing. The mold is significantly cooler than the glass, so when the surface of the heated glass sample touches the mold, it rapidly stiffens. The rapid increase in stiffness prevents the high-frequency surface imperfections of the mold to be copied to the glass. This, in turn, means the sample can be utilized immediately after the press process, without additional surface treatment. In addition to increasing the surface quality, the technique also increases the production rate due to accelerated cooling pace [24]. This technique is elaborated in section 1.4.

1.3.6 Design thinking and rapid prototyping

Design thinking, an iterative process involving breaking down a complex problem into multiple simpler steps. consequently contributing to suitable and creative solutions. The steps involved in the process can be summarized in these phases, empathize, define, ideate, prototype and test. These are all iterative steps, meant to optimize a product or design. The steps are not necessarily sequential and can be run in parallel or in different order. Typically this is a process run in teams of designers, but the principles can apply in individual processes as well [25]. Although not always intentional, the steps of this process are often executed in some way or other, particularly in the context of an iterative design process. During this project, one can put the different stages of the project into the design thinking process.

- Emphasize, gain an understanding of the challenges and existing solutions of the problem. Mainly executed through literature research and meetings with the supervisor. In addition to consulting other students and researchers.
- Define, find a problem statement, and define what we are trying to solve, building on knowledge acquired in the above step.
- Ideate, find alternative ways of creating the design and innovate by looking for different solutions to the problem.
- Prototype, start creating the solutions, split the problem into simplified models, and iterate to a better design. Within this project, rapid prototyping techniques have been practiced extensively.
- Test, evaluate what was successful and what needs improvement. Return to previous stages to improve the design if necessary.

Rapid prototyping, fast fabrication of physical parts, models or assemblies using CAD. In addition to producing it with rapid prototyping techniques. Typically Additive manufacturing (AM) is the modern go-to production technique within the field. Though not limited to AM, this is a fast and flexible technique viable for creating working prototypes for a variety of functionality and form in a fast manner. In addition to AM, rapid prototyping includes some machining processes, molding, casting, extrusion, and a few other techniques [26].

1.3.7 Imaging

There is a substantial amount of imaging in this research, therefore, some key properties of most imaging systems are mentioned and explained in this section. The section is parted into lens,

camera, and microscopy. Additionally, variable focus microscopy is presented.

This section explains the lens properties, aperture, focal length, and focus. **Aperture**, how much light the lens lets through to the camera, typically given by an f-number of focal ratio. Less light through the lens gives a greater depth of field. **Focal length** is how far away the lens is from the camera when it is in focus. this is a constant for a lens. While the **Focus** adjusts how far the lens is away from the camera, meaning it moves the lens so the desired focus distance is achieved between the camera and the object being photographed.

This paragraph explains the key imaging variables of the camera itself, namely shutter speed and sensor sensitivity(ISO). **Shutter speed** is how long the shutter stays open, to expose the sensor or film to light. This variable should be adjusted together with the aperture, a higher aperture means less light to the camera, while a longer shutter speed gives more light and vice versa. **Sensor sensititvity** or ISO is how sensitive the film or sensor is to light, a increase of this value makes the camera more sensitive to light and can increase graininess and noise in the image.

Variable focus microscopy, is a technique where a camera, usually inside a microscope is set with a fixed focus. By capturing images with the camera at different heights, different areas of the piece will be focused. These focus points are recognized by the software. Further these points and height coordinates are saved in a point cloud. The x and y of the focus points are given by the camera, while the height(z) is given by the relative travel of the camera. In turn a 3 dimensional image or point cloud can be created.

1.4 Previous research

In this section, some previous research for rapid prototyping of optics is presented. Previous research presented spans from altering commercial printers for higher precision to comparing polymer materials in optical 3d-printing in addition to the non-isothermal molding of glass and a photo resin containing glass, that can undergo a burnout and sintering process, to form a glass structure.

There are multiple ways to reach a better "resolution" of a stereolithography printer, one way is to use a fiber optic taper between the print tray and the LCD screen, as demonstrated by Parvathi Nair S et al.in [27]. They were able to shrink the image output of the LCD screen in the printer by 44%, on a hobbyist printer. Meaning that all details and minimal feature sizes in this plane are scaled down an equal amount. Within optics, this can be quite feasible, due to how small details and minimal features a 3D printer can manufacture, is a measure of how well it can manufacture optical pieces.

In a master's thesis for the University of Arizona Sandra Glynn explored the possibilities of diamond-turning 3D printed lenses as a precision imaging optic. The study used different commercially available photoresists and compared their optical properties to a similar diamond-turned PMMA specimen. The photoresist used included Accura ClearVue, the same resin used in this research. A key outtake from this study is that all of the materials could reach a satisfactory optical surface roughness with the right machining process. [28]

Non-isothermal molding, by utilizing a cold mold, with a lot of thermal mass, one can produce glass with specular surfaces, with relatively rough molds. This is due to the fact that if one cools down the surface rapidly enough, the glass blank is not able to copy the mold surface completely. This is attributed to the surface tension keeping the surface smooth. This process is employed in large-scale production, due to the fact that it accelerates the production rate, by minimizing cool-down time. Researchers created a lens, where the glass was heated to 880℃ while the stainless steel mold was kept at 550℃ and constant pressure of 125 psi, after 5 seconds the top surface was cooled down to 600℃ while the center was at 700℃ [29].

An additive manufacturing way of producing glass is presented in this research. A photoresin containing silica can be 3D printed to the desired geometry called a green part. Then undergo a burnout process so the polymers dissipate. Due to the evaporation of the polymers, the part shrinks to whats called a brown part. Following the burnout procedure is a sintering process that binds the silica grains together, forming a glass part, demonstrated by Kotz et al.[30] [31].

Though this project focuses on 3d-printing within prototyping, some companies have commercialized and scaled production lines based on 3d-printing, particularly within SLA technologies. A company named Carbon, has helped Adidas commercialize a 3D printed midsole for sneakers. Enabling geometries, previously impossible, demonstrating an interesting step for mass-scale additive manufacturing. One of the key setbacks of this type of printing is the slow production rate. The time between light exposure for each layer is a contributing factor to the slow manufacturing rate. A technology that removes part contact between the vat and the printed part completely is the Digital Light Synthesis that the company Carbon uses on some of their printers. They use a permeable vat, that is fed oxygen to create a small "dead zone" between the vat and the part. Meaning the printer can continuously expose the part to light. Reducing time between each layer and minimizing stairing effect on the parts [32]. The Formlabs printer used in this study, utilizes a flexible vat, to minimize the force exerted on the printed part when the part peels from the vat, thereby increasing printing speed. Though none of the printers mentioned here is optimized for speed, it's important to note how different technologies solve the challenges related to peeling in 3D printed parts.

2 Methodology

This chapter presents the methodology employed for structuring the project, finding a production technique, conducting the prototyping phases, collecting and processing of the data in addition to the tools utilized during this process. As well as elaboration for why these methods were chosen, and the strengths and limitations of each of the methods.

2.1 Problem approach

The overall goal of the project is to identify and compare accessible and simple prototyping techniques for non-imaging optics. Specifically, advanced geometries within the non-imaging optics field. This is done by limiting the tools for manufacturing to commonly available tools for both RD departments in universities, industry, or well-equipped hobbyists.

2.1.1 Project phases

Due to the short time span of the project a progress plan was sketched out to ensure a structured project process. The plan was split in 5 phases of equal length. Below is a list of the phases and the key takeouts for each of them.

1. **Explore resources, available equipment and emphazise(design thinking)**. Since the pre-project isn't an exact precursor to this project, a lot of the formalities and available resources had to be re-explored or redone. This also included formulating a problem statement.
2. **First iteration design and prototyping**, do the techniques and equipment from the previous phase comply with the goal of the project?
3. **Second iteration prototyping**, A more thorough prototyping based on the experiences from the previous phase.
4. **Datacollection and manipulation**, Creating a setup for testing the prototypes and collecting data.
5. **Documentation**, finish the report, and discuss the outcome.

While the progress plan is followed during the research, slight hick-ups are met. A key challenge is the hard nature of imaging specular surfaces. This will be elaborated on later.

2.1.2 Exploring accessible and relevant prototyping techniques

In the intention of creating an optimal free-form lens prototype, multiple manufacturing techniques are considered. This section lists some considered prototyping techniques and their key features. Due to the short time span of the project, a key consideration is the availability of the necessary equipment and resources. Additionally, the chosen prototyping technique should be easily accessible for industry trying to recreate the procedure later.

3D printing directly, could be considered the most straightforward procedure. Most SLA printers have some capability of printing clear resins. Meaning an optical prototype could be printed directly and undergo some later surface treatment to achieve a specular surface and remove the layer stepping in the 3D printed part. Chapter 1.4 mentions a study where 3D printed lenses are diamond turned and further inspected to gain knowledge about the material properties.

2- photon printing or two-photon absorption printing is an exceptionally precise printing technique. Its key distinction from traditional SLA printing lies in the non-linear optical process, allowing a specific point in the photoresist to be cured without affecting the surrounding voxels

with light. This means that one can achieve very small and precise features. NanoONE states that their UpNano printer can print with a minimal surface roughness of $\geq 10nm$, a minimal horizontal feature size of $\geq 170nm$, and a minimal vertical features size of $\geq 550nm$ [33]. This would imply that one might be able to print precise optics directly without further surface treatment. Though the lenses in this project are too big for such printing, additionally the availability of such printing technology is very limited, making it unsuitable for the scope of this project.

Press-forming, An additional prototyping technique is creating a negative of the desired part and then utilizing the negative to form a material blank to the desired shape. The material blank is put inside two molds before being pressed to the desired shape. The material and specifics of the process can be varied, like temperature, force, and speed. The supervisor of this project Håkon J.D. Johnsen demonstrated a version of this in his master thesis for a different lens array [34].

Epoxy casting, an additional technique where one creates a negative of the desired part geometry. The negative mold is then filled with epoxy resin, that can cure to the desired geometry. This technique can recreate a huge variety of different geometries and is more flexible in terms of geometry compared to press-forming. If one uses soluble molds, one can create any desired geometry as long as it's possible to remove the mold by dissolving it. The molds can also be flexible enabling easy removal of the mold after the epoxy has cured.

2.1.3 Landing prototyping technique

From the previously listed production techniques two of the production techniques are considered the most relevant. one of these is 3D printing directly, due to the widely accessible market solutions, and the simple process of printing. Additionally, we considered it one of the most widely adopted rapid prototyping techniques. So a reference between this technique and one of the others, yields a valuable result for a wide range of applications. Due to the less adapted and expensive equipment, 2-photon printing is considered irrelevant. Press-forming is a simple technique, viable of producing an extensive amount of geometries. In addition, if the process could be performed with standard widely-adapted 3D-printing techniques, it would demonstrate a wide scope of possibilities for simple prototyping of optics. Epoxy casting is a just as viable technique, and if the time span of the project would have been longer. This might have been a worthy process of investigation.

2.2 Calculations and prototyping

This section describes the process from concept to prototype. Starting with the generation of a virtual model, continuing with calculations regarding heat-flow in the lens geometry. Proceeding with the process of finding a professional manufacturer, and finally, a press-forming process to manufacture the lens geometry with additive manufacturing.

2.2.1 Creating virtual model

A few virtual models were optimized with the project supervisor's software. The main variable for the simulation was the concentration factor compared to the acceptance angle of the light. The higher the acceptance angle of the lenses, the looser the tolerances in production. The optimized lenses with their acceptance angles and their corresponding concentration factor are listed below. Note that this is the increased concentration the lenses yield, and not the concentration of the whole system, which is significantly higher.

- 1°, resulting in 3.7x concentration in PMMA.
- 1.5° resulting in 3.5x concentration in PMMA.
- 2° resulting in 3.3x concentration in PMMA.

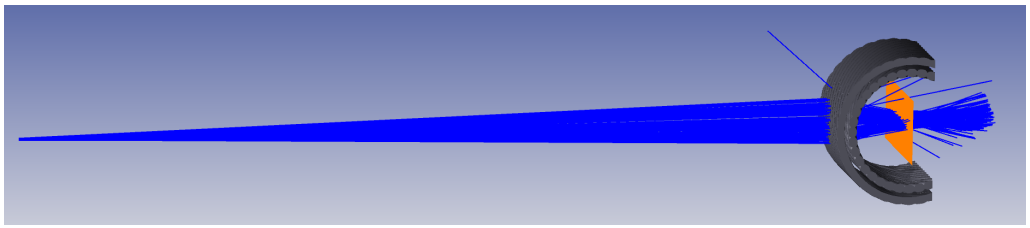

Figure 9: Zemax OpticStudio ray-tracing simulation with 1.64° dispersion.

After considering concentration and theoretical efficiency the 1.5° design was chosen for manufacturing. The key factor in this decision is fresnels law, described in section 1.3.1. To elaborate in short, one has to balance the trade-off between loss of light, against the thermodynamic laws saying that higher energy density gives better efficiency.

For simulating and visualizing how the optimized model would behave in the test jig a simulation in Zemax OpticStudio 17.5 was conducted.

2.2.2 Calculations

In this section, the calculations and estimations of how the PMMA would act in the press-forming process are presented.

Heat conduction through a flat PMMA plate
In addition to press-forming lenses the research investigates if a cooled press-forming operation yield lenses with less surface roughness. In this liquid-cooled process, the punches are kept at about 20℃ with water running through cooling ducts as observed in Figure 10b. This is the same process as in the non-isothermal molding procedure mentioned in subsection 1.3.5. The hypothesis is that if the surface of the PMMA is cooled fast enough below glass transition temperature, the imperfections of the punch will not be copied to the PMMA. The PMMA utilized in this research has a glass transition temperature of about 100℃ .

To get familiarized how the material would respond to a cooled press vs an uncooled press. A few calculations were done. Figure 10 shows how the heat flux of a PMMA specimen would be distributed over time. The initial condition was 200℃ over the whole plate. Then we assume that both ends of this graph are cooled to 20℃ (to emulate how a cooled press would behave). This is an optimistic estimate because the cooled punch doesn't have this temperature at the surface, but inside the actual cooling ducts. In addition, this assumes a flat plate with perfect heat transfer between the surfaces of the PMMA and punch, not the valleys and tops the punch geometry actually possesses. Observing the figure, we note that the material should have even heat distribution after 10-20 minutes.

2.2.3 Professional manufacturer

Since one of the project goals is to compare rapid prototyping techniques to a commercial supplier's product. A few manufacturers were considered. One of the key requirments was that it was 3D printed, affordable enough for commercial use and short delivery time. Among the considered suppliers were:

- **Luxexcel**, Which produces lenses through a additive manufacturing process, in which droplets are cured ontop of each other. And since the droplets have surface tension, there is no stairing between surface layers on the part. In contrast to traditional 3d-printing processes.
- **Prototal Levanger**, A company specializing in "time-to-market" strategy, involving a lot of additive manufacturing processes, amongst them SLA, which was relevant for this project. [35]

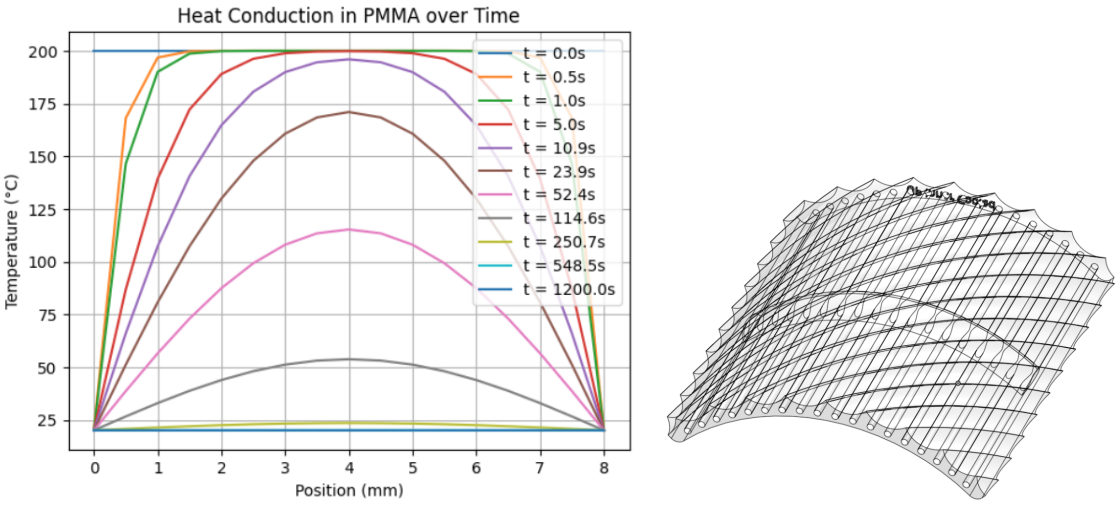

(a) (b)

Figure 10: 10a Numerical calculation of heat/time distribution with 1-Dimensional Heat Equation, assumed constant temperature on each side of PMMA specimen. 10b shows how the tubes are routed through the punch, minimum distance to surface is shy of 1mm, while maximum is about 3.5mm. This is further elaborated in chapter 2.2.5

2.2.4 3D printed lenses

The lenses are ordered from Prototal based on the virtual model that is optimized for the refractive index of the 3D printed material. The lenses are printed with the material Accura ClearVue. Further, it is polished by the manufacturer using a handheld rotary tool. Then the lenses are clear-coated. All of these operations are processed by the manufacturer, as per their recommendation. Additionally, some unprocessed lenses are also ordered to act as a reference for certain evaluations. In this research, these lenses serve as a representative of current market solutions for professional 3D printing.

2.2.5 Press forming process

As a rapid prototyping technique, a lot of 3D printed presses were made and utilized to create the PMMA lenses.

Press, a donkraft hydraulic press, built rigid ensuring parallell travel and minimal yield of the surfaces relative to each other. Capabillity of 20 tons, but any hydraulic press capable of 2 tons would suffice. Figure 12b illustrates the press utilized in the research.

Load cell, A load cell loaned from fatiguelab at NTNU MTP was used to monitor the exerted force.

Machined parts, as observed in Figure 12a, the first iterations used wooden blocks with aluminium plates on top and bottom. To ensure precision and easier use of the press, some parts were machined in nylon and aluminium, as observed in Figure 12b. This also moved the load cell above the press assembly, so that liquid cooling could be used without coolant running over the cell. Potentially disturbing the sensor or destroying it.

Infrared thermometer, Biltema 15-254, ±2% 20 ∼ 500°C, fixed emmisitivity at 0.95 [36]. Thermometer was used to measure the samples in the oven,

3D-Printers and material Multiple printers were considered for use in the project. Equipment accessible through personal and university resources were considered. The personal resources are through a volunteer organization based at the University, namely Omega Verksted. Two types of printers were used extensively, namely Prusa i3 mk3/mk3s in addition to Formlabs Form3+. The

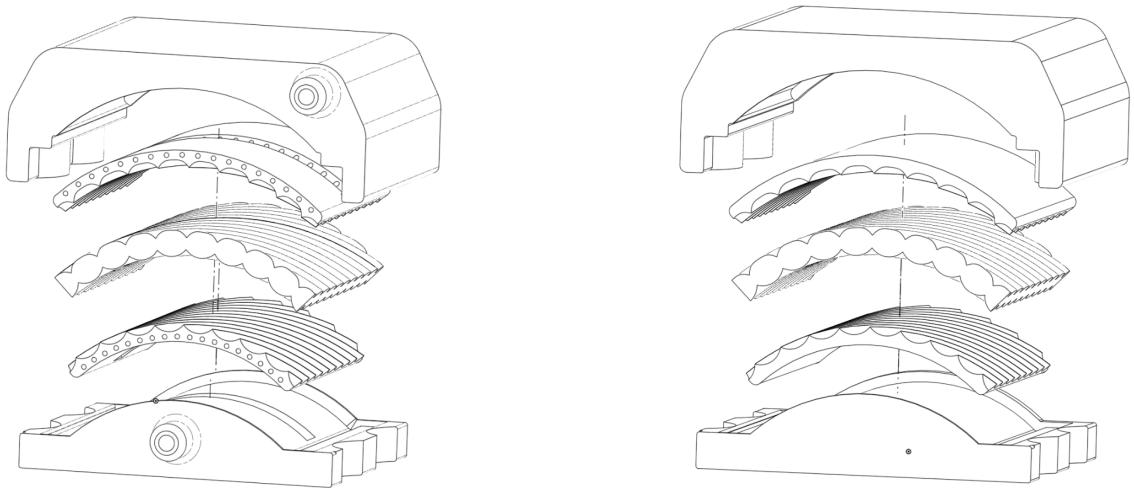

(a) (b)

Figure 11: Two revisions of the press for the inner lens. 11a, a press that is liquid cooled to research the capabillities of non isothermal molding with polymers. 11b a revision without liquid cooling. The middle parts is the produced specimen in PMMA, the upper and lower part acts as guide and fixture for the punches themselves. The punches are the two skinnier parts above and below the PMMA.

printers are described in further detail in the following paragraphs.

Formlabs 3+ a low force stereolithography printer. Used to make the punches for the press form tool. As observed and explained in Figure 11. 85µmeter Full width at half maximum (FWHM). 25µmeter XY resolution, and minimal layer height of 25µm [37].

Solflex 650, a precise DLP 3D printer. Unfortunately with minimal online documentation, making it harder to use and familiarize with. In addition to an advanced user interface, the printer was deemed less relevant, than the user-friendly Formalbs 3+.

Prusa sl1s An SLA printer capable of third-party resins. XY-resolution of 50µm. Minimal layer height of 25µm [38].

Prusa i3 mk3 and mk3s A standard FDM printer, capable of printing layer heights of 0.05mm. The extruder nozzle diameters can be changed, but in this project 0.4 and 0.6mm have been used. Of the mentioned printers, this is the only printer using thermoplastic to extrude structures. A fast printing technique, designed to print larger structures than the SLA printers listed above. Though the precision and level of detail is more limited in this printing technology. Additionally, the thermo-plastic material is extruded at just above 200℃ implying it can't withstand the heat involved in this project directly.

Formlabs High temp resin material was utilized for all the punches in this project, printed in the Formlabs 3+. Punches can be observed in Figure 12. The hi-temp resin have a heat deflection temperature of 238℃ at 0.45MPa and a ultimate tensile strength of 49 MPa with a tensile odulus of 2.8 GPa. [39]

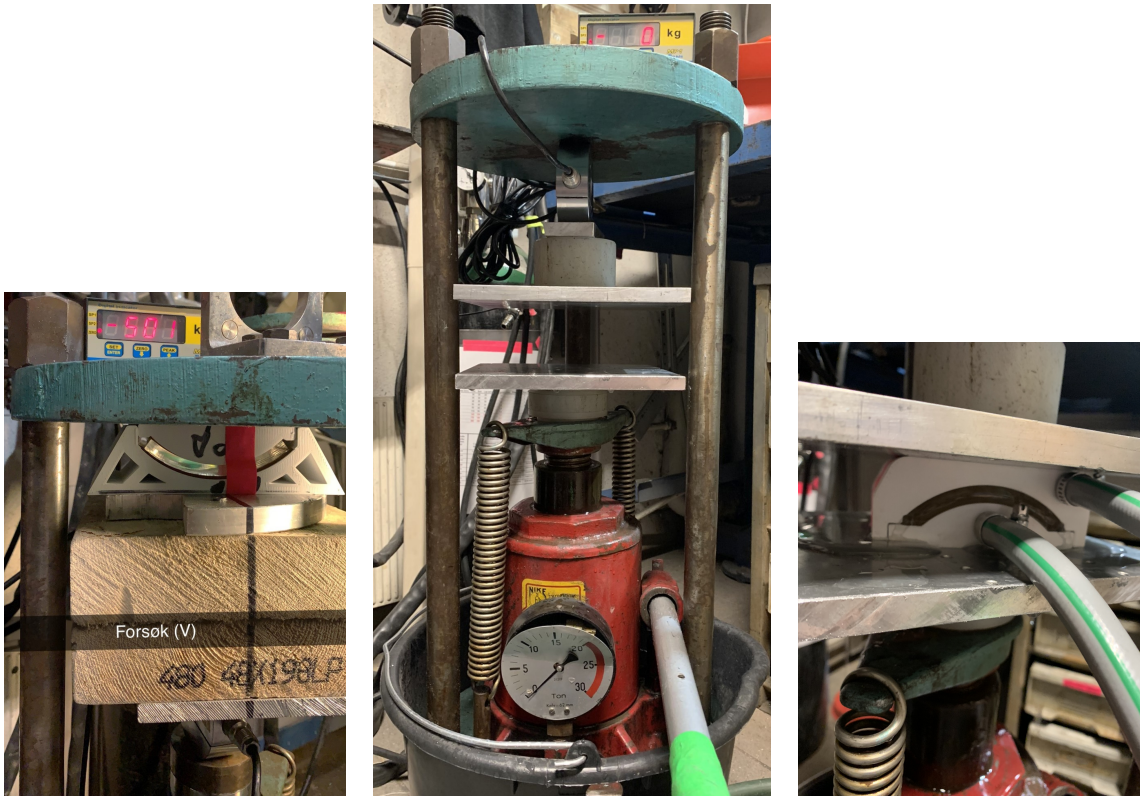

(a) First iteration (b) Improved press (c) Improved press with cooling

Figure 12: Press set ups. (12a) Press set up with wood blocks to space the press to the correct height. Aluminium plate is used on each side to distribute forces and have a flat contact surface. observe the load cell in the bottom of the picture and the load in the upper. (12b) A improved set up, the load cell is moved to top of press, and new aluminium plates are bolted to turned nylon cylinders for increased load distribution. Bucket for watercollection in the bottom. (12c) press with cooling in improved press.

2.2.6 Press tool iterations

As part of the prototyping process, multiple iterations of the 3D printed press are created to optimize the press-forming process and its yielded result. In the previous subsection, one can observe which changes are made to the hydraulic press setup itself. This subsection provides some key changes about the different iterations of the 3D printed tool. The 3D printed molds and punches had multiple revisions, the following is a summary of the considerations with Figures to illustrate the iterative process.

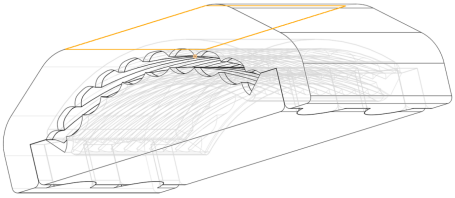

Figure 13: 1. iteration of inner press

Figure 13 illustrates the initial design, notice the narrow roof structure designed to spread the force from the middle section and out to the walls. Initially designed to be used in a press not spanning the whole area of the roof and floor. All of the presses are designed to withhold the Punches with a snap-fit inside the molds. The second iteration, observed in Figure 14a has increased roof size, ensuring stabilizing forces, so the top mold doesn't rotate due to forces exerted by the PMMA. Designed to be used in a press covering the whole roof and floor surface like the one illustrated in 12b. Pay attention to the highlighted walls, designed to receive the PMMA blank from the oven, ensuring easy lineup between the heated blank and the punches. Further, the third iteration, observed in Figure 14b holds water-cooling capabilities. The highlighted manifold leads water into small cooling channels inside the punch. Observe the cooling channels inside the punch in detail in Figure 10b and mold with hoses attached and active cooling in 12c.

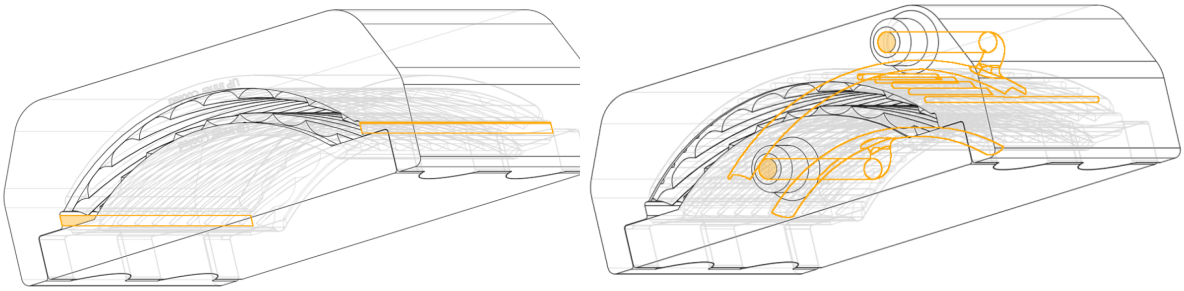

(a) 2. iteration

(b) 3. iteration

Figure 14: Second and third iterations for the inner lens mold

The first iteration of the outer mold observed in Figure 15a is quite similar to the inner press, with the exception of size. Some considerations related to less material use and printing time was different. Additionally, the deformation in the outer lens is less than in the inner, so it's designed with slightly slimmer walls. The second iteration, observed in 15b similar to the inner press, has an increased roof size, for stability when placed inside the surfaces of the hydraulic press. The third iteration observed in Figure 16a have received the parallel walls, to place the heated PMMA blank into. Though this iteration was unsuccessful due to too low guide rails, which can be observed under the mold, the 4 radis , which act as guides during the press operation. Iteration 4 was scaled up quite a lot, consequently, some material and print time measures were utilized as observed in Figure 16b. Additionally, the guide rail was changed to a taller design, and 6 guides instead of 4.

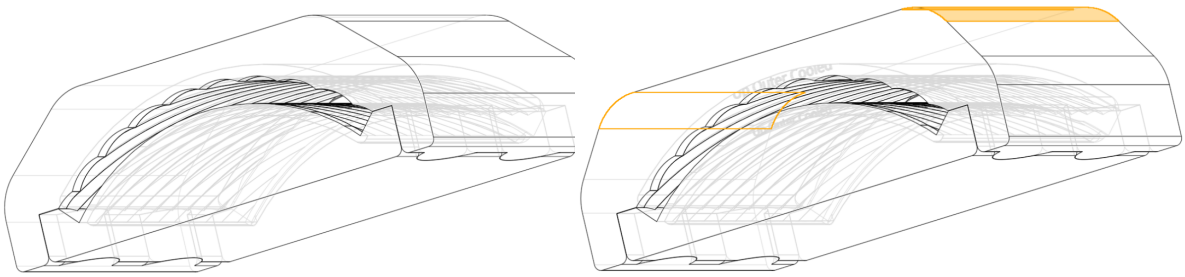

(a) 1. iteration (b) 2. iteration

Figure 15: First and second iterations of outer lens mold.

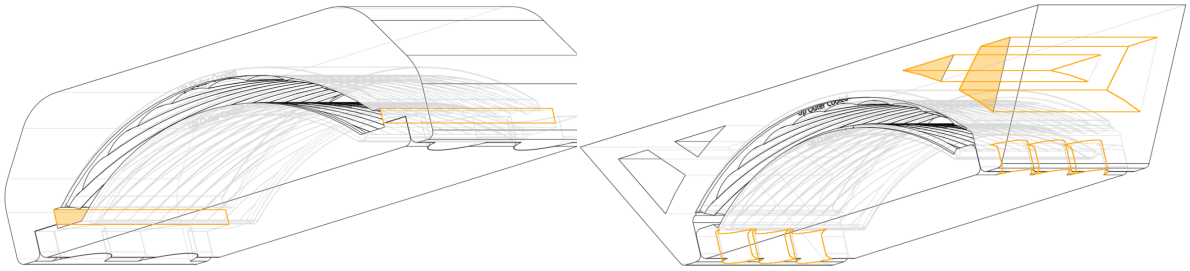

(a) 3. iteration (b) 4. iteration

Figure 16: Third and fourth iterations of the outer lens mold.

A concept for printing the whole mold in Hi-temp resin was thought of. Observe Figure 17, the roof exhibit a honeycomb pattern, to be able to transfer vertical forces and minimize material usage. Additionally, the SLA printing technique has quite a lot of thermal tension during curing, which means that its desirable with a constant wall thickness, and easily light-exposed designs. This design was thought of to reach even higher precision in addition to enabling a better cooling solution, with a designated input and output port for coolant. Though the design was never finished or printed.

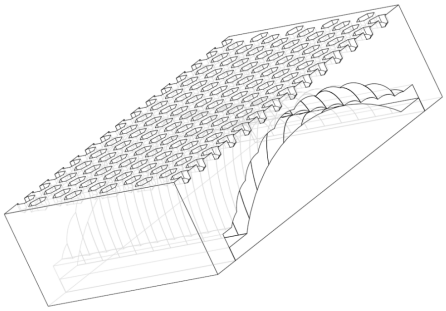

Figure 17: 5. iteration of inner press, not completed, nor used

All of the above designs are designed to be printed without support structure, the z-axis of the printer can be regarded as going inwards in the Figures. With the face of the molds laying directly on the build plate. Some pictures of the actual molds and punches are provided below, in Figures 18 and 19. Figure 18 presents a mold after it's been used, observe the crack in Figure 18a, in the lower left corner of the punch.

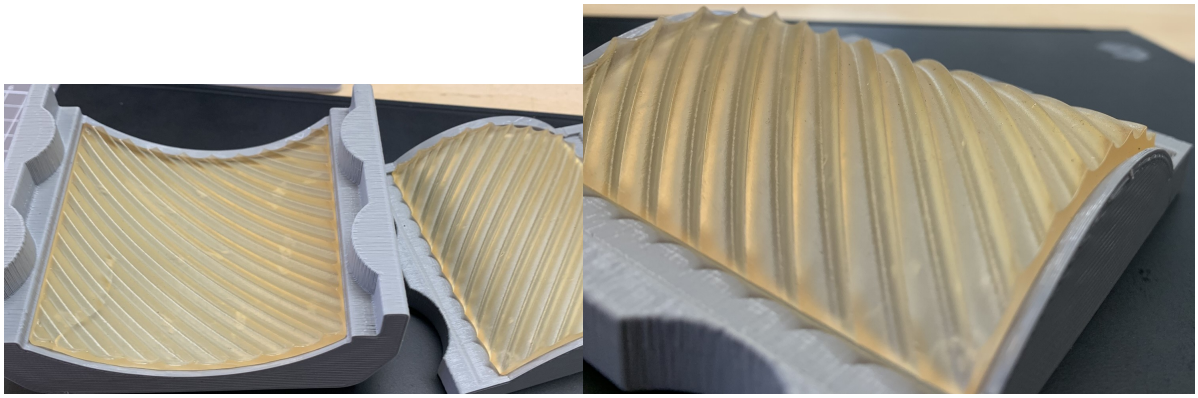

(a) Inner lens mold, with hi-temp punches mounted

(b) Inner lens mold, observe the surface quality of the punch

Figure 18: Second iteration of Inner Press

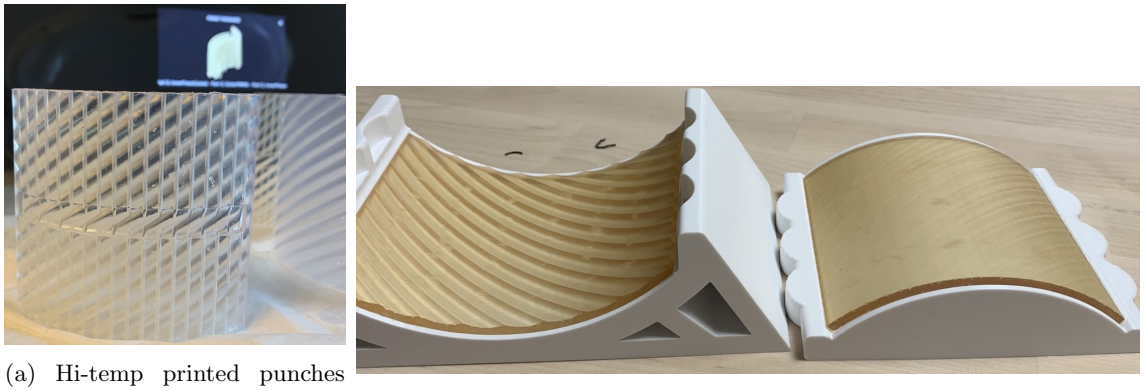

(a) Hi-temp printed punches with cooling ducts

(b) Fourth iteration of the outer press with punches

Figure 19: (19a) Inner punch with cooling before being UV-cured, (19b) outer press with punches mounted, the bottom punch is glued to the surface of the mold.

2.3 Evaluating the results

In this Section the methods and equipment used to evaluate the results are presented. As well as the assumptions and limitations of each of the tests are discussed. In addition the properties and limitations of the utilized equipment.

During the evaluation process, a few of the lenses were chosen for thorough analysis, hereby referred to as the highlighted lenses. In addition to visual inspection, these lenses underwent an optical test that resembles the light reflected from the trough mirrors. A few of them is 3D-scanned to check form, and all of them is measured in a stylus profilometer, to quantify the roughness, and give an indication of the optical surface quality. The following subsections present the roughness measurements, form and waviness measurements and the image analysis.

2.3.1 Roughness

Mitutoyo sj-301(178-952-3d) differential induction surface roughness tester. In this project, roughness where measured with 0.008mm and 0.8mm cut-off length. Minimal measurable roughness, Ra, Rq: 0.01µm = 100Å [40].

To be able to accurately measure roughness, one has to choose the λ_c for the measurement. This is the cut-off of the measurement, and the total evaluation length was chosen to be 5 times the

cut-off length, which is quite standard. The λ_c is listed with the Ra and Rz values in Chapter 3. The cut-off distance is an indication of what order of magnitude the roughness lies within. The smallest measurable cut-off on this profilometer was 0.08mm, for machined parts, one usually measures in the 0.8mm region.

2.3.2 Form and waviness

Alicona g4 infinite focus microscope, a microscope that can create point clouds of surfaces through "variable-focus" microscopy. The 3D printed lenses used in the scan are the untreated lenses because of the hard nature of imaging specular surfaces. Meanwhile, the matt surface of the untreated lenses allows for easy focusing and image capture. For the press-formed lenses, multiple coatings were tried with varying degrees of success. The glossy transparent surface of the specimens is inherently hard to capture. A coating technique tested is fine chalk powder spread over the surface, as recommended by the staff in the lab. Another coating tested is a fine mist of fermented milk, left to dry on the surface, yielding a smooth matt surface. Observe Figure 20 for a lens being scanned with the milk coating in the microscope.

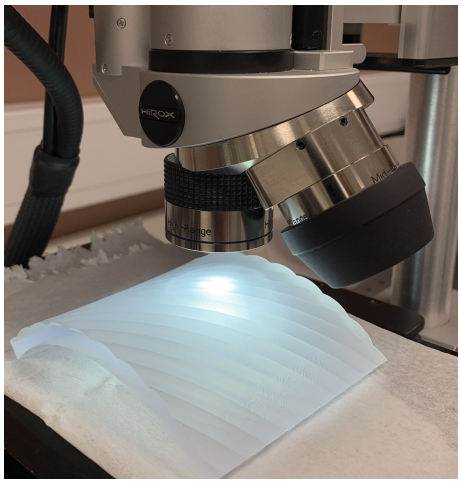

Figure 20: Press-formed lens with coating in microscope

Exporting data the data was exported as an STL file, with 4 points in the cloud scan converted into one triangle in the STL mesh. This was further compressed due to the large size of the data, elaborated in subsection 2.3.3.

2.3.3 3D map manipulation

Meshlab is utilized to compare the results from the microscope with the virtual model. The software is an Open-source system for working with mesh models. In the scope of this project the STL file format was used for mesh representation [41].

Iterative closest point, a process where the software chooses sample point from each mesh, that its trying to match. The software is given the number of sample points, minimal starting distance (how far away the software is looking for matching point on the other mesh.) Target distance, how close we want the algorithm to try to match the sample points together and the max iteration number, the number is a average alignment error of the sample points.[41]

Quadric edge collapse decimation, algorithm in MeshLab was utilized to compress the mesh file to a more manageable size, computing-wise. [42]

Hausdorf distance algorithm, was used in Meshlab to calculate the distance between produced shape and the virtual model. [43]

The mesh comparison process visualized:

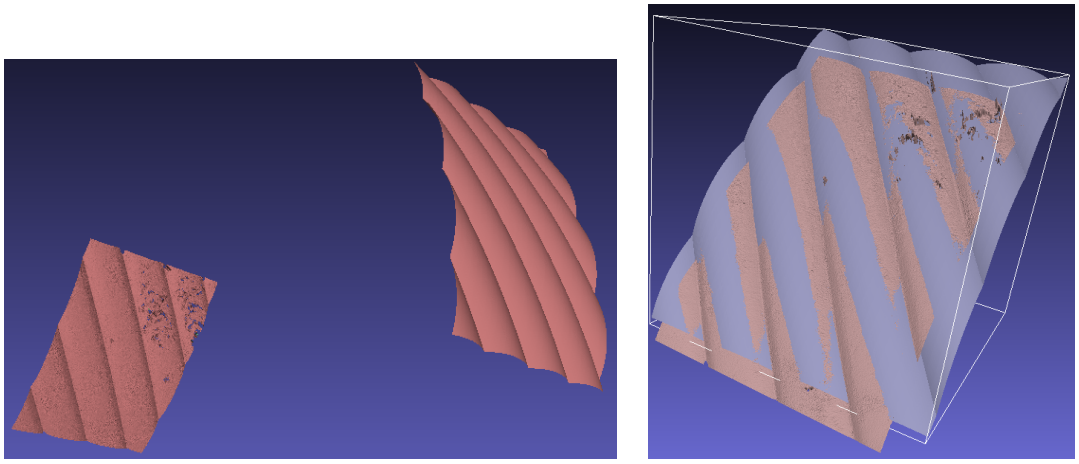

(a) Imported Geometry (b) Point glued geometry with mouseclicks

Figure 21

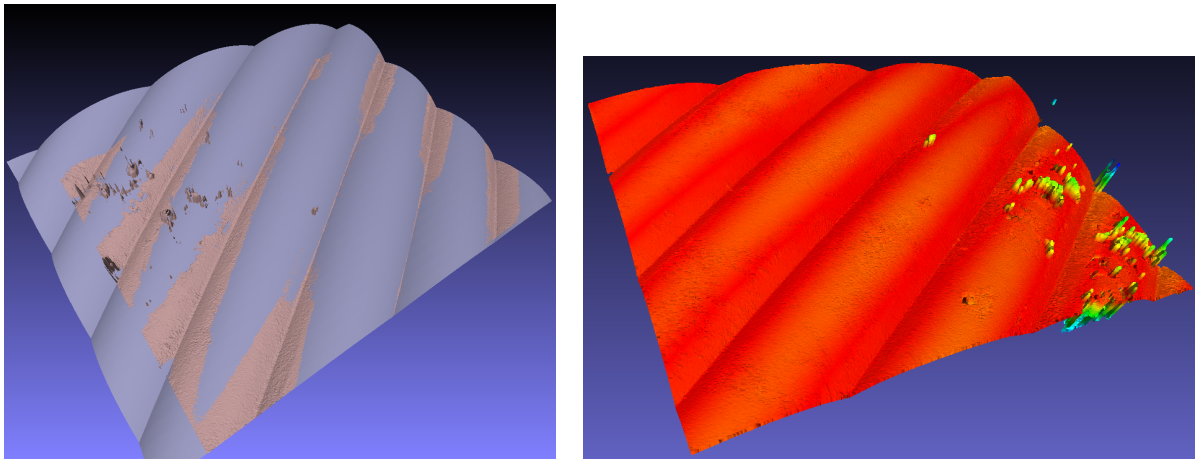

(a) Geometry after ICP (b) The hausdorf sample points on the 3D printed geometry

Figure 22

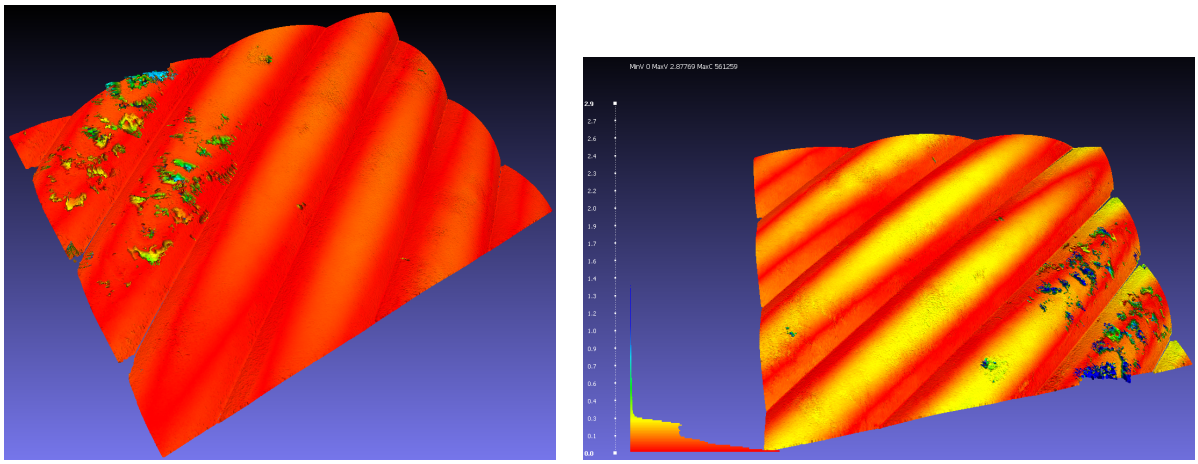

(a) Hausdorf minimal distance map

(b) Hausdorf minimal distance map with histogram and adjusted colors

Figure 23: Observe how the 23b histogram shows how close each color on the sample is from the virtual model, measured in mm

2.3.4 Image analysis and optical test jig

A image-analysis setup was made to resemble actual sunlight reflected from the mirror of the solar trough. The critical aspect of the setup is the divergence angle of the solar rays hitting the lenses and the distance from the light source to the focal plane.

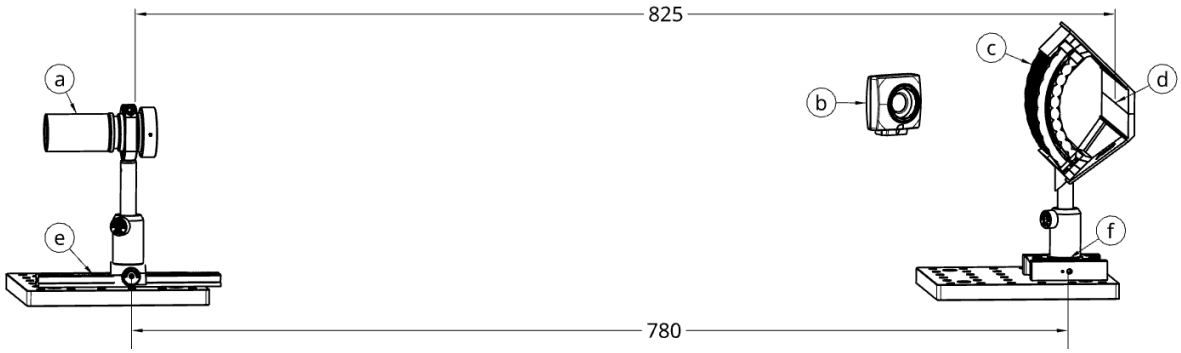

Figure 24: (distances are not to scale) a) Optical prototyping tube to mimic the light reflected from the mirror, with 1.64° divergence. b) Camera, fixed to the stem of the rotational plattform, thereby following the lenses rotation. c) The lenses for focusing the light. d) Jig for fixturing the lenses in the correct position, with the focal plane marked by the arrow. e) A linear rail to accurately move the lenses relative to the lenses, depending on the angle of incidence of the light. f) Rotation plattform, to emulate angle of sun through a day.

Figure 24 illustrates how the test setup is designed. An optical prototyping tube, is fitted with a led, dispersion filter, a pinhole hole and a lens, that creates a uniform light, with 1.64° divergence angle. The lens can be adjusted so the light is focused at the focal surface, depending on which solar altitude that is researched. A camera is mounted so that it rotates with the lenses, at a fixed height. The lenses are fixed with a 3D printed mount, that can rotate accurately on a platform to the desired angle. The assembly is screwed onto optical prototyping breadboards, which in turn are fixed to a flat plate. The optical test setup in action can be observed in Figure 25.

The optical prototyping tube is supposed to emulate light with the same properties as the one the model is optimized for with 1.5° dispersion angle. In contrast a slightly bigger angle is used, due to availability of parts. The actual acceptance is 1.64° , which means that we get slightly conservative

Figure 25: Actual optical test set up

results, than what could have been achieved with an exact replica. The lens has a focal length of 35mm, combined with the pinhole of 2000 µm, gives the acceptance angle of 1.64°

Test Procedure optical test:
To ensure comparable test results, a test procedure is followed. Each of the samples is tested at 3 different angles corresponding to the elevation angle of the sun. Since the lenses are optimized for 0°latitude (the equator) they are symmetric, so we only need to test with rotation in a single direction. As a side note, an Etendue rotator system optimized for other latitudes would not have a symmetric geometry, therefore the test procedure would be a bit more comprehensive.

1. Set the correct distance between the lens and the focal plane. Distance between the rotation table and the slider:
   - $780mm$@0°
   - $808mm$@11.75°
   - $864mm$@23.5°

   Note that these distances are not between the lens and the focal plane but between the rotational platform and the stem of the light fixture. As illustrated in Figure 24.
2. Focus the lens on the focal plane.
3. Remove the lens fixture and mount the lenses
4. Mount the lens fixture with the lenses, and tweak the lens positions so the light is the most concentrated.
5. Make sure everything is straight, and the rotation table is set to the desired angle.
6. Take the concentrated picture.
7. Disassemble the lenses in place, so everything is in the exact same position.
8. Take the reference picture.
9. Repeat for all the lenses and combinations, without changing any other parameters than the angle of the light and the focus of the light (not the camera lens).

Test procedure image manipulation:

1. Run the script with the desired test setup and without background removal.
2. Check the background light intensity with the mouse, run the script again with the chosen background threshold. Check the data the test provided, in relation to the performance of lens.
3. Rerun the test with different background removal thresholds and choose the background threshold giving the least pessimistic results. (see elaboration below)

Bullet point 3. needs some elaboration. The script produced to extract data for the image analysis deletes all pixels with intensities set below a user-defined threshold. The remaining pixel values are also subtracted this threshold value. This is done to compensate for background noise, but if the threshold is set too high, this process impacts the performance data pessimistically. To inspect the script used, see Appendix E.

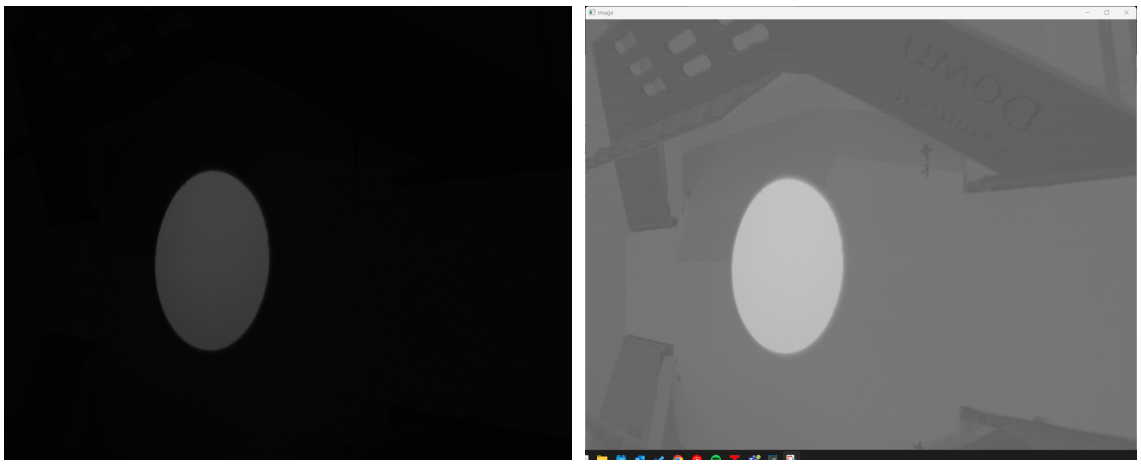

(a) Original image (b) Gamma adjusted image

Figure 26: The original image and the gamma adjusted, this is done in the script to be able to se where our reference points in the image is located. The image is not permanently altered, its just when the script displays image for the user.

3 Results

In this chapter the data and findings are presented and described. Keep in mind that one of the goals of the project is to compare professionally 3D-printed lenses to equal press-formed lenses, an additional factor in this is the cooled press, and how that process might create a different result than a non-cooled press. In total 24 lenses have been pressformed, however only a select few were chosen for in-depth analysis due to the extensive workload of these tests. Section 3.1 will elaborate on this process.

The data presented in this chapter was collected through 3 different methods: stylus profilometer, 3D mapping with a microscope and image analysis. Additionally, its relevant to introduce the lenses with a visual inspection and elaborate on the observations. Through these acquisition methods, we collect data for the different properties of the specimen. The stylus profilometer and visual inspection provide indications regarding the level of optical quality exhibited on the surface. The 3D mapping provides data about the deviations between the virtual model, and the manufactured one in terms of geometric form. In addition the image analysis indicates how well the manufactured lenses compare to the simulation and expectations.

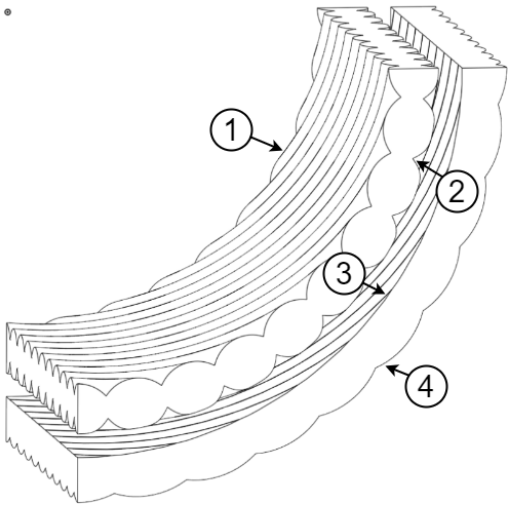

Figure 27: (1) Inner surface on inner lens. (2) Outer surface on inner lens. (3) Inner surface on outer lens. (4) Outer surface on inner lens.

Before presenting the findings of this research, the reader should be somewhat familiarized with the different surfaces of the lenses, Figure 27 shows an overview of the lenses manufactured in this project, and how they are referenced later on in this section. keep in mind that the pressformed inner lenses will be referenced with numeric numbers(1,2,3...), the outer with roman(i,ii,iii,...) and the 3D-printed with its full name.

3.1 Highlighted Lenses

In order to minimize the workload, while still maintaining a representative dataset from both the 3D-printed and the press-formed lenses, it was necessary to narrow down the lenses worth testing from 24 to only a handfull. These criteria were considered when choosing which lenses should be highlighted:

- A perfectly closed press in the press forming process.
- Surface roughness from visual inspection
- No obvious defects in the production or on the surface of the specimen.
- A span of different force and tempratures of the specimens
- Cooled press and not cooled.

Based on these criteria, a limited number of lenses were chosen. Below is a table representing which lenses was chosen and which tests each underwent. For more detailed pictures and explanation of the lenses, see appendix A.

As one observes from Table 1, not all lenses underwent the same tests. The test each underwent was carefully thought out, in terms of how each of their qualities could be compared to each other. An example is lenses 15 and 16, which are almost identical, the only difference being that one is from

Lens specification				Tests		
Lens	**°C**	**kg**	**comment**	**Profile**	**3D scan**	**Image analysis**
Press formed inner lenses				—	—	—
7	160	800	1100kg peak	✓	x	✓
9	155	650		✓	x	✓
15	200	650	with cooling	✓	✓	✓
16	200	650	same as 15, but w/o cooling	✓	x	✓
Press formed outer lenses				—	—	—
i	160	750		✓	✓	✓
iv	150	500		✓	x	✓
vii	175	400		✓	✓	✓
Professionally 3D-printed lenses				—	—	—
Outer, polished, clear coated				✓	x	✓
Inner, polished, clear coated				✓	x	✓
Outer, w/o surface treatment				✓	✓	x
Inner, w/o surface treatment				✓	✓	x

Table 1: Highlighted lenses evaluation and manufacturing specifications

a cooled press and another is from the same press, but without cooling. These comparisons will be elaborated in chapter 4.1. In addition, some lenses were too smooth for the 3D-scan microscope, meaning the equipment could not create a proper 3D image of the surface.

After undergoing each test it was clear that one pair of press-formed lenses had a result most similar to the expected results. These lenses were nr. 15 and outer lens nr. i, this lens pair will be the reference for the pressformed lenses, when comparing it to the 3D printed lenses in the further sections. The other highlighted lenses will still be of importance, but not in terms of comparing them to the professionally manufactured ones performance vise.

3.2 Visual inspection

In this section, the lenses that have been manufactured as part of the research are presented. This section aims to provide an overview of the lenses esthetic. The press-formed lenses are also compared to the 3D printed ones in side-by-side pictures, so it's easy to get an impression of how they compare visually. The key takeouts of the images are provided but with minimal discussion as to why. For the discussion, read chapter 4.

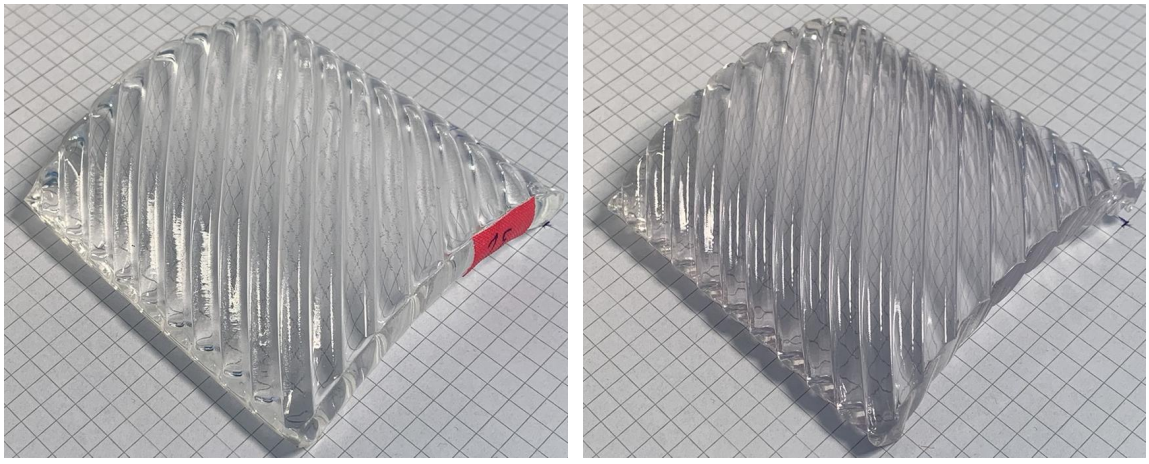

(a) Pressformed lens 15 (b) 3D printed lens

Figure 28: The two inner lenses that is being compared.

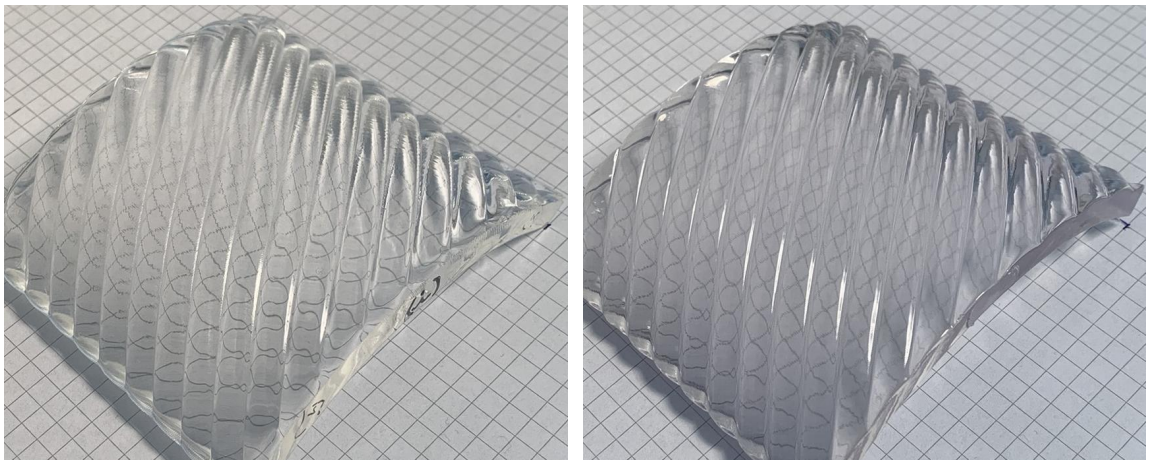

(a) Pressformed lens i (b) 3D printed lens

Figure 29: The two outer lenses that is compared

Pay special attention to how one can observe the layer stepping in both the press-formed lens and the 3D-printed lens in Figures 28a and 28b. On the press-formed lens, these steps can be felt by the touch, so it is an outside feature, while on the 3D printed lens, this can only be observed with the eye, not by the touch. Another noteworthy observation in the Figure is the darkening effect observed in the 3D-printed parts.

Another key takeout from observing the inner lenses in Figure 28 to the outer in Figure 29. Is the more aggressive geometry in the inner lenses. This means that straight light is deviated more in this lens than in the outer. Consequently, it's harder to observe the background grid through these lenses.

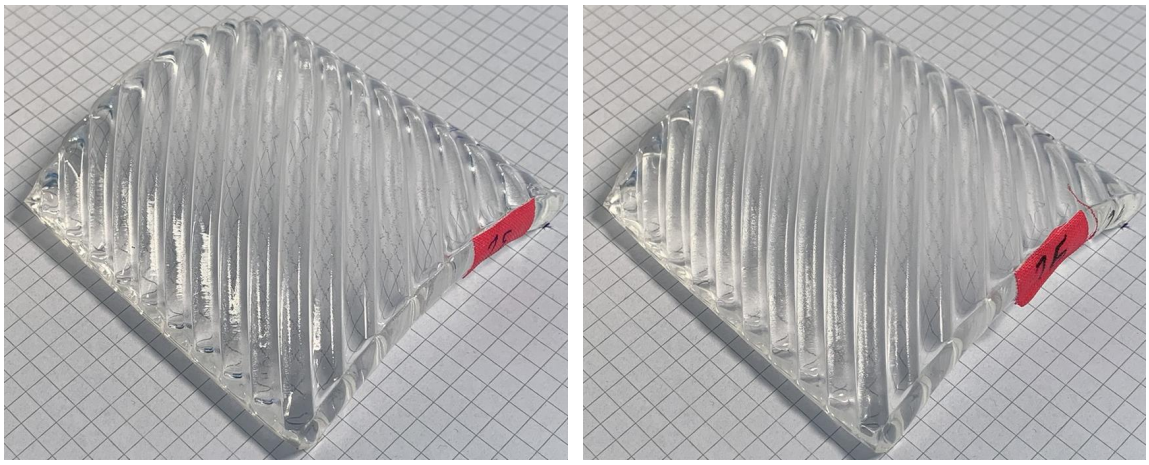

(a) Lens 15, press-formed with cooling (b) Lens 16, press-formed without cooling

Figure 30: Two lenses press-formed equally, with and without cooling

In addition to comparing professionally manufactured lenses with press-formed ones, the research explores different press-forming procedures. Figure 30 illustrates two lenses press-formed under identical parameters, with the exception of liquid cooling applied to one of them. Inspecting the lenses the differences are subtle, however, Lens 16 as depicted in Figure 30b, exhibits slightly more haze compared to its counterpart. A detailed analysis of this difference will be elaborated in section 4.1.

3.3 Surface roughness

A key aspect of optical parts is surface quality, more specifically surface roughness. The visual inspection in section 3.2 gives initial indications of the parts roughness. More particulary, if we observe a matt surface, this would imply that the light is scattered in multiple directions, giving a diffuse effect. A glossy surface indicates less scattering, and less divergence of the light rays from its intended path. In a solar concentrator its desireable with a a glossy surface, with minimal scattering, so the light rays travel in the path we intend.

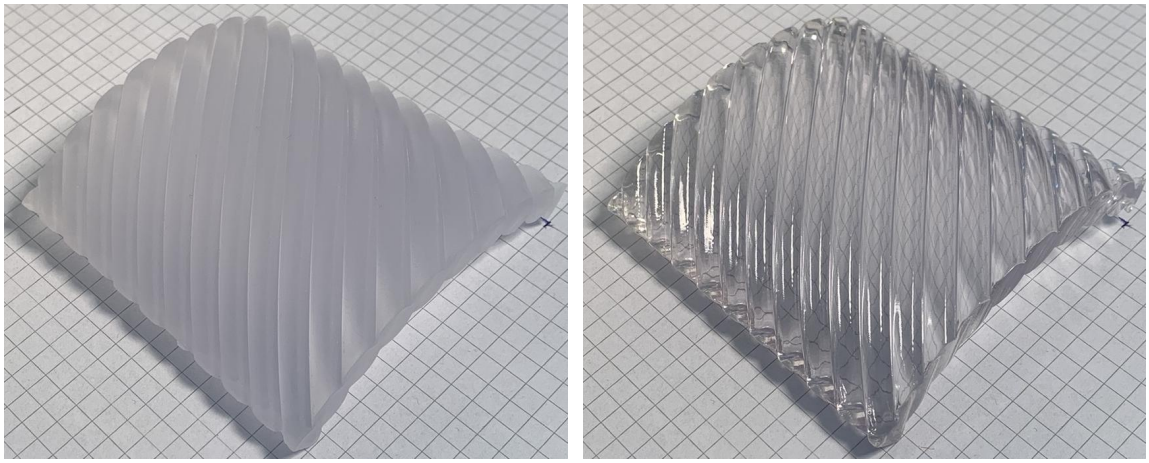

(a) 3D printed inner lens, untreated (b) 3D printed inner lens, polished and clear coated

Figure 31: The inner lenses that's 3D printed, both the same material and printing procedure, 31a representing a matt surface, while 31b is a glossy surface

Observe the two equal lenses, with different surface treatments in Figure 31. These are printed the same way, but one has been polished and clear coated, while the other has only been cured after printing. These two images show how significant difference the surface roughness of a part has relating it to its optical behavior. One is very rough, with a lot of waviness, while the other inhibits characteristics in the range of a specular surface.

3.3.1 Profilometer roughness

In this subsection we present the findings, obtained with a stylus profilometer. The roughnesses presented in this section should not be used quantitatively, but more as an indication of which order of magnitude the roughness of each part lies within. This is due to varying roughness across different sections of the parts, in addition to varying roughnesses between top and bottom of valleys. As mentioned in chapter 2.3.1 the minimal Ra value the profilometer can measure is 0.01µm, which within optics is considered a surface on the rougher side of the scale, but still, an specular surface, see section 1.3.1 for elaboration. In addition to the limitation of the equipment and different roughnesses across the part, the geometry measured in this research is doubly curved, which also makes the measuring of the surface harder. This is attributed to the traveling direction of the stylus tip, meaning in any direction it travels on the part the surface will curve. Observing Figure 32 we can see that on both the outer surface and inner surface of the lenses, the stylus traveling direction was directed along the least curved direction of the lenses.

(a) lens 16 Outer surface

(b) lens 16 Inner surface

Figure 32: Lens 16 in the stylus profilometer, observe that that the stylus is placed on top of the valleys and along their revolved direction. The outer lenses were measured on the top of the lens when placed flat 32a. While the inner lenses had to be measured closer to the edge as seen in 32b.

specimen	Outer Ra µm	Outer Rz µm	Inner Ra µm	Inner Rz µm	λ_c (cutoff)mm
7	0.46	1.88	0.42	3.03	0.8
9	0.09	0.61	0.02	0.34	0.25
15	0.85	3.85	0.17	1.07	0.8
16	0.99	5.59	0.43	2.34	0.8
i	0.02	0.15	0.38	2.24	0.25(outer) 0.8(inner)
iv	0.01	0.13	0.03	0.22	0.08(outer) 0.25(inner)
vii	0.01	0.07	0.12	0.68	0.08(outer) 0.25(inner)
3D outer	0.09	0.36	0.37	2.27	0.8(outer) 0.25(inner)
3D inner	0.23	0.96	0.24	1.23	0.8
3D outer untreated	5.99	32.73	8.96	58.55	2.5
3D inner untreated	7.99	45.47	-	-	2.5

Table 2: Roughness of the highlighted specimens

Observe the variation in λ_c in table 2, this implies which order of magnitude the roughness lies within. We observe that the outer surface of lenses iv and vii is measured using 0.08 cut-off distance. This would imply that they have a very low roughness, i and iv measure Ra = 0.01µm, meaning they both are within a production-grade optical surface.

Continuing the comparison between the liquid-cooled representative 15 and its uncooled counterpart 16 we observe a slightly lower roughness for the cooled lens in Table 2. This finding might be misleading and the results will be discussed in chapter 4.1.

3.4 3D mapping

This section presents the findings after the parts are 3D-scanned with a variable focus microscope and compared to the virtual model in software. Both the 3D-printed and the press-formed lenses are presented. We quantify two measures for surface deviation between the virtual and physical parts, distance deviation and angle deviation. The distance deviation should be considered a measure of how well the manufacturing process reproduces the virtual part. Meanwhile, the angle deviation, measures how well the parts resemble the virtual model in terms of optical behavior. The 3D printed results are from the untreated lenses. The reason is the challenging nature of imaging a specular transparent surface. The microscope struggles to identify a point of focus on a transparent, smooth surface. The untreated lenses have a rough matt surface, easily focused on and imaged, as observed in Figure 31a. Meanwhile, the press-formed and post-processed 3D printed lenses inhibit a glossy, smooth surface that is hard to image. Though different surface coating techniques are attempted, none were really successful.

3.4.1 Distance deviation

In this subsection the Meshlab Hausdorf distance results are presented. The findings are the distance between the virtual model and the 3D-scanned surface. Keep in mind that the colors of the Figures are not necessarily equal between Figures in terms of distance, therefore, it's important to keep an eye on the histogram in the left of the pictures, which is measured in mm deviation between the virtual model and the scanned model.

Before presenting the lenses, it's important to remember the inherent measurement error and resolution of this scanning process. These limitations are dictated by the magnification of the lens on the microscope, which was chosen to be the least amount of magnification (2.5x). We can assume that points appearing visually correct have a minimal deviation from their actual position, a topic further discussed in chapter 4. For the following results, we will assume that the scans in the subsequent Figures are precise to within $\pm 0.05mm$. We will justify this later in section 4.2.3.

For the sake of orderly presentation, the different lenses are grouped into inner and outer lenses, where the inner lenses are presented first. The inner lenses are numerically numbered when press-formed, while the outer press-formed lenses are marked with roman numbers(i,vii and so) and the 3D- printed lenses is named specifically. Keep in mind that the outer lenses possess a less aggressive geometry than the inner lenses. Meaning that the slopes and valleys have smoother transitions and less steep curves.

Inner lenses inner surface:

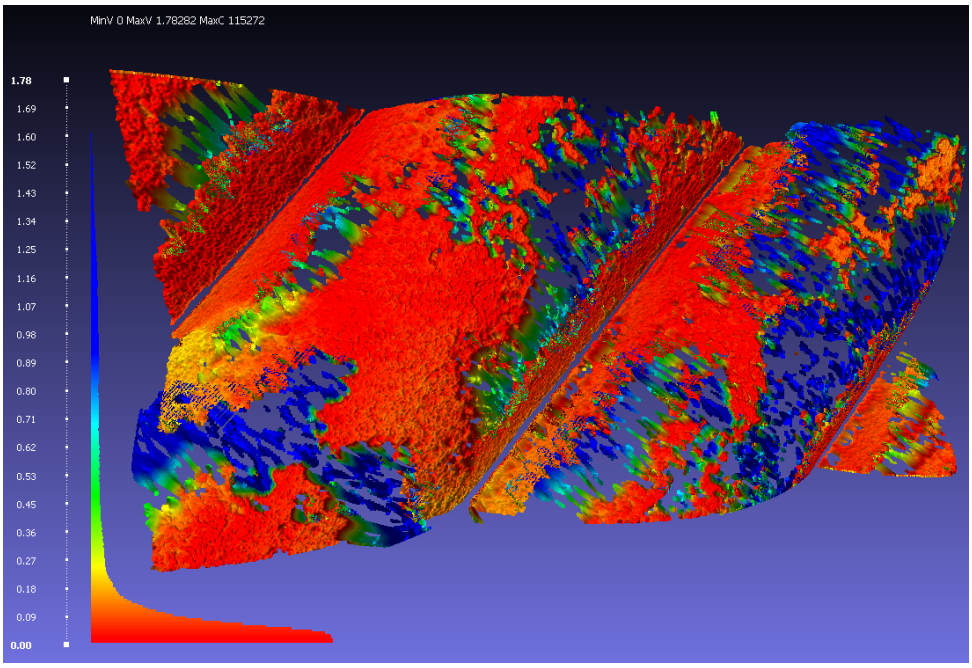

Figure 33: **Specimen 15 inner surface**, Observe the histogram and distribution of distances on the left of the image.

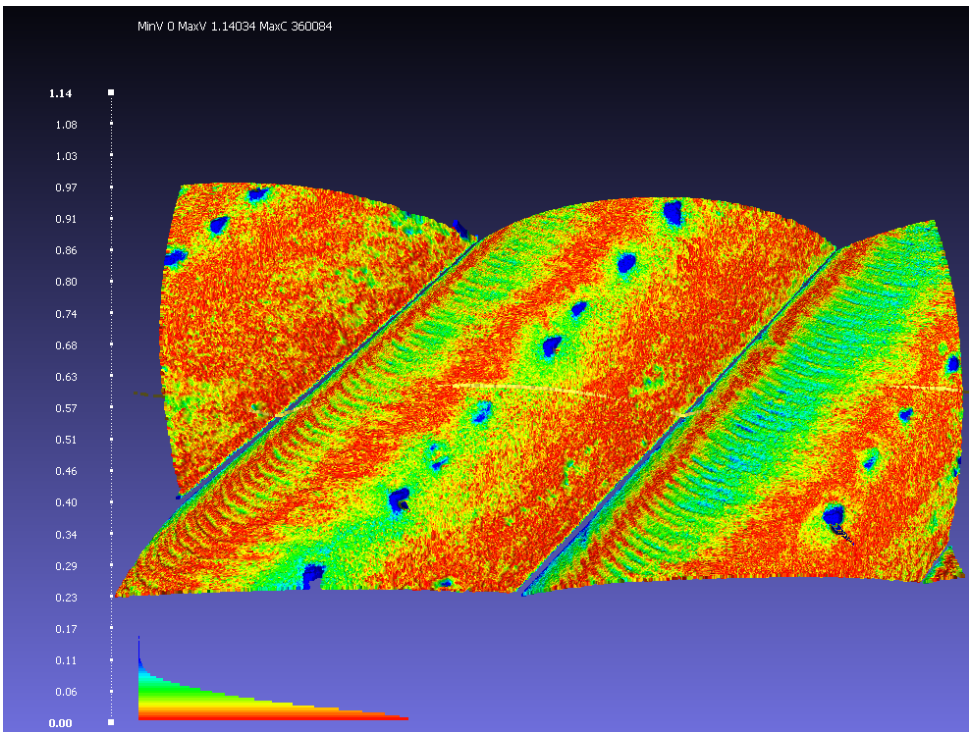

Figure 34: **3D Printed inner lens inner surface**, Observe the histogram and distribution of distances on the left of the image.

Observing Figure 33 one notice that most of the data including the top section of the hills have a distance deviation $\leq 0.15mm$. Meanwhile Figure 34 indicates that most of the part is precise to $\leq 0.1mm$, implying that the 3D printed surface have a better form compared to the virtual model, than the press-formed lens.

Inner Lenses outer surface:

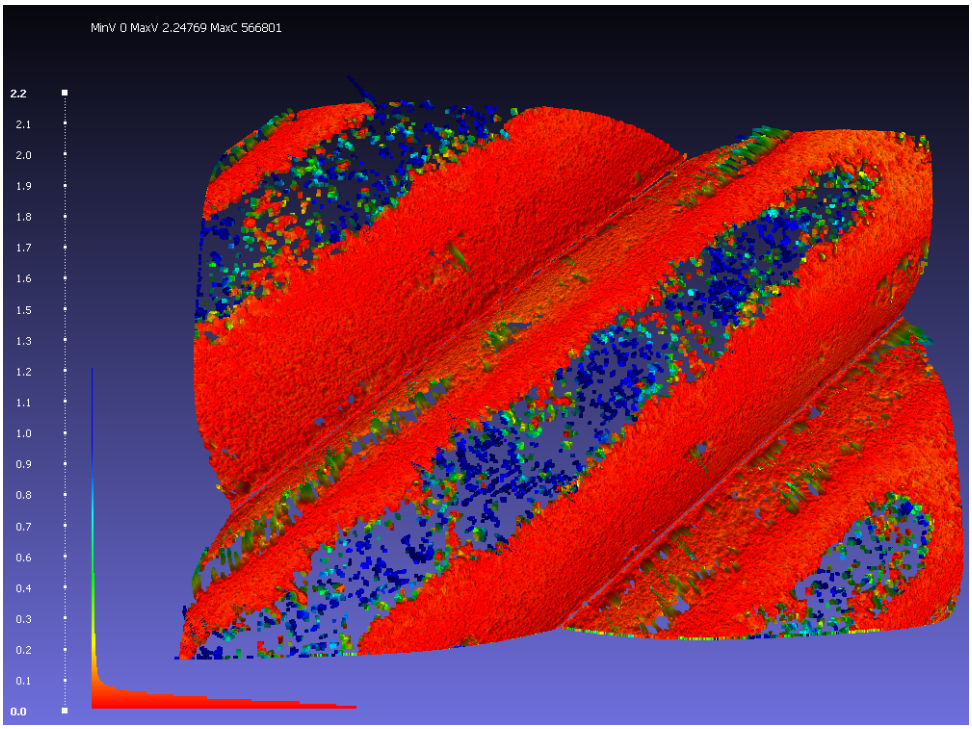

Figure 35: **Specimen 15 outer surface**, Observe the histogram and distribution of distances on the left of the image.

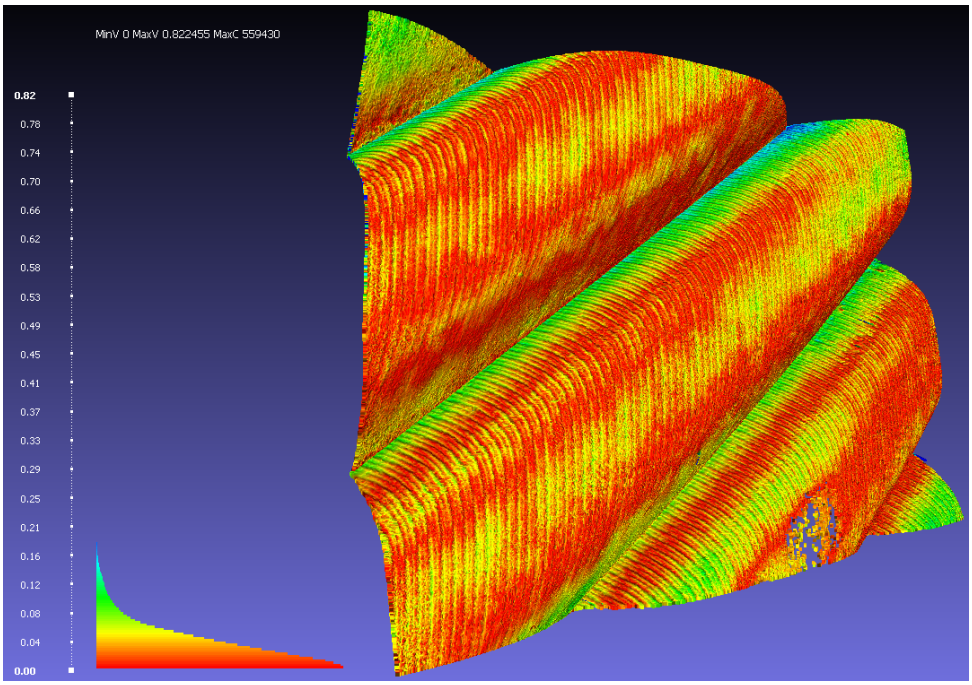

Figure 36: **3D Printed inner lens outer surface**, Observe the histogram and distribution of distances on the left of the image.

Observing Figure 35, notice that the upper part of the hill is missing from the scan. A small portion is left in the upper right corner, based on the histogram, this deviation seems to be $\leq 0.1mm$. Comparing to Figure 36 most of the data suggest a distance deviation $\leq 0.08mm$.

Outer lenses, outer surface:

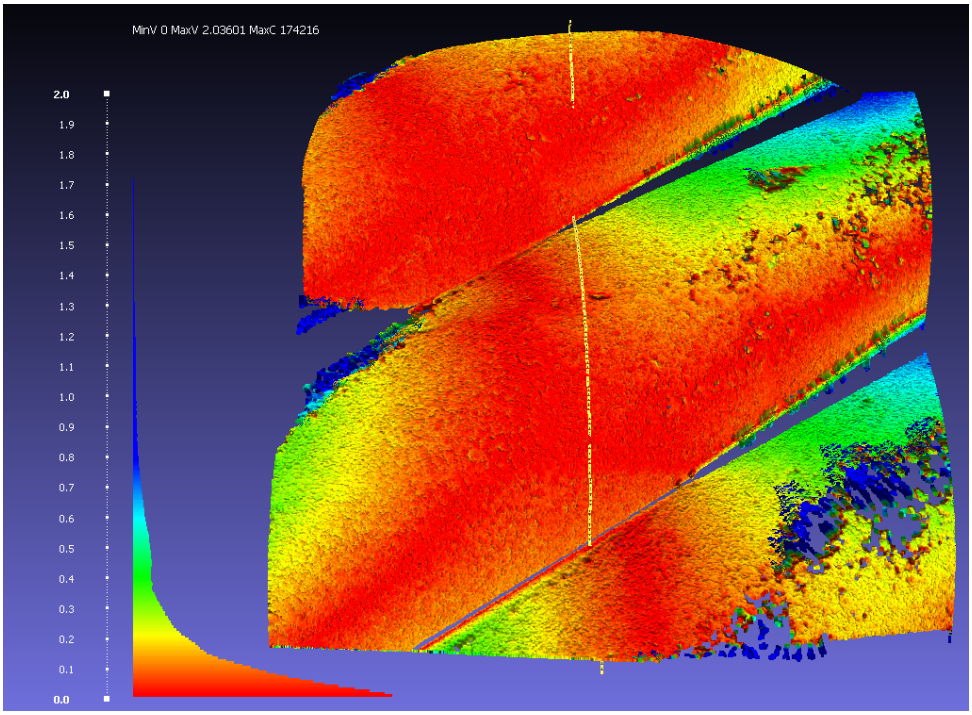

Figure 37: **Specimen i outer surface**, Observe the histogram and distribution of distances in the left of the image.

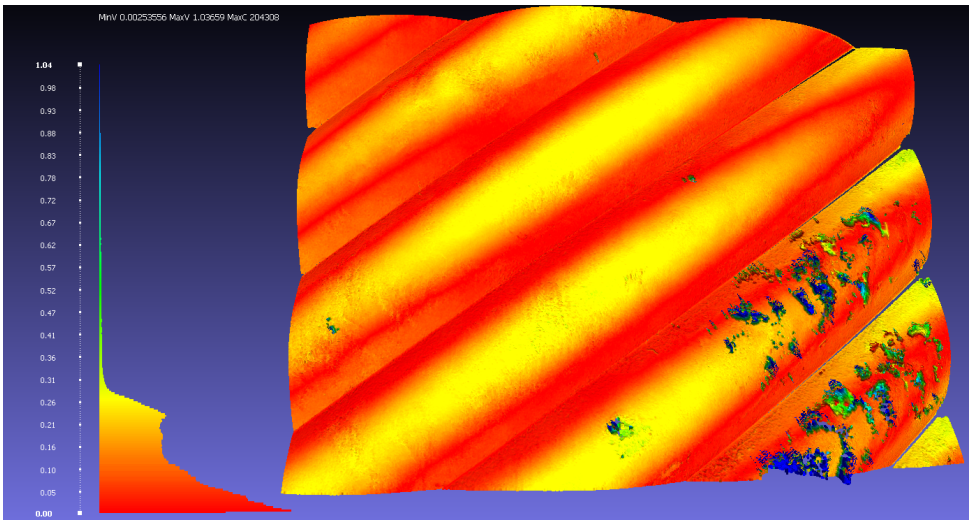

Figure 38: **Specimen vii outer surface**, Observe the histogram and distribution of distances in the left of the image.

Figures 37 and 38 originates from two different outer lenses, as observed in the caption. Pay close attention to the yellow fields in the upper part of the hills in Figure 38, this deviation is in the range of $0.25mm$. Meanwhile a different press-formed lens, namely i in Figure 37 seems to have the same area within $\leq 0.1mm$.

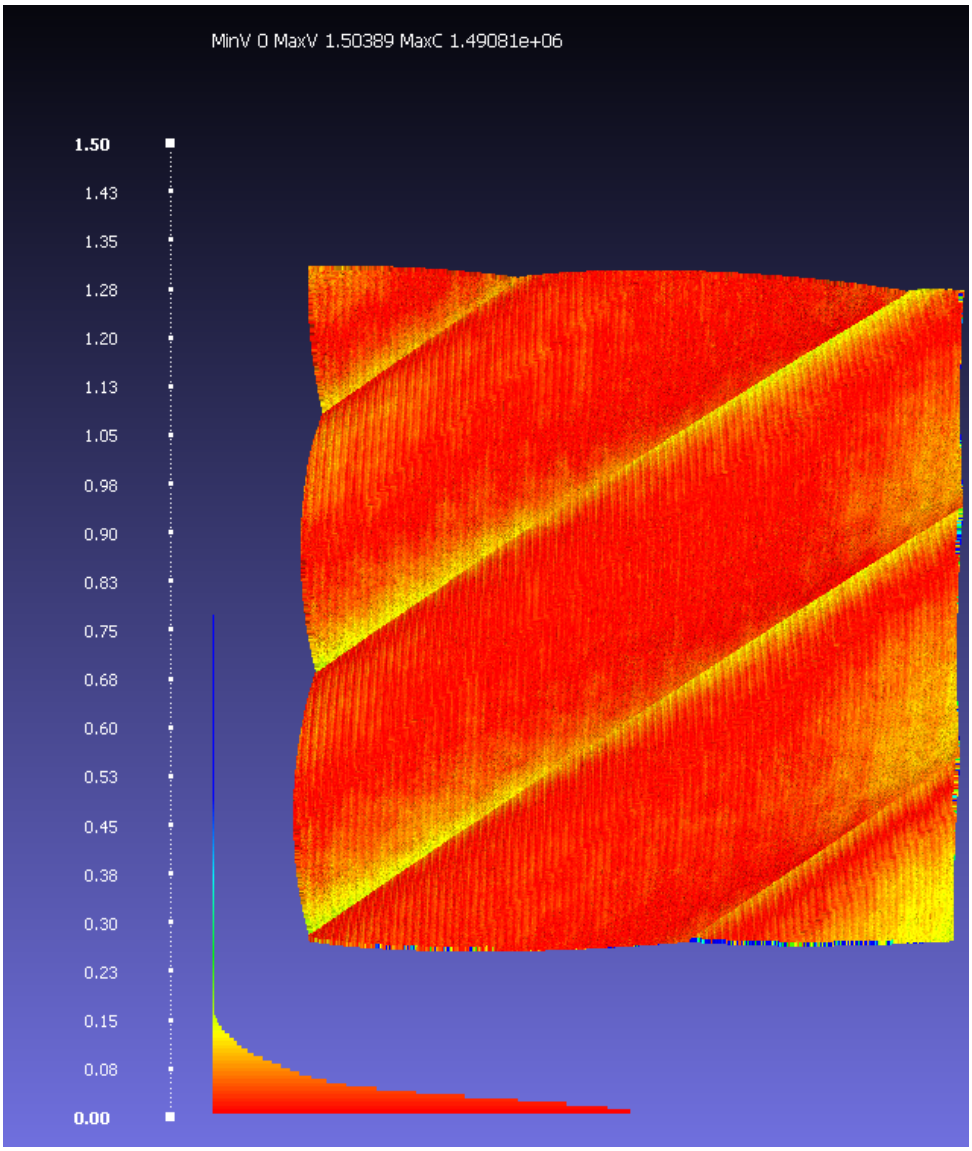

Figure 39: **3D printer outer lens, outer surface**, Observe the histogram and distribution of distances in the left of the image.

The two previous Figures, 37 and 38 should be compared to its 3D-printed counterpart in Figure 39. Observing the histogram, most of the surface indicates a accuracy $\leq 0.08mm$.

3.4.2 Angular deviation

This subsection is dedicated to the measure of angular deviation. As previously mentioned the distance deviation results presented earlier doesn't provide accurate measure of optical behavior. A more accurate measure within non-imaging optics, is the angle deviation of the surface, compared between the virtual and physical part. This concept is elaborated in chapter 1.3.2. In short, the precise translational distance becomes less critical, as the angle of incidence has a more profound influence on the light ray direction. Additionally, the translational distance also influences the angle deviation. For this reason, this research quantifies the angle deviation as the representative measure of optical form. The data from the 3D microscope are quite rough, and its necessary to extract the form of the meshes. This is done by interpolating the data with a smoothing factor. The smoothing factor is set equal for all the data sets. These data, as well as the distance deviation data, shouldn't be used quantitatively, other than to compare the plots to each other, and not to be

referenced outside of this research, due to the inherent uncertainty of the microscope measurement.

The graphs presented illustrate the distance on the left y-axis and x-axis. Meanwhile, the angle deviation is presented in degrees on the right y-axis. The yellow line, noted as "Virtual" in the legend illustrates the virtual reference surface. Accordingly, the blue graph named "Scanned surface" is the data from the 3D scanning process. Additionally, the red, dotted line is the interpolated and smoothed scanned surface. Angle deviation is shown in dotted green, as noted by the legend. The measured deviation is between the interpolated line and the virtual line, calculated at each individual point in the data.

In Figure 40a observe the slightly longer distance between the valleys in the scanned plot compared to the virtual surface. In Figure 40b note the gap between the hills of the scanned surface compared to the virtual. Additionally, observe the repeated pattern between each of the hill's angle deviations, two almost identical "waves". The 3D printed outer surface demonstrates the least deviation between these 3 plots, as observed in 40c

Unfortunately, the 3D scans from the other press-formed lenses have too much non-manifold surfaces to be able to section it properly as observed in the previous section: 3.4.1, specular surfaces are inherently hard to image, thereby hard to post process due to the lack of data points.

In Figure 41 we observe the inner and outer surfaces of the 3D-printed inner lenses overlap the scanned surface almost exactly. With minimal deviation between the Virtual line and the scanned surface. Some deviation is found at the bottom of each valley. Consequently the angle deviation peaks in these areas. Observing Figure 41a notice the slight shift to the left between the scanned surface and the virtual surface.

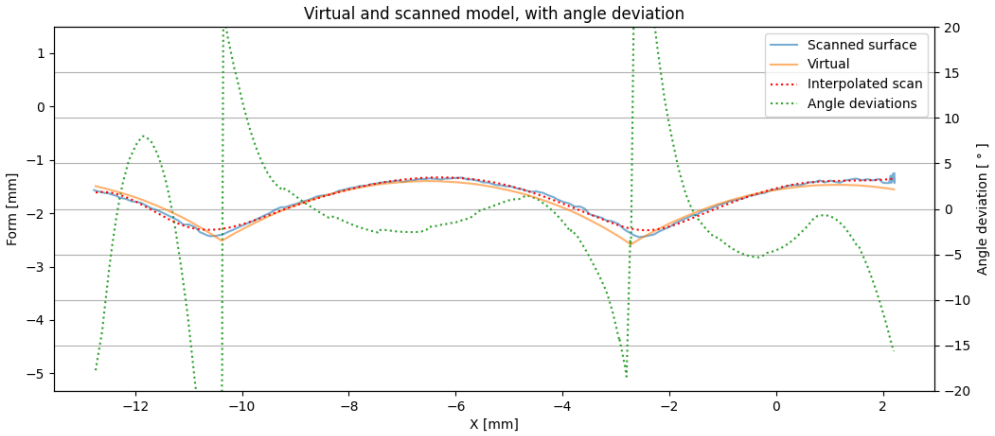

(a) Lens i, outer surface

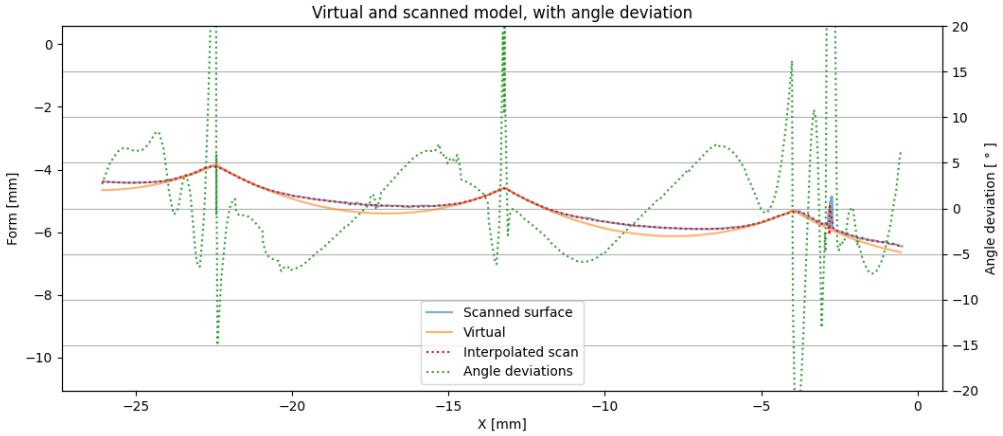

(b) Lens vii, outer surface

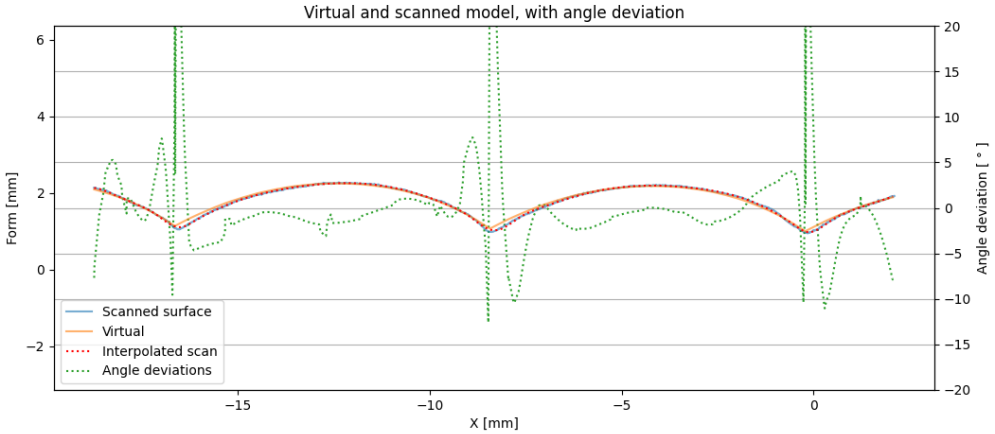

(c) 3D printed Outer Lens, outer surface.

Figure 40: Three angle deviation os outer surfaces on the outer lenses

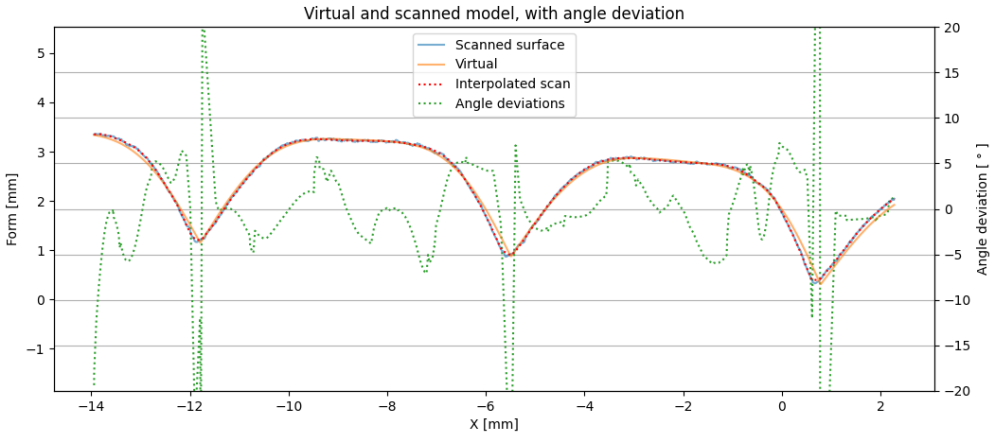

(a) 3D printed inner lens, outer surface

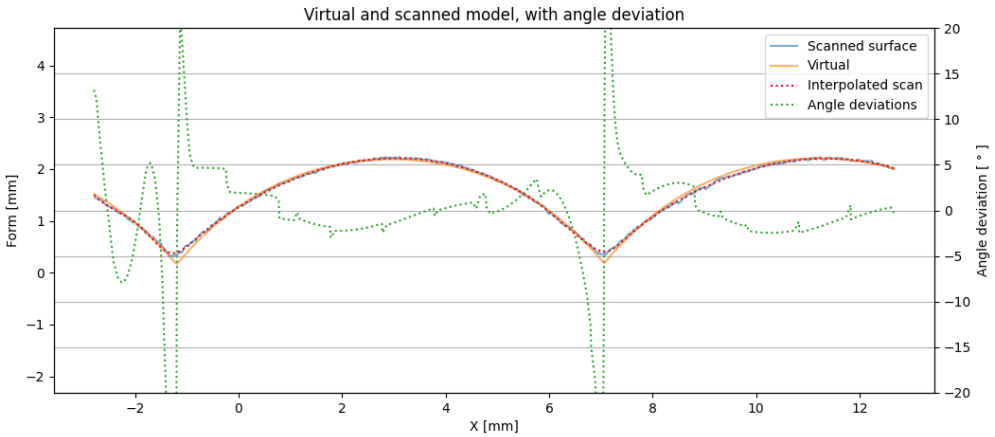

(b) 3D printed inner lens, inner surface

Figure 41: Two 3D printed inner lenses angle deviation

3.5 Image analysis

In this section, an image analysis is presented in a purpose-built test setup. The image analysis set-up is designed to resemble light traveling from the outer edge of the parabolic mirror and onto the lenses, with the acceptance angle that the lenses are optimized for. In addition, the setup is designed for testing light at three different solar zenith angles. The data gathered in the image analysis is processed in different scripts to extract the desired data. A camera is positioned to measure the light intensities in a repetitive and equal manner in a purpose-built test-jig. In addition to data manipulation of the images for measuring the performance of the prototypes. Keep in mind that all of the presented lenses are measured with three incident angles to simulate different solar zenith angles. The three different angles being 0°, 11.75° and 23.5°, where 0° corresponds to the sun being straight up, and the 23.5° is the lowest solar zenith angle at equator, meaning we test the two extramas in addition to a middle value.

One key attribute of the project is to research a viable production technique and compare it to a commercially available substitute. This section compares the best results from the press-forming process to the commercially manufactured lenses. Additionally, the test setup is simulated in a virtual setup, so a set of theoretical virtual data will also be presented.

3.5.1 Overview images

In this subsection images during the image analysis are presented. Some of these pictures have been taken at different background lights. For that reason, some images exhibit different lighted situations. This information is given in the subcaptions. Later in the research, it was found that all pictures should be taken with the same background noise, so the image analysis was redone so the background noise would be consistent for all tests. Consequently, all of the image analysis is carried out with the same lighting situation, but not all the overview images are redone. For that reason, the pictures presented in this subsection should only consider the lighting pattern, and not the intensities of the lighting in the images. The background lighting is stated as strong or weak background noise in the subcaption, corresponding to strong or low background lighting.

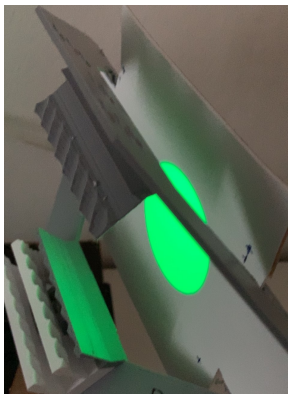

Figure 42: Test jig without lenses

Figure 42 illustrates how the light is emitted in the test jig without any mounted lenses, try to gain an understanding of how wide the circle emitted to the test jig is compared to how wide it appears with the lenses mounted.

(a) 3D Printed lenses, weak noise

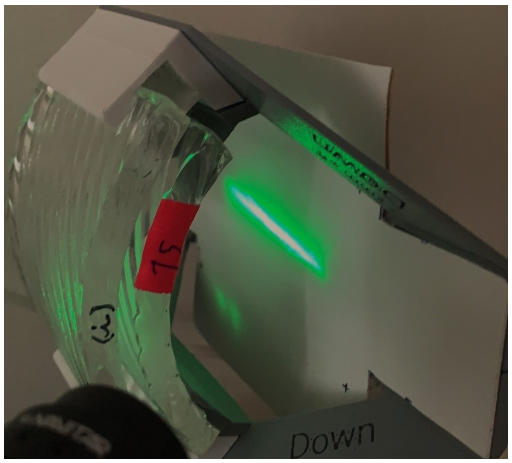

(b) 15 and i, strong noise

Figure 43: Pictures show the resulting light with 0°solar zenith angle.

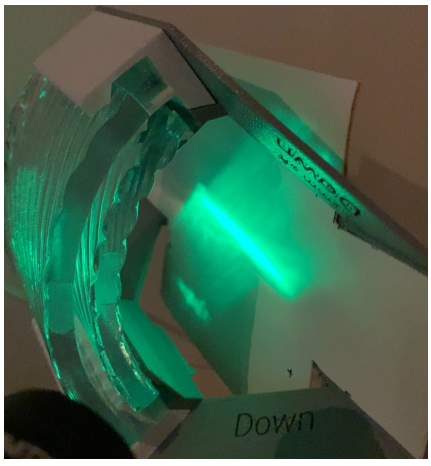

(a) 3D Printed lenses, weak noise

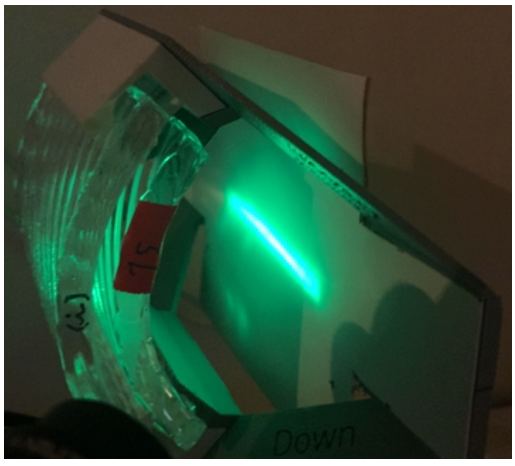

(b) 15 and i, weak noise

Figure 44: Pictures show the resulting light with 11.75°solar zenith angle.

Figure 44 showcases the only two pictures in this section that can be some-

what directly compared to each other. This is due to the background lighting being the same. On the other hand, the pictures are taken without manual adjustment of shutter speed, ISO sensitivity and aperture on the camera. With this in mind, one can consider more than just the pattern of the image. Observe especially how the light in the middle of the focal line Figure 44b is so bright it almost looks white in the image, despite the background being darker than in 44a in terms of exposure. The intensities of the light in the image will be further elaborated in section 3.5.3, with proper imaging techniques for comparing intensities.

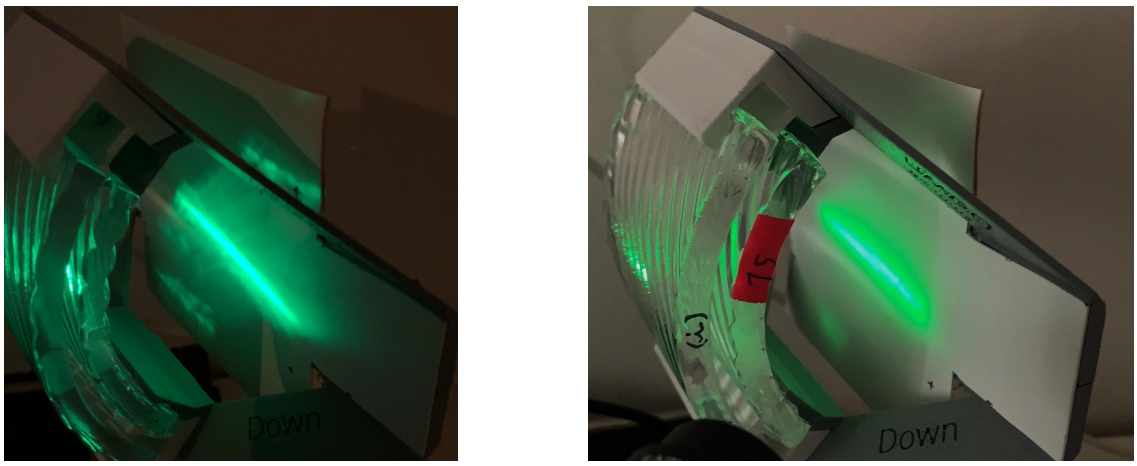

(a) 3D Printed lenses, weak noise

(b) 15 and i, strong noise

Figure 45: Pictures show the resulting light with 0°solar zenith angle.

Figures 43, 44 and 45 display how the 3D printed lenses compare to lens 15 and i. In the optical test jig. Lens 15 and i was found to be the best-performing lenses of the press-formed lenses. Pay special attention to how wide the different focal lines are in each image, and how the light is scattered across the surface, with attention to how the light is scattered, is it a diffuse scattering or a line-like scatter?

3.5.2 Image capture compared to simulation

This subsection is dedicated to providing insight to the image analysis and how the image analysis images compares to the simulation. In addition these results are meant to prepare the reader for the next subsection, which presents the key findings for the image analysis, and the project in general. A more comprehensive guide to how the image analysis was carried out, can be found in chapter 2.3.4.

The section begins by presenting the raw images, before and after transformation compensating for camera angle. Followed by the corresponding images generated by simulation in Zemax OpticStudio. With one exception in the simulation, no additional transformation is needed in the simulation, we have the desired angle immediately.

(a) Reference image without the lenses

(b) Same image as 46a with the lenses

Figure 46: The right images show the uncropped raw image, the left image is the same image, but transformed to compensate for camera angle. In addition it has been cropped to our area of interest.

Figure 46 illustrates how the image is cropped and transformed for further image analysis, the intensities in these images are equal, notice how Figure 46b have a brighter and narrower light than in 46a. With a close inspection, we observe that the background in 46b looks somewhat brighter than in 46a. This is due to reflection and scattering of the light hitting the focal plane and lenses. Keep in mind that these images are taken with the exact same background noise and manual camera settings.

Observing the ray-traced images in Figure 47 we notice that 47a looks brighter than 47b. This is not accurate, its just that the image has been normalized by the software, so the brightest value is totally white, while the darkest is totally black. This can be somewhat misleading, as it's not the same in Figure 46. Section 3.5.3 will give a qualitative insight into the actual intensity distributions in these images.

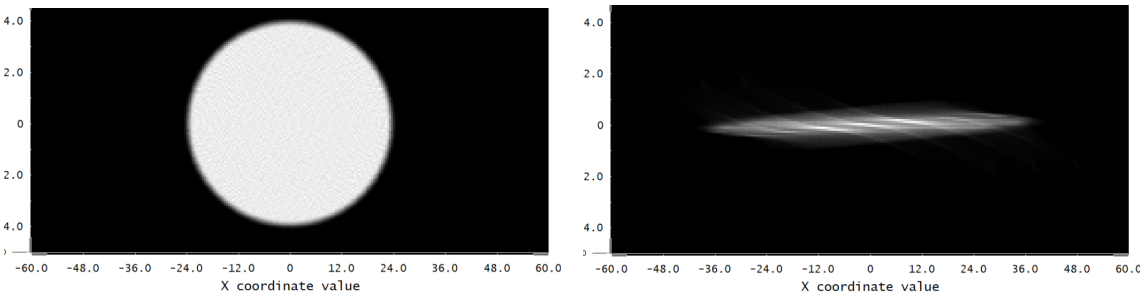

(a) Simulation without lenses

(b) Simulation with lenses

Figure 47: The simulated result corresponding to how the image should look like in a theoretically perfect model

3.5.3 Intensity plots and transmission

This section showcases the intensity plots derived from the image analysis. Two different plots will be presented, one illustrates how the Etendue lenses intensify light compared to without the lenses. This plot will be referred to as the intensity plot. Additionally, an enclosed intensity plot will compare the different lens configurations and how much of the light that's actually hitting the focal tube, in addition to how much light is transmitted through the lenses.

The section begins by presenting the simulation plot, depicting the ideal behavior of the physical lenses. The simulation was carried out only at one solar zenith angle, namely 0°. Consequently, the plots for 11.75° and 23.5° doesn't have the same ideal comparison reference. After presenting the simulated results, the physical results are presented. when reading the plots, don't give too much thought to the units on the x-axis, just imagine that it's a relative measure of intensity, and can not be compared between plots. The y-axis represents the focal plane of the optical jig and is measured in millimeters.

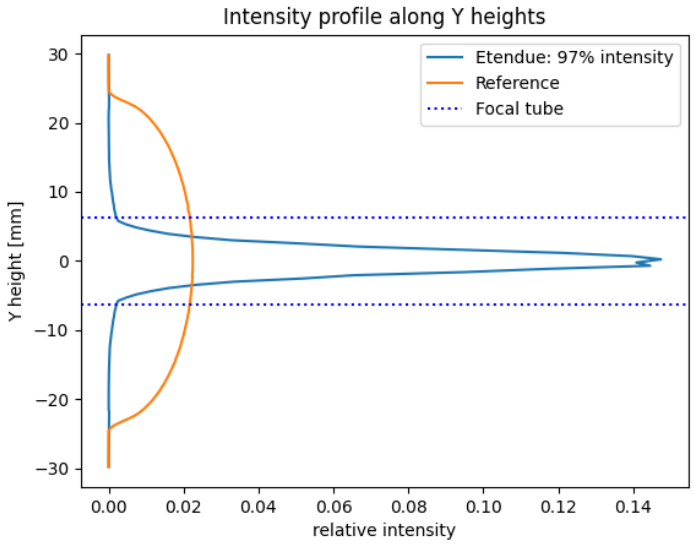

Figure 48: Simulated intensity profile at 0°zenith angle

Figure 48 provides an illustration of the intensity distribution from the simulated ray-traced image in Figure 47. It showcases the overall profile for both the reference light(no lens) and the lenses. The x-axis in 48 shows the arithmetic intensity at each height of the image. The focal tube lines illustrate the diameter of the focal tube, all light between 0 on the x-axis and Etendue graph not between the focal tube lines is lost light. The focal tube in all the presented data have a diameter of 12.45mm in this research. Observing the legend in Figure 48 there is a percentage, this indicates that 97% of the light the etendue lenses concentrate hits the focal tube, meaning 3% of the light that passes through the lenses will miss the focal tube. A key take out from the x-axis is the relative difference between peak value of the Reference graph and the Etendue graph. Which is about 0.02 for the reference, and 0.15 for etendue, meaning its 7.5 times brighter. This is not a direct measure of the light concentration, but it implies that the arithmetic sum of intensities in each row of the image would be 7.5x bigger. This value is the peak optical concentration and not a geometrical concentration. The geometrical concentration intensification of the lenses will be presented with the enclosed intensity plot, later in this section.

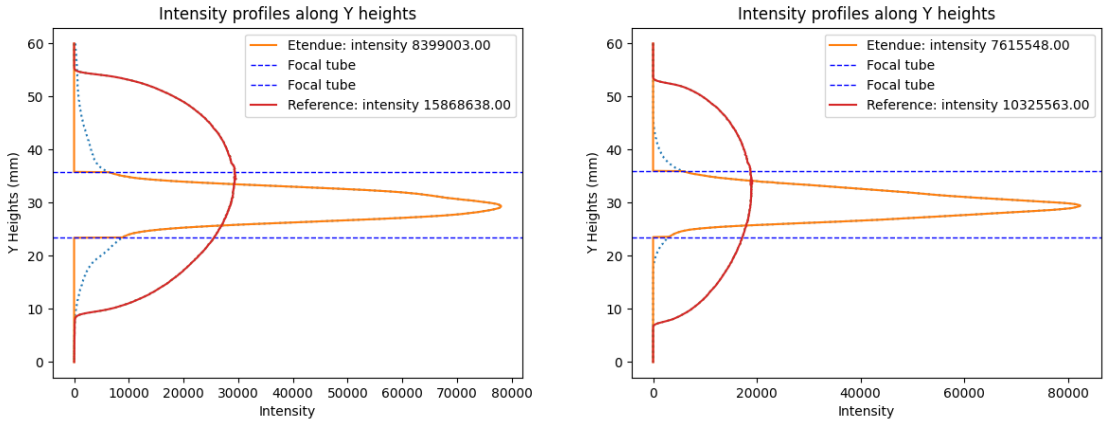

(a) 3D Printed lens

(b) 15 and i press-formed lens

Figure 49: Intensity profile of the manufactured lenses, at 0°solar zenith angle

Figure 49 showcases the intensity plots from the physical parts after the data has been extracted from the raw data of the images. Observe that the relative distance between the peak x-values of Reference graph and Etendue graph in the two plots Figure 49a and 49b. In addition its important to note the narrower profile of the etendue graph in 49b than 49a. The next graphs presented is the same plots, but at solar Zenith angle of 11.75°and 23.5°.

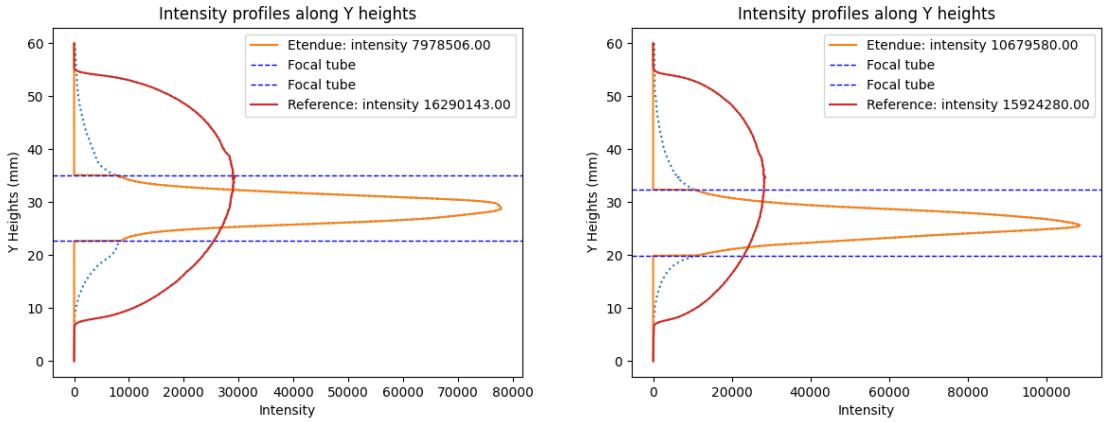

(a) 3D Printed lens

(b) 15 and i press-formed lens

Figure 50: Intensity profile of the manufactured lenses, at 11.75°solar zenith angle

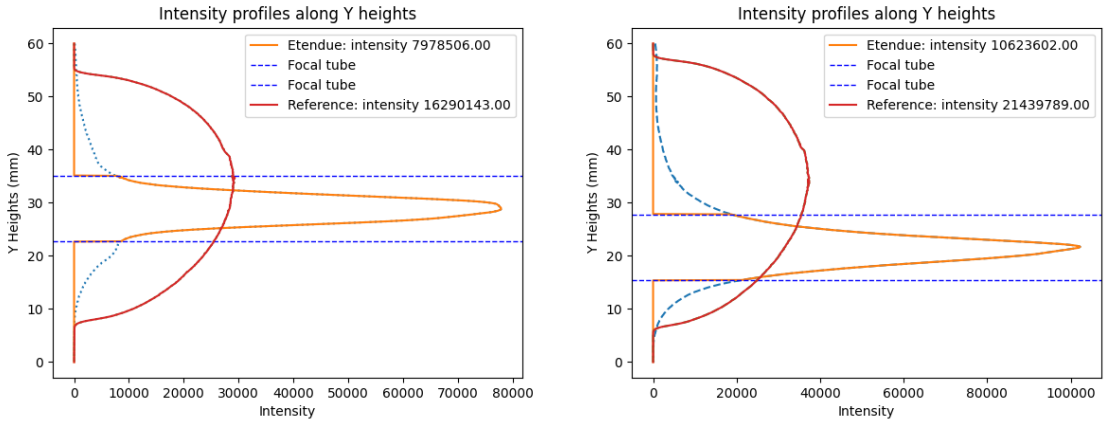

(a) 3D Printed lens

(b) 15 and i press-formed lens

Figure 51: Intensity profile of the manufacture lenses, at 23.5°solar zenith angle

Notice how the Etendue graph in 51b is slightly shifted down from the center compared to the reference graph. This shift leads to an increase in Fresnel reflections on the lenses, consequently giving falsely pessimistic data. The reason for this shift is discussed in chapter 4. The result of this misalignment will also affect the corresponding plot in Figure 52.

The preceding Figures, have provided an insight into the behavior of each lens configuration as an individual assembly. The subsequent Figure 52 depicts how each lens configuration behaves compared to one another. More precise, each lens configuration, the press-formed, 3D printed and the simulation is showcased. This includes their corresponding graphs, both in terms of how they act depending on solar zenith angle, and how they compare to the reference light and a perfect simulated virtual model. The simulated data is only for 0°solar zenith angle and does not apply for 11.75°and 23.5°.

Figure 52 presents a significant amount of data, and can be considered one of the key findings in this research. The dashed Reference line illustrated in the legend presents the round circular reference light that's been observed previously. This line provides the amount of light for the system as a whole, therefore touching the 100% line on the y-axis. The dashed Simulation line represents how the lenses act in a virtual ray-traced simulated model, note that it peaks at about 81%, implying that the rest of the light is lost to Fresnel Reflection. For comparison, two flat glass plates would lose about 85% light. However, due to the geometry in this system, a greater amount is lost upon incidence on each surface. This is due to the angle of incidence of the light rays, is not perpendicular to the surface. Additionally, the legend states a percentage, (79%), representing the amount of light in the system hitting the focal tube. The focal tube line represents the width of the focal tube, and the location on the y-axis of where each graph incidence this line, gives how much light that hits the focal tube, this number corresponds to the percentages in the legend for each graph. Lastly, the "°s̈ymbol in the legend tells which solar Zenith angle each graph corresponds to. Implying that each graph is a result of an individual image analysis.

Now that the plot and its virtual lines have been explained, the performance of the manufactured lenses should be presented. We observe that the best-performing line is 15i. The "15" and "i" means that the inner lens used is specimen 15 and the outer is specimen i. Notice how the graph has miminal growth after passing the focal tube line, meaning the lenses have focused most of the transmitted light onto the focal tube. Another key observation is how the 3D printed lenses have quite similar behaviour until about 35% flux. These observations will be further discussed in Chapter 4. As mentioned previously lens configuration 15i at 23.5° had a shift between the etendue line and reference line in Figure 51b. Observe how the line in Figure 52 stops somewhat sooner than the others in this Figure as well.

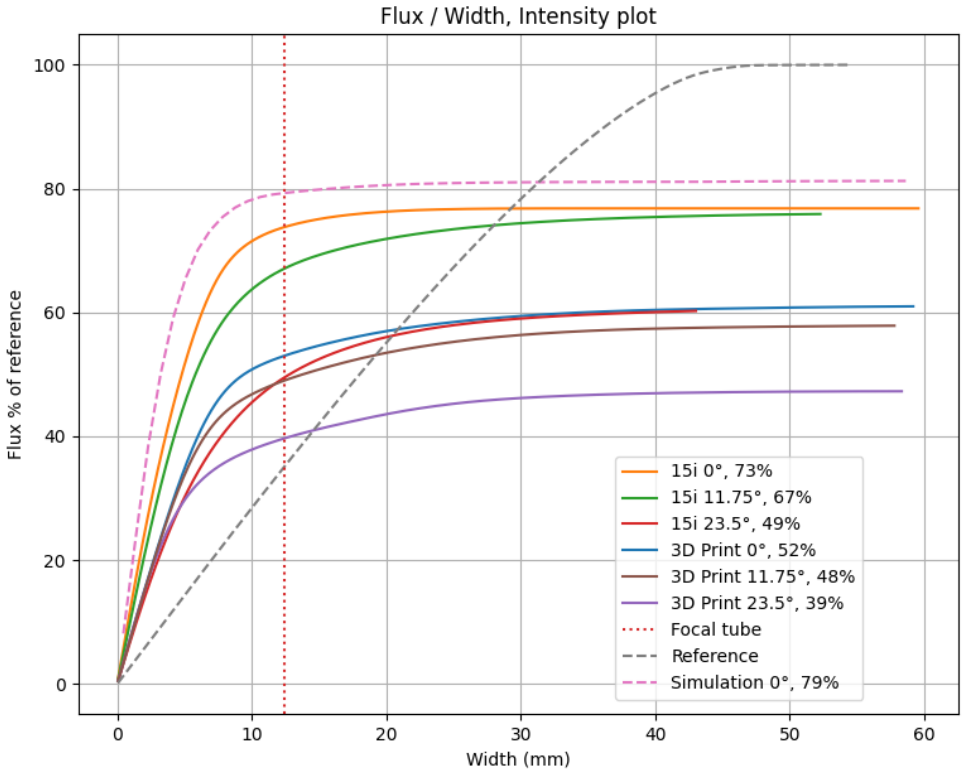

Figure 52: Enclosed intensity plot of the 3D printed and pressformed lenses, refered to as 15i. The left of the vertical focal tube illustrates light hitting the tube. The percentages are how much light that is hitting inside the focal area.

4 Discussion

In this research, we investigate two distinct approaches to rapid prototyping. The first involves manufacturing a part directly, while the second employs additive manufacturing to manufacture negatives of the lenses, subsequently press-forming the actual geometry. This chapter introduces the findings from the preceding chapter, followed by an in-depth interpretation and discussion of the contributing factors for each result. It further explores the limitations of the methodologies employed throughout the research and proposes areas for future study. The chapter concludes with a conclusion and reflections on the discussions presented.

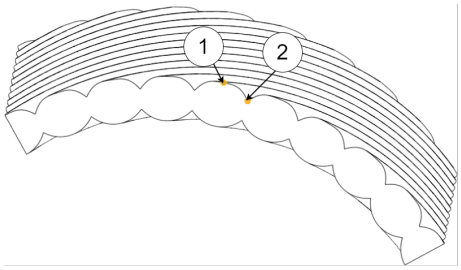

Figure 53: (1) Hill top, (2) Valley bottom

Throughout this chapter, there will be a detailed examination of the shape of the lenses. For the sake of simplicity, Figure 53 illustrates some reference terms. The observed inwardly curved sections will be referred to as valleys. Meanwhile, the outwardly shaped portion will be referred to as hills.

4.1 Interpretation and explanation of findings

This section delves into the findings presented in the preceding Result chapter. Each data-gathering method is discussed in its own subsection, providing an in-depth analysis of the findings.

4.1.1 Visual inspection

The inner press-formed lens(Lens 15) exhibits a certain degree of waviness, characterized by a glossy surface interrupted by valleys and irregularities. Observe Figure 28a in the Result chapter for reference. The waviness pattern resembles the layer stepping in the 3D-print punches. Indicating that the lens copies more of the mold surface than desirable. Implying that the punches should be treated to exhibit a smoother surface. Moreover, the valleys in the lens geometry, which undergo the most deformation during the press-forming operations, display a rough texture. Indicating degraded surface texture, additionally, there might be degradation within the material if high rates of deformation are exerted in localized points.

The outer press-formed lens (Lens i) exhibits a smoother observed surface on the waviness scale than Lens 15, the surface is glossy, indicating minimal scattering and roughness. However, some layer stepping can also be observed on this surface, though it's less pronounced than on the inner lens. This finding might be related to the less aggressive geometry on the outer lenses than the inner. Implying less deformation and pressure is needed to form the part into the desired shape. Observe Figure 29a for reference.

The 3D printed lenses have a noticeable darkening effect on the background, suggesting less light travels directly through the material, implying more volume scattering and volume absorption than on the press-formed lenses. The glossy surface finish suggests minimal roughness. Keep in mind that a rough surface gives a matt look. Upon examining the surface with the touch of the hand, minimal waviness is exhibited. The surface feels smooth with minimal irregularities. Looking through the lens, one can observe layer-stepping within the part, indicating irregularities below the coating. For reference, observe Figure 28 and 29. This layer stepping within the part itself might be related to the coating applied to them, either the coating hasn't successfully bonded to the whole surface, resulting in light rays not being transmitted directly through the coating to the 3D print material. Another explanation could be different indexes of refraction for the coating and the 3D print material. Ergo, the surface coating will not exhibit the exact same optical property as the part, and some deficiencies on the surface of the core material will still be visible through the coating. A perfect sanding and polishing procedure would remove these deficiencies as a result

of the layer lines being removed from the part completely.

Observing Figure 30 there's a comparison between the two lenses manufactured with the same parameters, with the exception of liquid cooling. As observed on lens 16 in Figure 30b, the lens press-formed without cooling, one observes a haze in the specimen. It's hard to distinguish if it's a surface feature or inside the material. This might indicate degradation of the material due to heat, and the cooling of lens 15 assisted in stabilizing the material, preventing the degradation. To further investigate the reason why, one would need more tests to quantify the data. No other lenses were produced at 200℃ like these ones. Early experiments revealed that this temperature is close to the degradation temperature of the material. The test was conducted with such high temp, in an attempt to exaggerate the effect of non-isothermal molding.

4.1.2 Stylus profilometer

A stylus profilometer capable of measuring $Ra \geq 0.01\mu m$ roughness was used to inspect the surfaces. See chapter 2.3.1 and table 2 for reference. In this subsection, the findings of these measurements are discussed.

Some of the highlighted lenses exhibit surface roughness in the minimal range of the stylus profilometer. From the lenses presented in the visual inspection(chapter 3.2 and later the image analysis(chapter 3.5, the outer surface of the outer 3D printed Lens exhibits the best roughness value. Measured to 0.09µm, implying roughness in the range of 90nm, which is still not a perfect optical surface, but in the upper range of acceptable optics, especially for non-imaging optics. While identifying the exact reason why the polished and coated 3D printed lenses don't perform even better, possible factors should be mentioned. The lenses are spray painted, which can result in surface roughness if each layer isn't applied with the correct thickness due to the coating not being able to use surface tension to smooth the surface. Other contributing factors in the coating process are: temperature, correct mixture, and application techniques.

The uncoated 3D prints have a really rough surface, in the range of 30 to 60µm Ra, indicating the surface treatment techniques underdone by the professional manufacturer have successfully reduced the roughness to an acceptable level.

Observing press-formed lenses, we notice the lenses that successfully recreated the desired form of the surface, exhibits a higher roughness value than the lenses with the correct form. Implying that the lenses, with exceptional roughness, haven't successfully copied the geometry of the form. Suggesting it may be difficult to achieve a smooth surface when using 3D printed punches in the press-molding process without any post-processing, especially if a specular surface is desired. An effective measure to reduce the waviness and roughness of the punches could be different sanding techniques.

As detailed in Section 3.3.1, observing Table 2, there is a minor distinction in surface roughness between Lens 16(press-formed without cooling) and Lens 15(press-formed with cooling). Indicating that lens 15 has a slightly lower roughness than 16. Keep in mind that both lenses are manufactured with identical parameters, except for with and without liquid cooling. The results are cross-checked by measuring different locations on the lens ranging:

- Lens 15 outer surface, Ra: 0.82 to 1.4 µm
- Lens 16 outer surface, Ra: 0.99 to 1.65 µm
- Lens 15 inner surface, Ra: 0.03 to 0.17 µm
- Lens 16 inner surface, Ra: 0.17 to 0.43 µm

Measured in 4 different locations on both the inner and outer surface, where each lens is measured in the same spot. The slight improvement in Lens 15 might suggest the influence of liquid cooling. However the overlap in the roughness range between the two lenses complicates this interpretation. Consequently, it's not definitive that liquid cooling contributes to reducing the surface roughness of the specimen.

4.1.3 3D mapping

Using a Infinite Focus Microscope, yielding a virtual representation of the physical part, the model is compared to the virtual model in software. The software calculates both distance deviation and angle deviation. In this subsection, the data gathered from the 3D mapping is discussed.

As previously noted, the 3D printed scans originate from the untreated 3D printed lenses, meaning the actual optically clear 3D printed lenses may have a slightly different form due to polishing and clear coating. Observing the Rz value of the untreated 3D prints in Table 2 we have the values 32.73µm and 45.47µm on the outer surfaces. This represents the measurement's max value between the lowest valley and the highest peak. The sampling length of the measurement is 2.5mm. When inputting an equal length traveled line in our cad software on the outer lens, this sample length on a smooth surface will account for a Rz value of $\geq$ 10µm. Consequently we have to subtract this measurement from the Rz value 45.47µmeter, resulting in a Rz value of approximately 35µm. This number indicates the minimal surface deformation the surface must undergo to reach an optically specular surface. Implying that the polishing and clear-coating will have at least this thickness. For reference, an automotive clearcoat usually ranges from 35-50µm [44]. With this in mind, we can assume that the treated surface deviates from the untreated surface $\leq$ 100 µm = $0.1mm$ given that it is both polished and clear coated, as a conservative estimate. The sanding and polishing will remove material, while the clear coating will add material, meaning the two processes kind of cancel each other out. Though it's important to note that the form of the lens can be affected differently across the shape. Meaning the post-processing isn't necessarily uniform.

Observing the 3D printed lenses, we observe minimal deviation from the virtual model, The 3D printed lenses in Figures 34, 36 and 39 all displays some deviation in the bottom of the valleys, but generally well below 0.15mm, and generally below 0.05mm. Meanwhile the press-formed lenses observed in Figure 33, 35, 37, and 38, with their respectively general deviation ≤ 0.15, ≤ 0.9, ≤ 0.2 and ≤ 0.26 observed from the histogram. One can argue that the 3D printed lenses have a superior form compared to the press-formed lenses.

Observing Figure 37 we notice that the outer parts of the map have a more significant distance deviation than the middle section. This might be due to inaccurate alignment between the virtual model and the physical scan within Meshlab. More explicitly, the surfaces could be slightly rotated relative to each other, creating a systematic error. This error will be propagated to the angle deviation plot in Figure 40a. As one can observe that the valleys of the scanned plot seems further apart than the virtual model.

Figure 38 demonstrates a key finding in this research. Noted in the previous chapter, the distance deviation on the top of hills in the scan have a greater deviation than in the valleys. The yellow color illustrates a deviation of 0.25mm, systematically on the top of the hills. Noting Lens vii row in Table 2 we observe minimal roughness on this portion of the part(Ra=0.01µm). This was found to be related to the PMMA not properly filling the press, or at least not copying the surface texture, reading Table 1 we observe that 400kg of force was used to create the lens, significantly less than Lens i which was manufacture with 750kg of force. As a result this deviation in distance, can also be observed in the angle deviation graphs for vii in Figure 40b. In comparison Lens i seems to have a more accurate form on top of the hills, based on Figure 40a and 37.

Although the angle deviation graphs provide some data on the surfaces, they are somewhat limited. However, the outer lens's outer surface is well-represented in the graph. Observing Figure 40 we notice that the distance deviation noted in the previous chapter is illustrated in 40b. The Virtual surface and the Scanned surface illustrate how the top of the hills in lens vii, have unsuccessfully replicated the virtual model. The 3D printed parts have recreated the angles to a higher degree, with exception of in the bottom of the valleys, as observed in Figure 40c. The angle deviation illustrated in the bottom of the valleys, might be due to slight misalignment in the measuring software. Additionally a portion of the bottom of the lens is not utilized for etendue rotating. Keep in mind that 3% of the light transmitted through the lens, will miss the focal tube, and the area in the bottom of the valleys makes up a portion of this.

Figure 40a suggests that there might be an alignment error in the comparison between the virtual and scanned part of Lens i, as observed in Figure 37. We observe that the virtual and scanned line

deviates from each other in the valleys. The scanned surface seems kind of stretched compared to the virtual model, this could be explained by a relative rotation between the two parts in the comparison software.

4.1.4 Image analysis

An image analysis purpose-built to resemble how light from the outer edge of the trough mirror behaves in the systems is carried out. The rationale for mimicking the light traveling from the boundary of the trough is that it gives the worst-case scenario for light in the system. consequently, light traveling from other locations on the trough mirror would result in increased performance of the lenses.

Observing the overview images in chapter 3.5.1 we observe that the 3D printed lenses exhibit systematic scattering lines. Implying that the scattering originates from a systematic error. Meanwhile, the press-formed lenses mostly demonstrate diffuse scattering, without the systematic lines. The systematic scattering might be due to the waviness lines inside the part as discussed earlier, while the diffuse scattering could be a result of surface roughness and volume scattering inside the material. Observe Figure 43 for a pronounced demonstration of the effect. Comparing these scatter lines to the press-formed lenses, it's hard to argue for the same systematic scattering. Observing Figure 47 illustrating the simulated image, we notice systematic lines in the image, implying that the lines observed in 43a might inhibit the same effect. Though the simulated image doesn't present the line-scattering over such a large area on the focal plane.

In addition to the scattering lines, we observe some light accumulation on top and bottom of the focal paper in Figure 43a, outside our area of interest. This effect is not as pronounced on the press-formed lenses. Even though some of the same effects can be observed for the Press-formed lenses in Figure 44b, an explanation for this might be that the system is optimized for 1.5°divergence angle light, while in reality it's tested with 1.64° divergence angle.

A key observation within the intensity plots is the slight variation some of the Reference graphs inhibit. The Reference graph should be symmetrical in the vertical axis. This might be caused by a slight tilt of the lens jig focal plane or a uneven focal plane. The defect is clearly illustrated in Figures 44a and 45b.

In addition to the asymmetrical reference graph, we observe that some of the etendue graphs are shifted downwards from the center of the reference graph. Clearly observed in 45b, this is most lightly due to slight misalignment of the lenses in the optical jig. The light and the height of the jig were set to fixed heights. So the light is emitted to the center of the image, as observed by the reference plots. In one of the earliest image analyses in the jig, this error was prone in a set of measurements. The tests were redone later. In the redone test, the measurements had a performance increase of up to 4% measured in how much light hit the focal tube. Consequently one can assume that the 23.5° graph of 15i in Figure 52 would have had a performance increase similar to this if the misalignment was fixed.

Observing the enclosed intensity plot in Figure 52, one notices that neither the press-formed lenses nor the 3D printed lenses behave identically to the simulation. This is to be expected, but in theory, a perfectly manufactured PMMA lens would behave as the simulation graph.

Another key finding from the intensity plot is the press-formed lenses' superior performance compared to the 3D printed lenses. Based on the distance deviation and roughness measurements, we can assume that the 3D printed lenses inhibit better surface quality than the press-formed ones. As noted in the methodology, surface quality includes roughness, waviness and form. Consequently, we can argue that the inferior performance of the 3D printed lens is a result of volume scattering and absorption within the 3D printed material.

4.2 Limitations

This chapter presents the limitations of the study. The chapter is sectioned in chronological order, following the lifecycle of the project. Starting with the optimization of the virtual model, continuing with the design of the press mold, followed by the process of manufacturing the presses and prototypes, and finally the data-gathering processes.

4.2.1 Optimizing the lens geometry

The software for optimizing the etendue rotator geometry is outside the scope of this project. But it's still important to outline the limitations of the optimization conducted for creating the geometry for this project. As mentioned in chapter 2.2.1, the different acceptance angles give different concentration ratios for the etendue rotator. The optimization is computed without Fresnel reflection in mind, meaning the lens geometry is optimized for having an anti-reflection coating on the lens surfaces. If the lenses were optimized with the Fresnel Reflection parameter, the lenses would most lightly have had a less aggressive geometry, thereby reducing the Fresnel reflection. Even though this gives slightly more pessimistic data than we might have achieved, it would most likely not have changed the performance gap between the press-formed and 3D-printed lenses. As mentioned earlier in the best-case-scenario we would have had at least $100\% - 85\% = 15\%$ Fresnel reflection, compared to the simulated $100\% - 81\% = 19\%$ transmittance, meaning that we might have reduced the reflection slightly, but not significantly. The assumption that the performance gap between the press-formed and 3D-printed lenses would remain unchanged is due to material properties. The research have indicated that the 3D-printed lenses exhibit superior surface quality in terms of form, waviness and roughness. Suggesting the parameter resulting in inferior performance can be attributed to within the material, specifically volume scattering and volume absorption.

4.2.2 Press-forming

This subsection highlights the drawbacks and limitations of the press-forming process. Some additional thoughts regarding design and engineering related to the mold are also discussed.

Heating, A lab oven is used to heat the PMMA blanks before press-forming them. An infrared thermometer is employed to measure the temperature of the specimens. The oven was preheated to a temperature about 20℃ above the desired PMMA temperature. The thermometer has fixed emissivity and can not be adjusted to compensate for the specific emissivity of PMMA at the wavelength of the thermometer. This might lead to some deviation between the actual surface temperature and the measured temperature. The assumption of this being a viable technique for measuring is the low transmittance of IR radiation in PMMA. The time in the oven was also slightly varying, ranging from 15 to 20 minutes in the oven, waiting for the PMMA to reach the desired temperature. Observing Figure 10a we observe that the core temperature in the PMMA should be around approximately 200℃ after 10 minutes, if the surface maintains a perfect heat transfer between air and surface and the oven is set to 200℃. Additionally, the PMMA blank is heated laying in the bottom of the oven, though the bottom of the oven is preheated, some variation in heat between the air in the oven and the bottom is to be expected.

Pressing **operation**

The FDM printed mold has guides to assist in closing the mold properly, though these guides have some play, meaning they can slightly rotate relative to each other. In addition, they have built-in stops when the PMMA is pressed to its desired thickness. The end-stops can be slightly mispositioned due to inaccuracies in the 3D print. Consequently, the surfaces are not exactly at their desired position. These two factors can create a misalignment between the two surfaces of the lens. Meaning the surfaces can slightly deviate relative to each other's intended position.

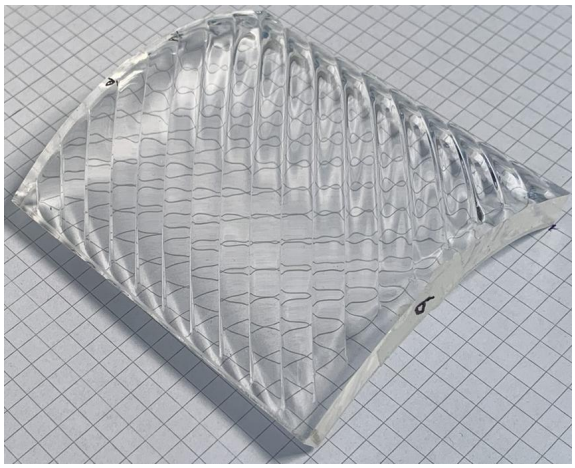

Figure 54: Lens 6, failed due to it shifting out of position in the mold. Observe the insufficient deformation of geometry in the closest section of the surface

In addition to inaccuracies in the printed molds, the PMMA blank is positioned inside the press before the whole mold assembly is transferred into the press. During this process, the PMMA blank can shift out of its intended position. The shift of this position can result in more force being exerted on one side of the press than the other, meaning the PMMA blank will have different forming pressures from one side of the mold to the other. The press forming tools are designed to have symmetrical force from two parallel surfaces, meaning that an asymmetry in the placement of the PMMA blank can result in slightly different results from one side to the other of the lenses. Figure 54 illustrates an inner lens that has shifted during press-forming, which resulted in an uneven geometry across the lens.

Additionally, the first iteration of the hydraulic press setup uses two wooden pieces with an aluminum plate on each side to distribute force and reach the desired opening of the press. This wooden piece will not be perfectly parallel and can introduce imbalanced force in the press. The later iteration of the setup used two nylon bushings with bolted-on aluminum plates to ensure parallel movement and rigidity. Lens i which is extensively documented in the Results Chapter 3, is manufactured with the wood solution, while lens 15 is manufactured with the upgraded solution. Observe Figure 12 for reference.

The force applied in the press is generated from a hydraulic hand pump. Which in turn drives the piston in the press. This operation requires manual effort- specifically, cranking the handle until the desired displacement or force is achieved. Mastering the precise application of force requires considerable practice, and it's easy to overshoot the desired force during press operation. Moreover, the force tends to decrease until the PMMA has cooled down and reached its desired shape. The force will decrease rapidly while the PMMA is hot, and decelerate with the temperature decrease in the PMMA. To counter this creep, one must continually adjust the force exerted by cranking the lever on the press. As a result, all of the stated forces in the result chapter have a deviation of $\pm 40kg$. Varying cyclic with the time the Lens is being pressed. A simple solution to this issue is to utilize an adjustable pressure valve to ensure that the intended amount of force is not surpassed.

4.2.3 Evaluating the samples

Stylus profilometer, The stylus profilometer is used to give an indication of the roughness of the surface, some results yielded its minimum measuring range. Indicating a quite impressive surface roughness. Though these results are not completely accurate, the stylus tip radi is 2µm, and the measured value of 0.01µm indicates minimal surface roughness, but all imperfections in a surface where a 2µm radi could slide over will consequently not be measured by the apparatus. Moreover only the hill tops of the structures were measured. These areas undergo the least amount of deformation inside the mold, consequently, less surface pressure is exhibited on these sections. Implying that they don't replicate the surface imperfections of the 3D-print punch to the same

extent as in the valleys.

Alicona IFM variable focus microscopy measurement deviations The threshold for the microscope software had to be set below the recommended settings, due to the aggressive geometry and shiny surfaces on the lenses. This implies that the microscope will give more false data points, as observed in Chapter 3.4. The XY and Z-resolution for the images were set to $\leq 15\mu m$ for all the scans. Implying that all points on the surface less than this can be distinguished as separate points. With this in mind, the microscope can provide data points with a detail level of 15µm. Without directly converting this data to accuracy, we can argue that all the points that look correct should be inside a range of $\pm$ 50µm. This is the assumption, that is provided in Section 3.4.1. With this threshold of accuracy in mind, the 3D print scans are the only ones where this accuracy is relevant in the histogram. Due to the accuracy indicated in the histograms. Consequently, the numbers aren't used quantitively to assert accuracy in this research, only to give indications as to which method recreated the virtual lenses best.

An additional element of uncertainty is related to data manipulation. To be able to handle the large datasets provided in the microscope, each point in the point cloud provided by the microscope was exported so that one triangle in the STL meshes corresponds to 4 points in the cloud, further introducing measurement uncertainty. Consecutively the mesh data is compared in Mashlab, where imperfect alignment of the two meshes may induce slight measurement deviations.

The angle deviation plots presented in the 3 are calculated by comparing two slopes of the graphs to each other in each data point. Consequently, the data is quite sensitive to changes in the geometry, as it only considers two data points and not a local average for creating the slopes. Accordingly, the data presented might be slightly exaggerated. A sliding window technique for comparing multiple data points to create a local average is implemented, but it is hard to tune correctly. So the presented plots are presented without.

4.2.4 Improved results from experience

Craftsmanship is important in all research, no matter which stage of academia or trade one belongs. Whether one is crafting reports, painting cars, soldering connections, building houses, or etc., there will be some degree of craftsmanship. In this research, a key motivation is to introduce as little physical craftsmanship as possible in the press-forming process. The primary reason for this is the introduction of an uncertainty parameter, which is difficult to document, making it challenging to repeat the process in the future. Consequently, some surface treatments weren't explored. A treatment discarded in an early stage of the project is sanding or matting the surface of the punch. Hence the data gathered from such a process haven't been collected.

4.2.5 Additional considerations and relevant measuring techniques

The form of the surfaces is compared in the 3D-mapping procedure. Another relevant measurement would be to measure the two surface positions relative to each other. As a first step in this process, one could measure the thickness of the lens at different locations with a caliper or micrometer. This would give an indication of how well the press-forming process is successful in creating the correct thickness between the surfaces of the lenses. A more advanced technique could have been simulating the image of each lens of the Etendue rotator individually, and comparing it to a ray-traced simulation image. A third relevant examination could have been more advanced 3D-scanning to obtain a virtual model of the physical part and compare it similar to what's been carried out in this research.

4.3 Implications

This section aims to explore the potential broader impacts of our research findings. Specifically focusing on the value of a simple prototyping technique for non-imaging optics. The results presented in the image analysis demonstrate significantly better results than the 3D-print reference, despite

some challenges in surface quality. As an alternative to direct 3D printing, the process demonstrates promising results, especially in a rapid prototyping environment. In a wider scope, the process is valuable for researchers, engineers, or designers trying to create a prototype of a non-imaging optics system. The press-forming process is an easy and adaptable technique, capable of creating multiple geometries.

4.4 Future Research

This section identifies areas for future study. The section outlines areas for continued study based on findings in the results and observations through the project.

From the beginning of the project, one goal has been to investigate a process easy to replicate with a minimal amount of variables. Meaning that variables that are hard to control or replicate have been excluded. One of these variables is craftsmanship, there is a minimal amount of craftmanship and manual labor in this thesis. During the early stages of the project, it was identified that surface-treating the mold before press-forming or post-processing the PMMA would have the potential of removing the roughness and waviness we observed in the lenses. This process would have introduced quite a lot of craftsmanship into the product, polishing, clear coating or sanding are all processes that yield improved results with experience. This is a variable hard to control or document, but in future research, a matting of the layer stepping in the SLA printed punch, would have the potential of removing the waviness observed in the results. Additionally, the non-isothermal process, which demonstrated little potential here, might have shown a lot of potential in a smoother mold. During the project's initial phase, we hypothesized that by cooling the form, we could eliminate the layer stepping. Specifically by cooling the surface rapidly, the surface tension of the PMMA would hinder the recreation of the small irregularities in the punch. It appears that this effect was not observed. One hypothesis is that although non-isothermal molding may eliminate small-scale irregularities in the roughness spectrum, the waviness of the layer lines may be on too large of a size scale to be affected. Thus an interesting study would have been to sand the layer stepping and use different sanding grits to reach different roughnesses and compare the result of the roughnesses of the differently sanded surfaces.

This study recreates a section of the whole etendue rotator and not the whole lens assembly. An interesting study would have been a rotational extrusion-like 3D-printed tool, in the High Temp material like the punches in this research. The extrusion process could have utilized a flat PMMA plate pushed through a spiral forming tool to recreate the lens configuration of the etendue rotator. This would have been a much more advanced setup, but the punches utilized in this research demonstrated no visible degradation due to heat.

This research utilized minimal CFD or FEA software to calculate dimensions, heat, and force, as a consequence of a rapid prototyping approach and limited time span. Though there are multiple suitable solutions for this type of calculation. A more detailed heat- and material flow simulation would be valuable to correctly perform the press-forming process and tooling design. Potentially leading to better surface quality and optical performance.

This 1-dimensional press-forming process certainly limits the possible geometries one can produce. The 90° part, which is manufactured in this project is only a section of the actual geometry. This would mean that press-forming the whole geometry in one batch would need a different approach to the press-forming process. Some companies specialize in soluble printed parts. Designed to be used as molds in an injection molding process. A negative of a part is printed as a mold, the material is injected into the mold. Then the mold is dissolved revealing the desired geometry. One of the companies branding this technology is Nexa3D and xMOLD [45], with a special resin and production line for this application. This would enable the production of complex geometries like the free-form lenses in this project. Though one would likely struggle with the surface quality of the PMMA, due to the strict optical surface quality demands.

In addition to the mentioned surface treatment of the punches, an alternative would be to surface-treat the press-formed PMMA lenses. This treatment could have been in the form of laser-, flame- or mechanical polishing. Additionally one could coat the PMMA parts, possibly with an anti-

reflection coating, reducing the Fresnel reflection. A purely utilitarian consideration would be the effort between sanding the punches or polishing the lenses. Given the hard-to-reach valleys in the geometry of the lenses, sanding the punches seems easier.

4.5 Concluding the discussion

This chapter has outlined and discussed the findings from the Result chapter. The visual inspection found a darkening effect of the 3D printed lenses, in addition to the internal waviness of the part. Hypothesized to be related to different indexes of refraction in the coating material and core material. Additionally, the press-formed lenses that demonstrated the best form, had adopted waviness from the punches in the press-forming process. Implying that further processing of the punches is necessary to exhibit a quality optical surface. The image analysis revealed some shifting in the test jig, yielding pessimistic data in some of the results. Though the image analysis indicated significantly better performance of the press-formed lenses than the directly 3D printed ones, the surface quality of the press-formed lenses was sub-par compared to production-grade optics.

5 Conclusion

This research explores an alternative approach to directly 3D printing a non-imaging optical prototype. By utilizing commercially available 3D-printing technology and simple tools, the research presents a press-forming procedure designed to press-form PMMA into a desired shape. The research is motivated by a concept named Etendue Rotating, utilizing two lenses to increase the efficiency of a solar trough.

The research spans a range of evaluation techniques for assessing the manufactured lenses. A stylus profilometer was utilized to indicate surface roughness. Indicating that the polished and coated 3D-printed lenses had superior roughness compared to the press-formed ones. A variable focus microscope was utilized to create a point cloud that was later compared to a virtual model in software. Finding the 3D-printed lenses to demonstrate better form recreation of the virtual model, than the press-formed ones. Additionally, a purpose-built optical test jig was manufactured, designed to emulate the behavior of light in a solar trough. Image analysis was used to compare the lenses in the jig, uncovering that the press-formed PMMA lenses significantly outperformed the directly 3D-printed ones. The superior performance of the lenses is assumed to be related to volume scattering and volume absorption in the 3D print material.

A limitation worth noting in the research pertains to the measurement of the relative positioning of each surface side of the lens. While individual analysis of the two surfaces is conducted, no explicit measurement of how precise the surfaces are positioned relative to each other is performed. This is an important aspect to consider, as it gauges how well the press-forming process performs, in terms of recreating the desired shape.

Multiple findings worth further research are uncovered. The press-forming process employed in this study doesn't post-process the 3D-printed tooling surfaces after curing at all. Due to the waviness and roughness found in the press-formed lenses, an interesting future project would be to smooth the layer stepping in the 3D-printed mold. A liquid-cooled press was utilized in this research to try and minimize the roughness of the surface, but the results were ambiguous. If the punch employed in the press-formed process exhibited less waviness, this technique might yield better results, leading to less waviness and roughness in the manufactured lenses.

In conclusion, this research has successfully demonstrated a novel approach to prototyping non-imaging lens prototypes. Highlighting the promising potential of the press-forming procedure. The study has revealed certain limitations pertaining to the measurement of the lens surfaces in relation to one another. Additionally, it has uncovered possible areas of study to further enhance the press-forming process. Despite the limitations and areas for future exploration, the superior performance of the press-formed lenses in an emulated solar trough environment, underscores the potential of this prototyping technique.

Bibliography

[1] *Nonimaging Optics*. In: *Wikipedia*. 7th Nov. 2022. URL: https://en.wikipedia.org/w/index.php?title=Nonimaging_optics&oldid=1120494611 (visited on 20/05/2023).

[2] *Parabolic Trough*. In: *Wikipedia*. 15th June 2023. URL: https://en.wikipedia.org/w/index.php?title=Parabolic_trough&oldid=1160286326 (visited on 29/06/2023).

[3] *Parabolic Trough*. In: *Wikipedia*. 27th July 2022. URL: https://en.wikipedia.org/w/index.php?title=Parabolic_trough&oldid=1100703978 (visited on 20/05/2023).

[4] Derek Curry. *Stirling Energy Systems - Dish Stirling Engine [Found]*. 3rd Oct. 2005. URL: https://www.flickr.com/photos/derek_curry/49083646/ (visited on 29/06/2023).

[5] Håkon Jarand Dugstad Johnsen and Juan C. Miñano. 'In Search of a Sharper Line Focus: Rotating the Étendue'. In: *Nonimaging Optics: Efficient Design for Illumination and Solar Concentration XVIII*. Nonimaging Optics: Efficient Design for Illumination and Solar Concentration XVIII. Ed. by Lun Jiang, Roland Winston and R. John Koshel. San Diego, United States: SPIE, 3rd Oct. 2022, p. 5. ISBN: 978-1-5106-5424-2 978-1-5106-5425-9. DOI: 10.1117/12.2633358. URL: https://www.spiedigitallibrary.org/conference-proceedings-of-spie/12220/2633358/In-search-of-a-sharper-line-focus--Rotating-the/10.1117/12.2633358.full (visited on 20/05/2023).

[6] *Understanding Optical Specifications — Edmund Optics*. edmundoptics. URL: https://www.edmundoptics.com/knowledge-center/application-notes/optics/understanding-optical-specifications/ (visited on 21/05/2023).

[7] *Understanding Surface Roughness — Edmund Optics*. URL: https://www.edmundoptics.com/knowledge-center/application-notes/optics/understanding-surface-roughness/ (visited on 21/05/2023).

[8] *What Is Light Scattering and How Does It Work? — Synopsys*. URL: https://www.synopsys.com/glossary/what-is-light-scattering.html (visited on 21/05/2023).

[9] Addoptics. *Optics Material: Glass versus Polymers*. Addoptics. 25th Feb. 2021. URL: https://www.addoptics.com/optics-explained/optics-materials/ (visited on 28/02/2023).

[10] *Transmission Curves of Optics Materials*. GS Plastic Optics. URL: https://www.gsoptics.com/transmission-curves/ (visited on 21/05/2023).

[11] *Measurement of the Solar Constant*. URL: https://www2.pvlighthouse.com.au/resources/courses/altermatt/The%20Solar%20Spectrum/Measurement%20of%20the%20solar%20constant.aspx (visited on 23/05/2023).

[12] *The Direct Standard Spectrum (AM1-5d)*. URL: https://www2.pvlighthouse.com.au/resources/courses/altermatt/The%20Solar%20Spectrum/The%20direct%20standard%20spectrum%20(AM1-5d).aspx (visited on 23/05/2023).

[13] *Introduction to the Solar Spectrum Lecture*. URL: https://www2.pvlighthouse.com.au/resources/courses/altermatt/The%20Solar%20Spectrum/Introduction%20to%20the%20solar%20spectrum%20lecture.aspx (visited on 23/05/2023).

[14] *Fresnell's Equations: Reflection and Transmission*. URL: http://hyperphysics.phy-astr.gsu.edu/hbase/phyopt/freseq.html#c1 (visited on 03/06/2023).

[15] *Anti-Reflective Coating*. In: *Wikipedia*. 22nd Feb. 2023. URL: https://en.wikipedia.org/w/index.php?title=Anti-reflective_coating&oldid=1140961422 (visited on 29/06/2023).

[16] *Thin Film Coating for Optics*. GS Plastic Optics. URL: https://www.gsoptics.com/thin-film-coating/ (visited on 29/06/2023).

[17] Torger Holtsmark. *aberrasjon – optikk*. In: *Store norske leksikon*. 12th Jan. 2023. URL: https://snl.no/aberrasjon_-_optikk (visited on 14/06/2023).

[18] Frank L. Pedrotti, Leno Matthew Pedrotti and Leno S. Pedrotti. *Introduction to Optics*. 3rd ed. Cambridge: Cambridge university press, 2018. ISBN: 978-1-108-42826-2.

[19] Roland Winston, Juan C. Miñano and Pablo Benítez. '14 - MANUFACTURING TOLERANCES'. In: *Nonimaging Optics*. Ed. by Roland Winston, Juan C. Miñano and Pablo Benítez. Burlington: Academic Press, 1st Jan. 2005, pp. 395–413. ISBN: 978-0-12-759751-5. DOI: 10.1016/B978-012759751-5/50014-2. URL: https://www.sciencedirect.com/science/article/pii/B9780127597515500142 (visited on 16/06/2023).

[20] *Guide to Stereolithography (SLA) 3D Printing*. Formlabs. URL: https://formlabs.com/blog/ultimate-guide-to-stereolithography-sla-3d-printing/ (visited on 11/06/2023).

[21] *4 Ways LFS 3D Printing Produces Better Parts*. Formlabs. URL: https://formlabs.com/eu/blog/benefits-of-lfs-3d-printing/ (visited on 11/06/2023).

[22] *Two-Photon Polymerization*. Microlight3D. URL: https://www.microlight3d.com/technology/two-photon-polymerization (visited on 30/06/2023).

[23] Katie Schwertz. 'An Introduction to the Optics Manufacturing Process'. In: ().

[24] *Non-Isothermal Glass Molding - Fraunhofer IPT*. Fraunhofer Institute for Production Technology IPT. URL: https://www.ipt.fraunhofer.de/en/technologies/forming-casting/glass-molding/non-isothermal-glass-molding.html (visited on 21/05/2023).

[25] *What Is Design Thinking?* The Interaction Design Foundation. URL: https://www.interaction-design.org/literature/topics/design-thinking (visited on 29/05/2023).

[26] *What Is Rapid Prototyping? - Definition, Methods and Advantages*. URL: https://www.twi-global.com/technical-knowledge/faqs/faq-manufacturing-what-is-rapid-prototyping.aspx (visited on 30/05/2023).

[27] Parvathi Nair S et al. '3D Printing Mesoscale Optical Components with a Low-Cost Resin Printer Integrated with a Fiber-Optic Taper'. In: *ACS Photonics* 9.6 (15th June 2022), pp. 2024–2031. DOI: 10.1021/acsphotonics.2c00125. URL: https://doi.org/10.1021/acsphotonics.2c00125 (visited on 09/02/2023).

[28] Sandra Glynn. *Evaluating the Validity of Manufacturing 3D Printed Lenses: Using Commercial SLA Materials and Diamond Turning Processes*. 2020. ISBN: 9798607302559.

[29] Roger Angel et al. 'A Highly Efficient, Low-Cost Hybrid Module, Built on a Full-Size Bifacial Silicon Module'. In: ().

[30] Frederik Kotz et al. 'Liquid Glass: A Facile Soft Replication Method for Structuring Glass'. In: *Advanced Materials* 28.23 (June 2016), pp. 4646–4650. ISSN: 09359648. DOI: 10.1002/adma.201506089. URL: https://onlinelibrary.wiley.com/doi/10.1002/adma.201506089 (visited on 21/05/2023).

[31] Xin Su, director. *Liquid Glass: Casting Glass like Cement*. 23rd Feb. 2016. URL: https://www.youtube.com/watch?v=XsZL7zajgr0 (visited on 21/05/2023).

[32] *DLS 3D Printing Technology*. Carbon. URL: https://www.carbon3d.com/carbon-dls-technology (visited on 21/06/2023).

[33] *NanoOne – UpNano – High-Resolution 3D Printing*. URL: https://www.upnano.at/nanoone/ (visited on 26/06/2023).

[34] Håkon Jarand Dugstad Johnsen. 'Novel Low Cost Solar Thermal Energy Concepts for Developing Countries'. MA thesis. NTNU, 2017. URL: https://ntnuopen.ntnu.no/ntnu-xmlui/handle/11250/2454573 (visited on 26/06/2023).

[35] *Forside*. Prototal. URL: https://www.prototal.no/ (visited on 03/06/2023).

[36] *Infrarødt termometer*. URL: https://www.biltema.no/verktoy/maleverktoy/maleinstrumenter/ir-termometre/infrarodt-termometer-2000044496 (visited on 31/05/2023).

[37] *Compare Formlabs SLA 3D Printer Tech Specs*. Formlabs. URL: https://formlabs.com/3d-printers/form-3/tech-specs/ (visited on 30/05/2023).

[38] *SLA Comparison — Prusa vs Formlabs*. 9th Nov. 2021. URL: https://www.solidprint3d.co.uk/sla-comparison-prusa-sl1s-speed-vs-formlabs-form-3/ (visited on 30/06/2023).

[39] *Buy High Temp Resin*. URL: https://formlabs.com/store/materials/high-temp-resin/ (visited on 30/06/2023).

[40] amc-magazin. *Rugozimetru SJ 201P.Pdf*. amc-magazin.ro. URL: http://amc-magazin.ro/PRODUSE-DOC/Mitutoyo/rugozimetru%20SJ%20201P.pdf (visited on 03/06/2023).

[41] European Association for Computer Graphics. *Sixth Eurographics Italian Chapter Conference: Salerno, Italy, July 2nd - 4th, 2008*. Ed. by Vittorio Scarano. Eurographics Italian Chapter Proceedings. Aire-la-Ville: Eurographics Assoc. [u.a.], 2008. 142 pp. ISBN: 978-3-905673-68-5.

[42] Michael Garland and Paul S Heckbert. 'Surface Simplification Using Quadric Error Metrics'. In: ().

[43] Paolo Cignoni, Claudio Rocchini and Roberto Scopigno. 'Metro: Measuring Error on Simplified Surfaces'. In: *Computer Graphics Forum*. Vol. 17. 2. Blackwell Publishers, 1998, pp. 167–174.

[44] *How to Use Paint Thickness Gauges for Better Automotive Detailing — Resources — DeFelsko*. URL: https://www.defelsko.com/resources/how-to-use-paint-thickness-gauges-for-better-automotive-detailing (visited on 27/06/2023).

[45] *xMOLD Tooling Resin by Nexa3D*. Nexa3D. URL: https://nexa3d.com/digitaltooling/ (visited on 22/06/2023).

Appendix

A Pressforming log

Inner lenses pressed

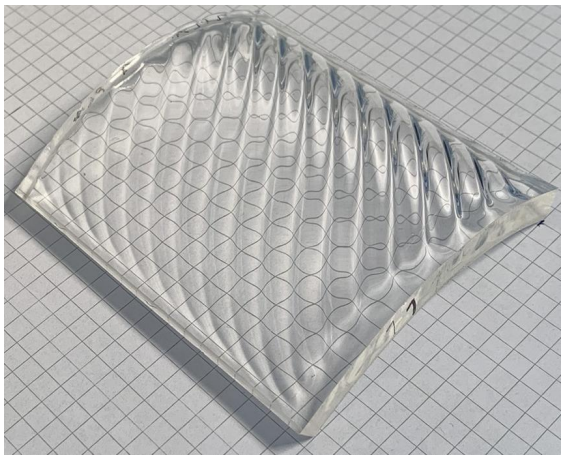

(1) PLA mold, 120℃, 2-3000kg(w/o load cell) a test of concept, to check if the PMMA keeps it transparency as well as if the press can stand the temperature as well as the press itself

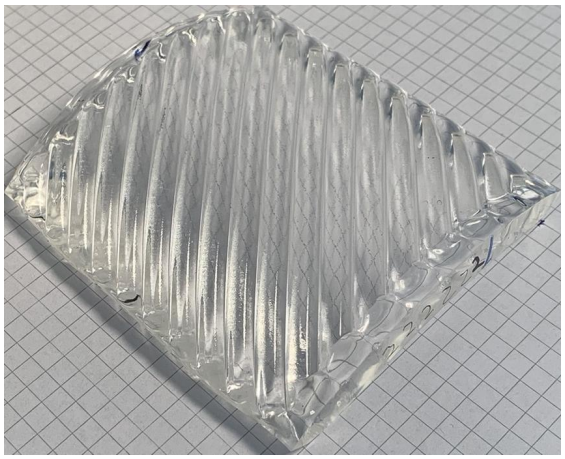

(2) Hi-temp mold, 160℃, 2-3000kg(w/o load cell), The PLA was destroyed due to excessive force. The lens was therefore not a 90 deg bend.

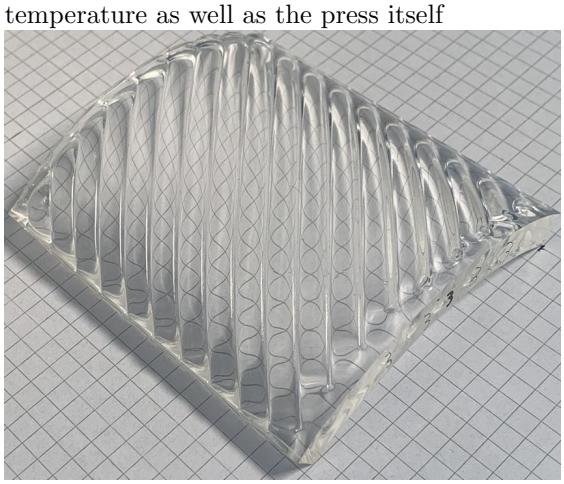

(3) Hi-temp mold, 165℃, 150kg(1min), 500kg(2min), 900kg(until no more force movement), first test with loadcell. The attempt to use different loads through the process was hard, and not repeat4able, in addition to introducing a lot of variables, therefore this was abandoned.

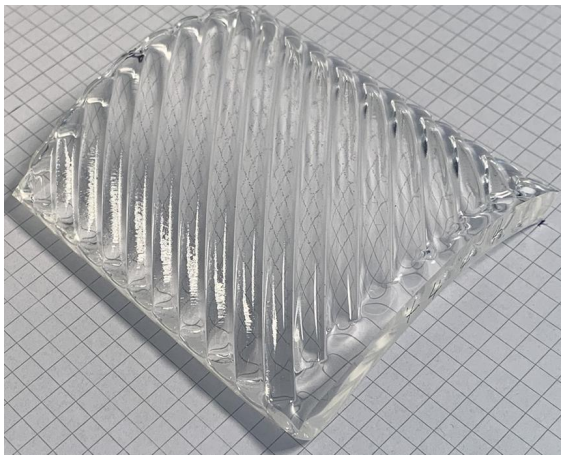

(4) Hi-temp mold, 175℃, 900kg

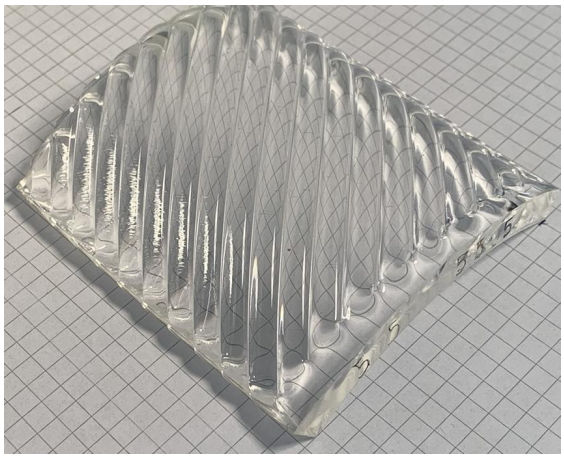

(5) Hi-temp mold, 155℃, —kg, operation failed due to misplacment of PMMA in mold.

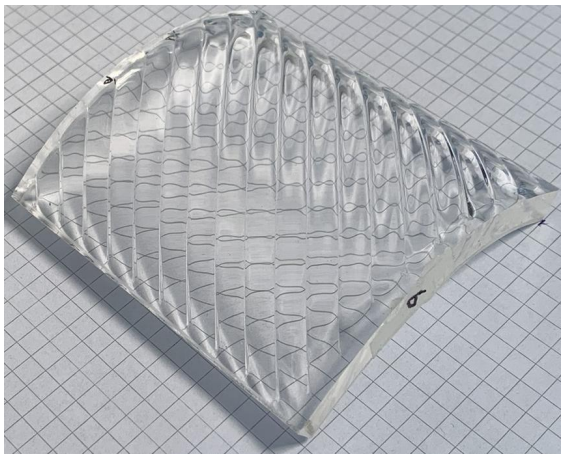

(6) Hi-temp mold, 165℃, —kg, operation failed due to misplacment of PMMA in mold.

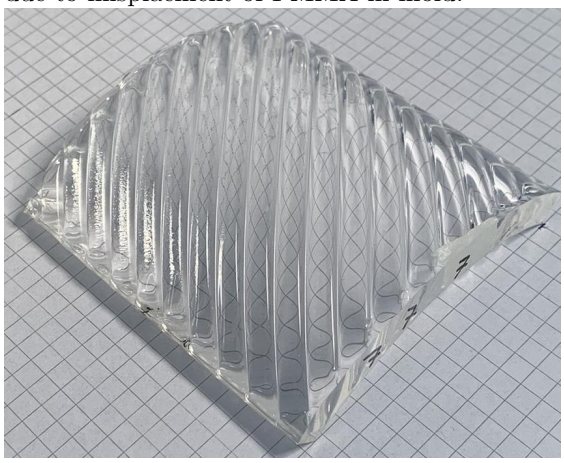

(7) Hi-temp mold, 160℃, 1100kg(1min), 800kg(15min), 500kg(15min)

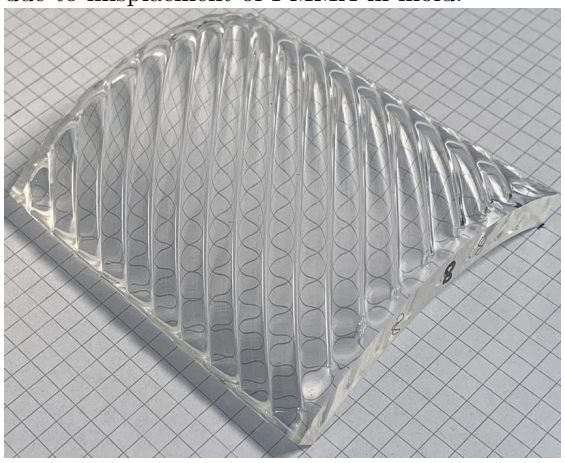

(8) Hi-temp mold, 160℃, 500kg, did not close properly

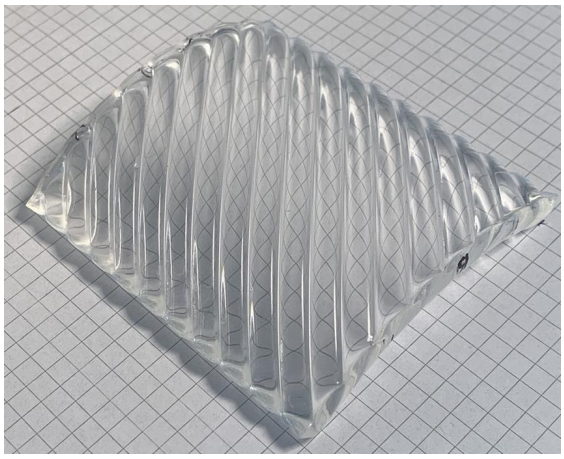

(9) Hi-temp mold, 155℃, 650kg

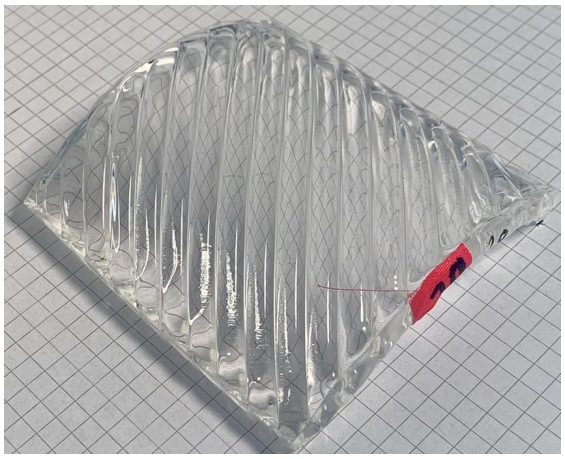

(10) Hi-temp mold, with cooling, 190℃, 1000kg, rapid cooling, much faster to cool down, not enough water flow. Mold did not close properly, turned on water to early, so the PMMA stiffened before being squeezed into shape.

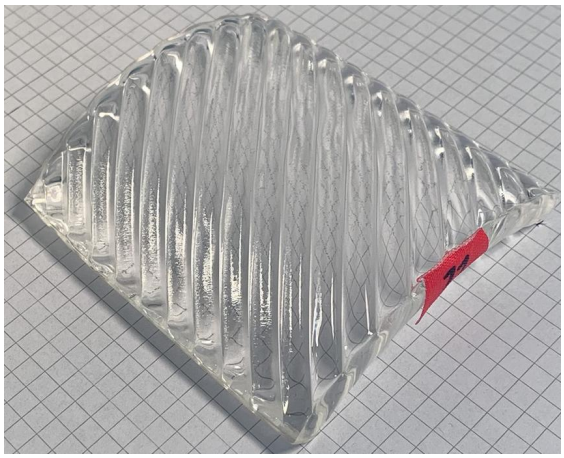

(11) Hi-temp mold, with cooling, 190℃, 1250kg, the load is quite constant, meaning i didn't need to apply pressure after first deformation. Uncertain if the cooling flows in all channels

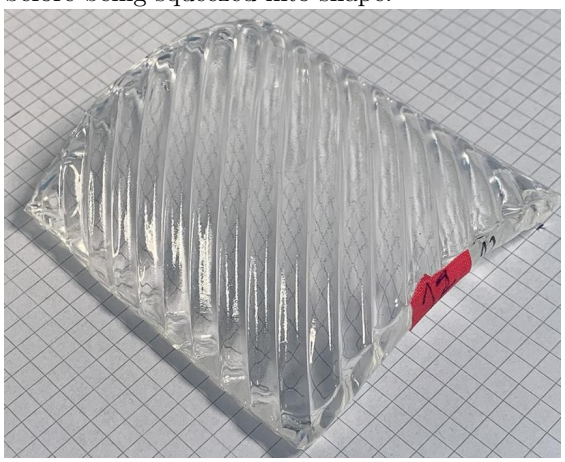

(12) Hi-temp mold, with cooling, 190℃, 900kg(small peak off 1600kg initially, but was fast compensated with pressure relief valve), some more cooling than in 11 to ensure cooling in all channels.

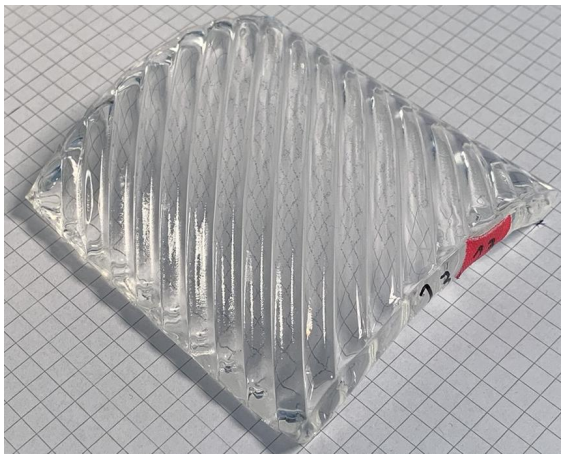

(13) Hi-temp mold, with cooling, 190℃, 900kg(1100peak), more cooling, lot of shrinkage pmma, was stuck in mold, which is unusual.

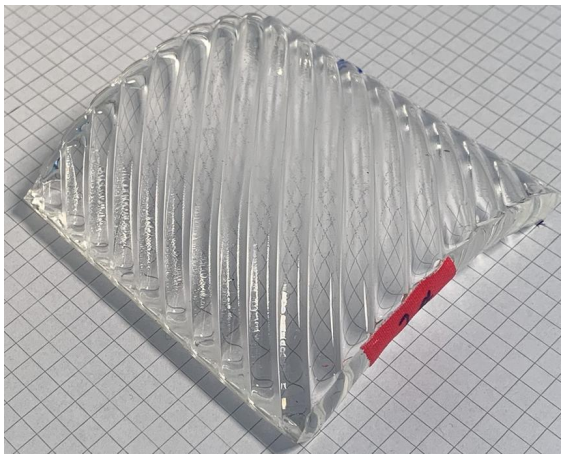

(14) Hi-temp mold, no cooling in cooled punch, 190℃, 650kg, perfect closing. New punch due to damage to old punch in 11,12,13.

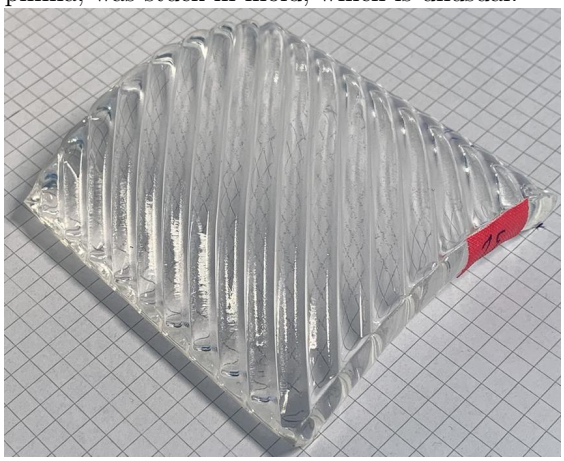

(15) Hi-temp mold, with cooling, 200℃,650kg perfectly closed. New punch due to damage to old punch in 11,12,13.

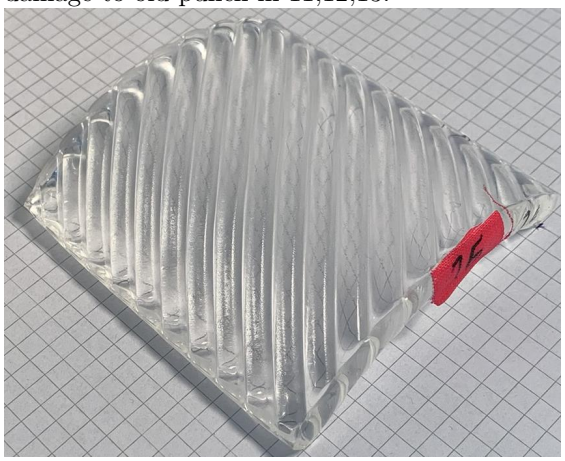

(16) Hi-temp mold, no cooling in cooled punch, 200℃, 650kg, perfect closing, but significantly slower than 15. made as reference for 14, to checxk if isolthermal molding decreases roughness or waviness.

Outer lenses pressed

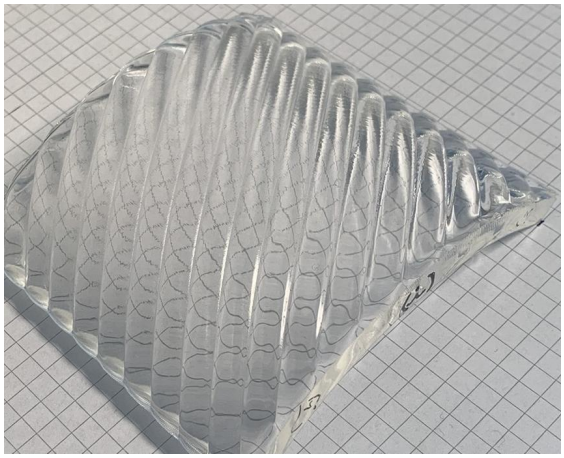

(i) Hi-temp mold, 160℃, 750kg, too much weight, rough surface.

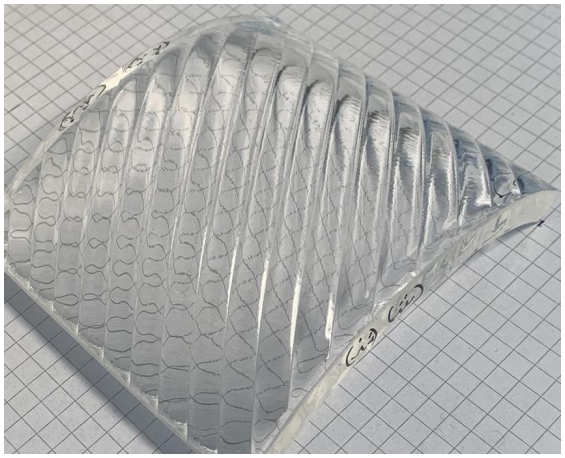

(ii) Hi-temp mold, 150℃, 650kg

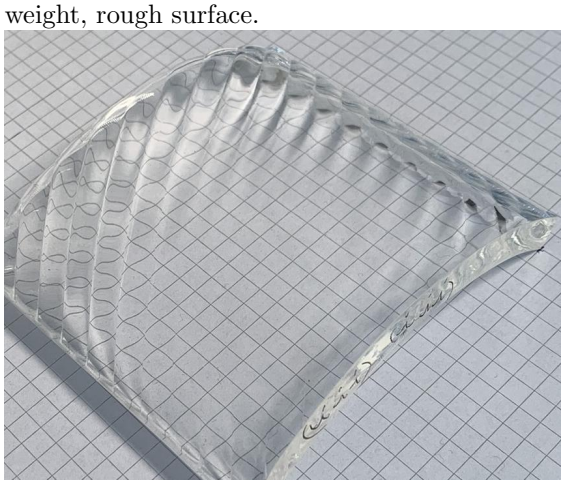

(iii) Hi-temp mold, 150℃, 500kg, mold did not close properly, lot of springback.

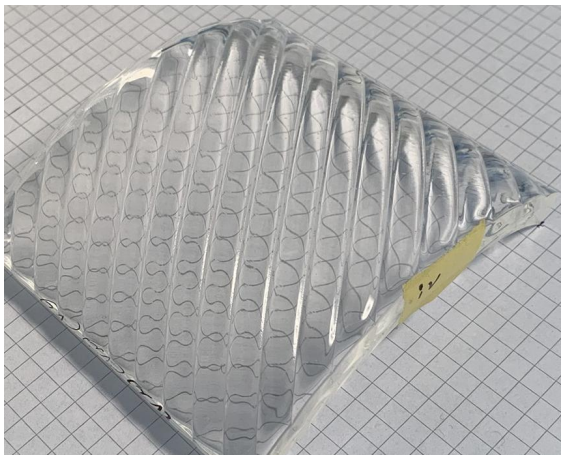

(iv) Hi-temp mold, 150℃, 500kg, upside down mold, some water residue in mold.

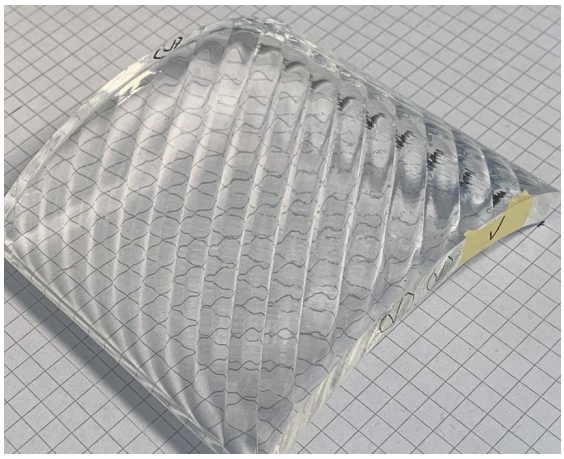

(v) Hi-temp mold, 150℃, 700kg(10sek by accident), 500kg, did not close properly.

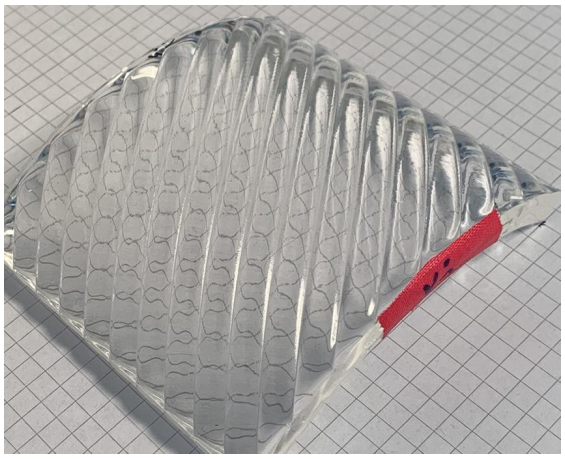

(vi) Hi-temp mold, 180℃, 500kg, some second adjustment needed due to misplacment of pmma.

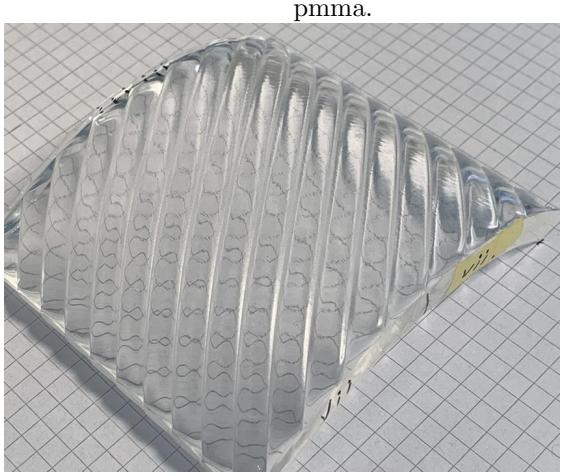

(vii) 175℃, 400kg, closed almost perfectly. same as vi

Printed lenses

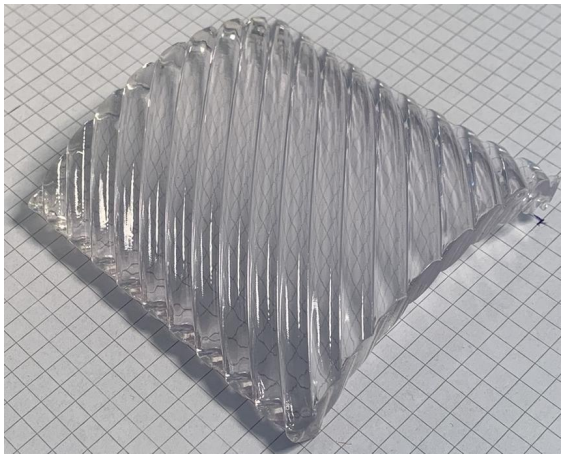

(1) Inner lens, printed, polished, clearcoated

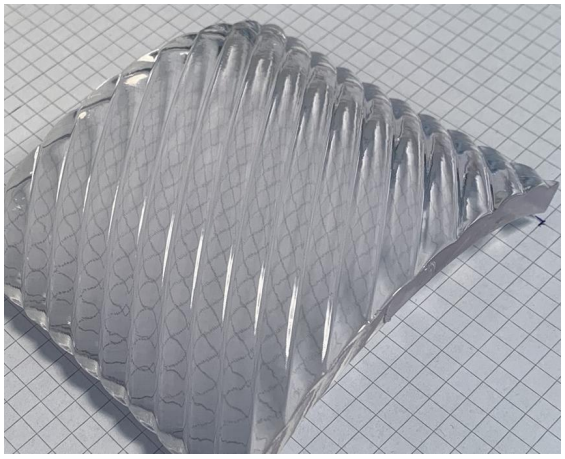

(2) Outer lens, printed, polished, clearcoat

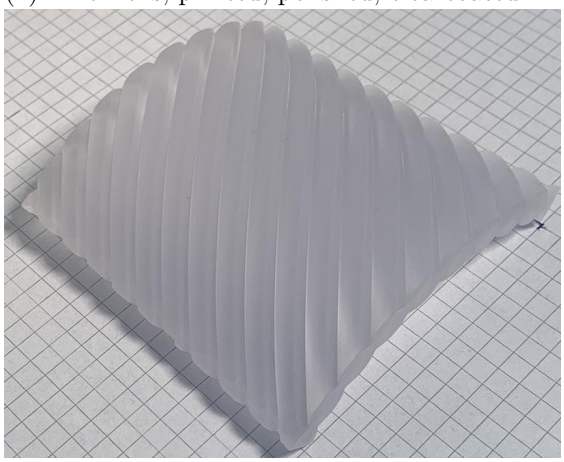

(3) Inner lens, printed, cured, unpolished

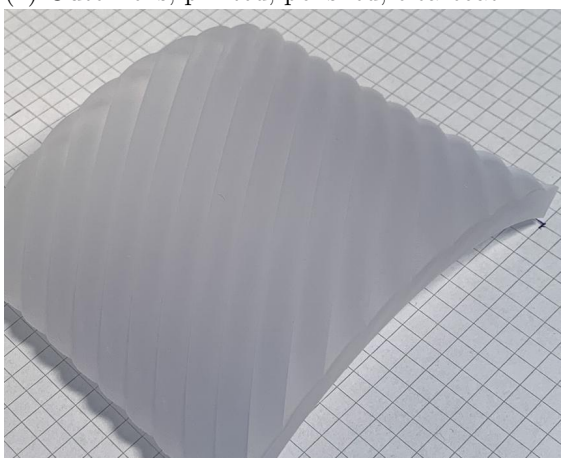

(4) Outer lens, printed, cured, unpolished

B Profilometer

Roughness table

Specimen 7

(7) Outer surface sampled

(7) Inner surface sampled

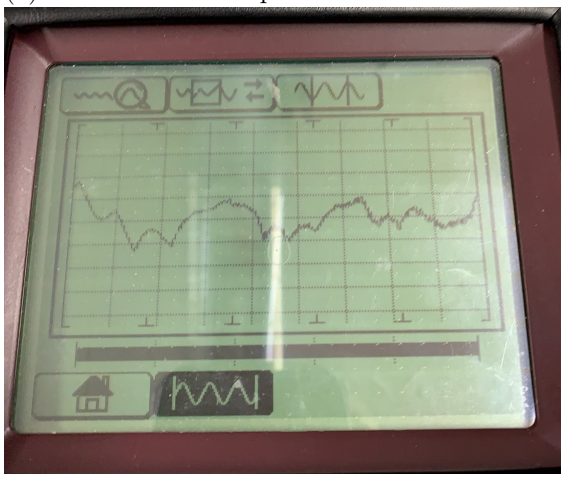

(7) Outer surface graph

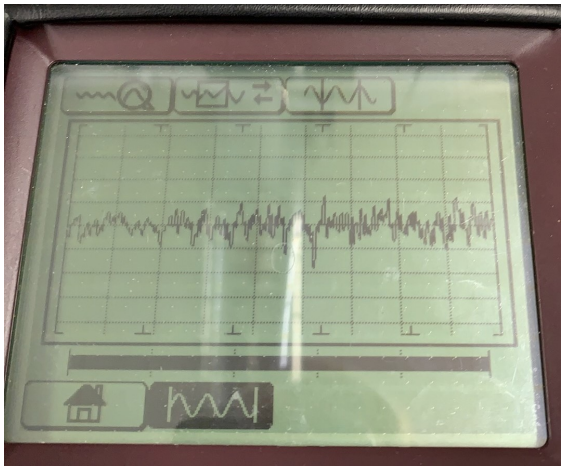

(7) Inner surface graph

Specimen 9

(9) Outer surface sampled

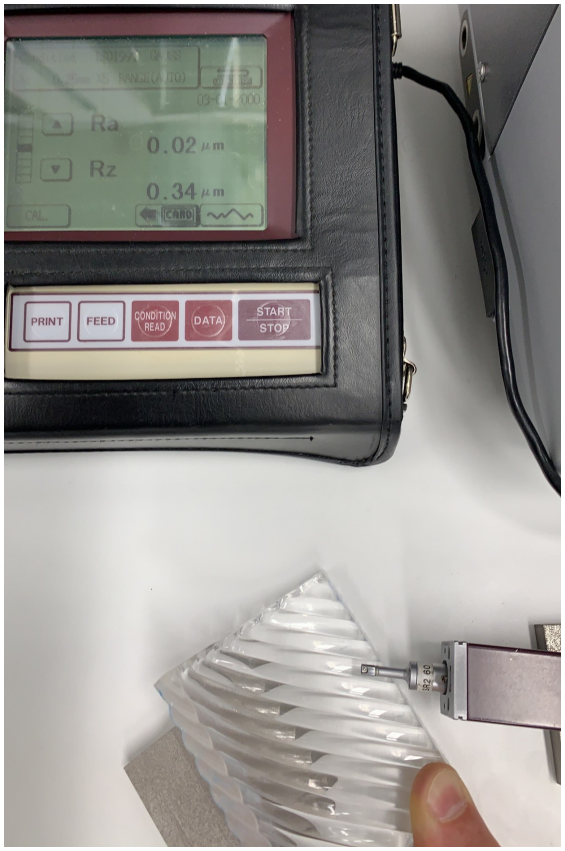

(9) Inner surface sampled

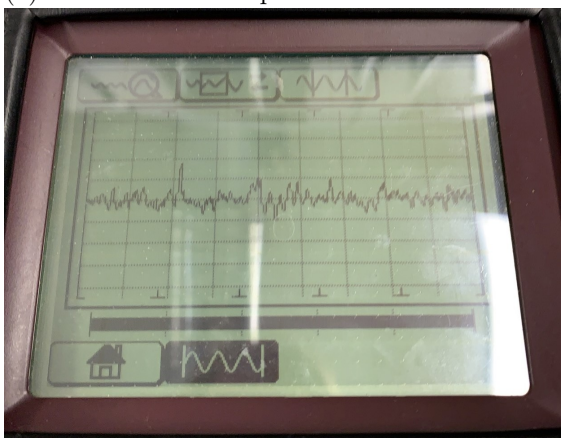

(9) Outer surface graph

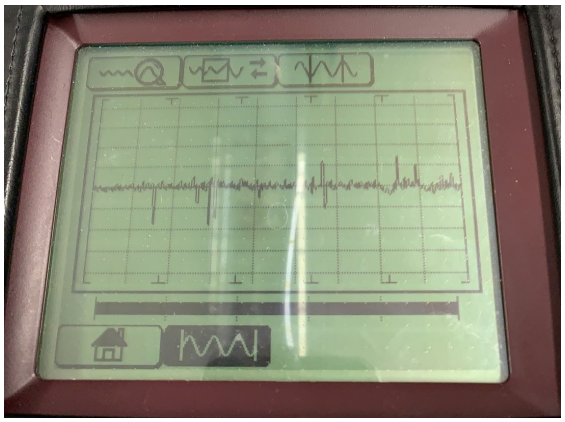

(9) Inner surface graph

Specimen 15

(15) Outer surface sampled

(15) Inner surface sampled

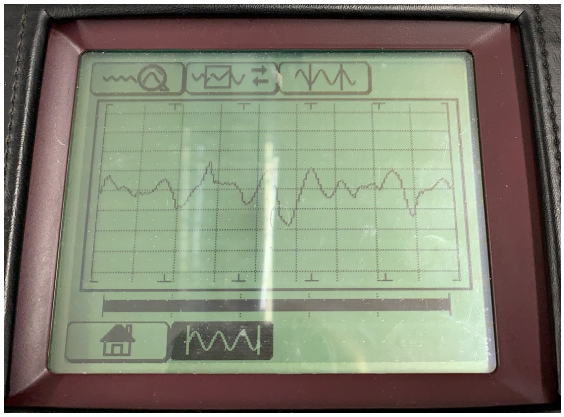

(15) Outer surface graph

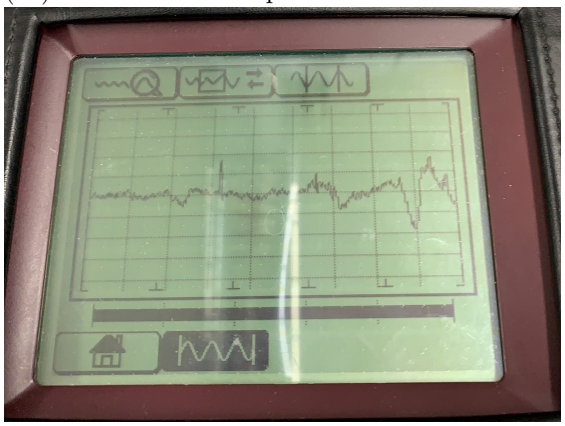

(15) Inner surface graph

Specimen 16

(16) Outer surface sampled

(16) Inner surface sampled

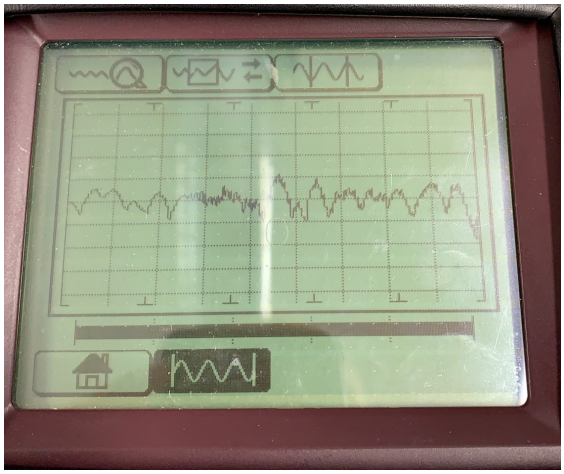

(16) Outer surface graph

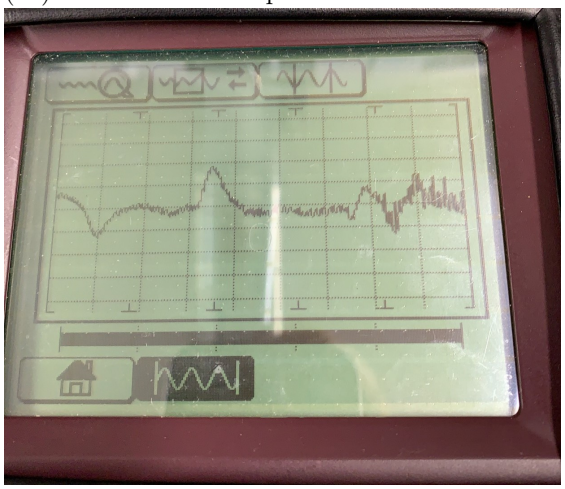

(16) Inner surface graph

Specimen i

(i) Outer surface sampled

(i) Inner surface sampled

(i) Outer surface graph

(i) Inner surface graph

Specimen iv

(iv) Outer surface sampled

(iv) Inner surface sampled

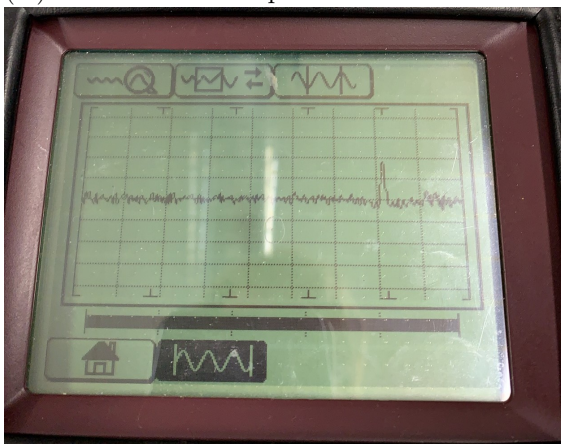

(iv) Outer surface graph

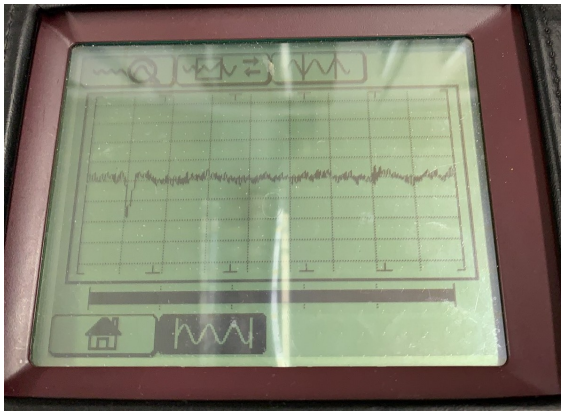

(iv) Inner surface graph

Specimen vii

(iv) Outer surface sampled

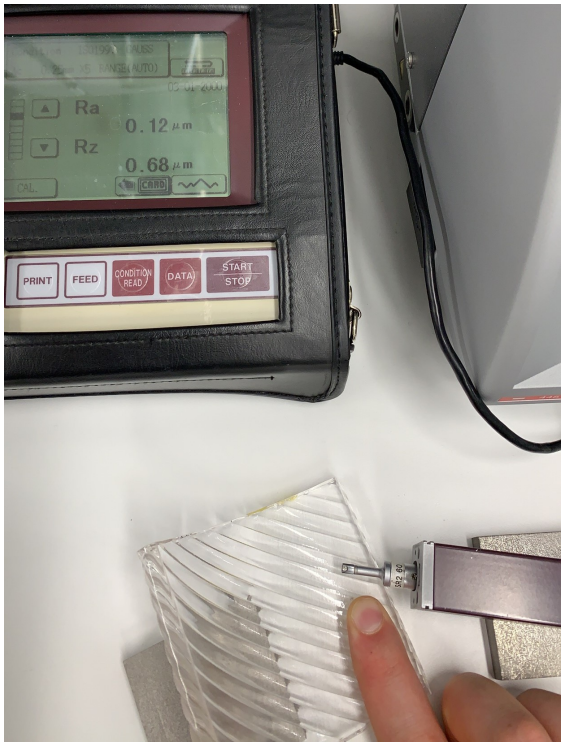

(iv) Inner surface sampled

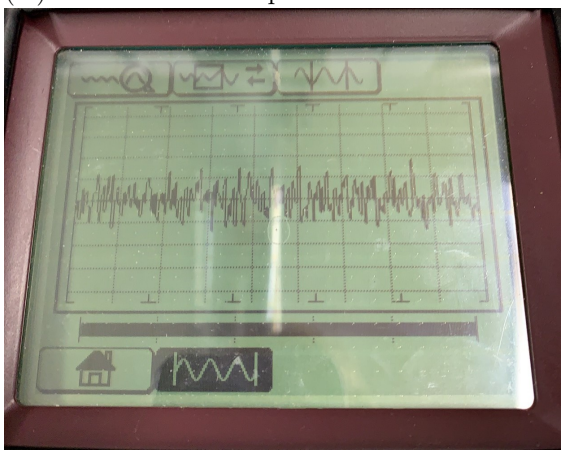

(iv) Outer surface graph

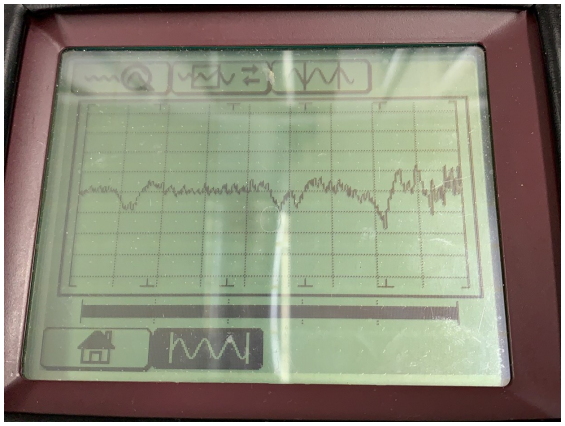

(iv) Inner surface graph

3D Outer polished

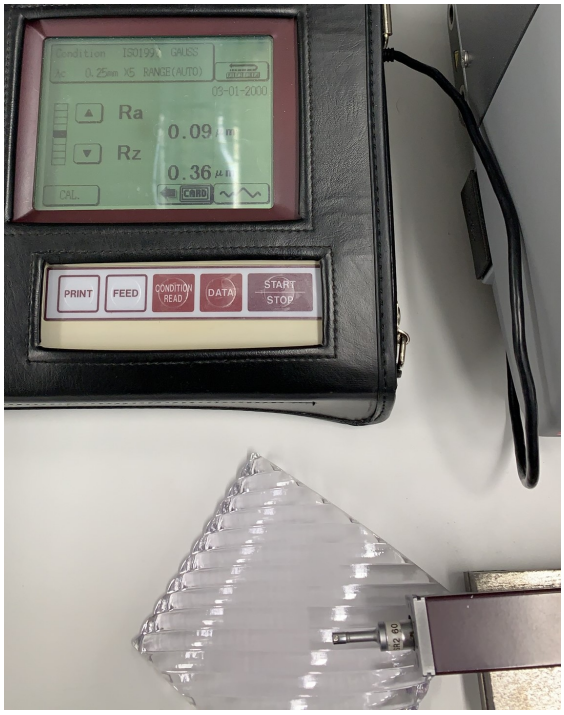

(3D outer) Outer surface sampled

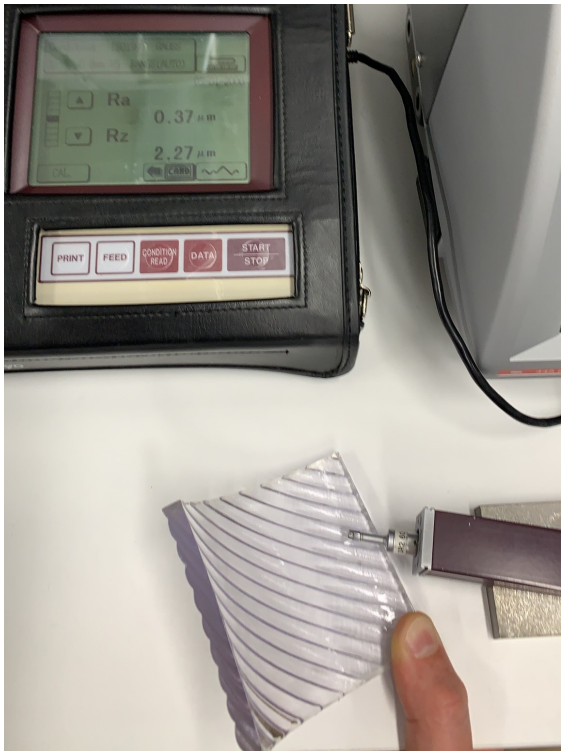

(3D outer) Inner surface sampled

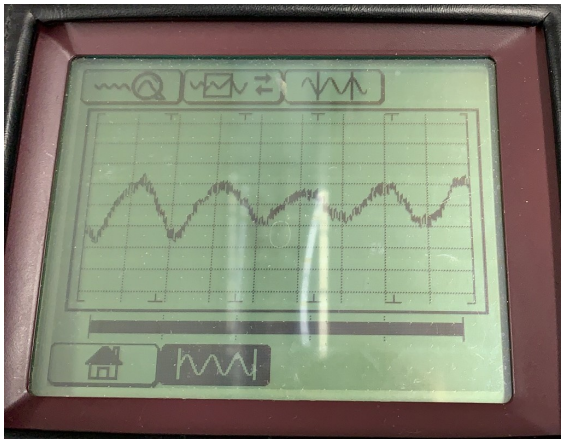

(3D outer) Outer surface graph

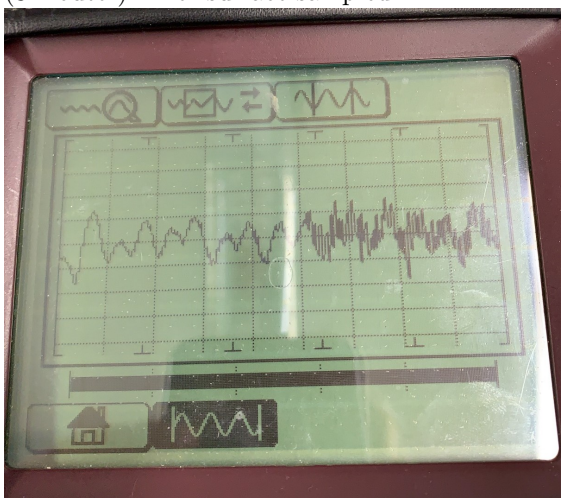

(3D outer) Inner surface graph

3D Inner polished

(3D inner) Outer surface sampled

(3D inner) Inner surface sampled

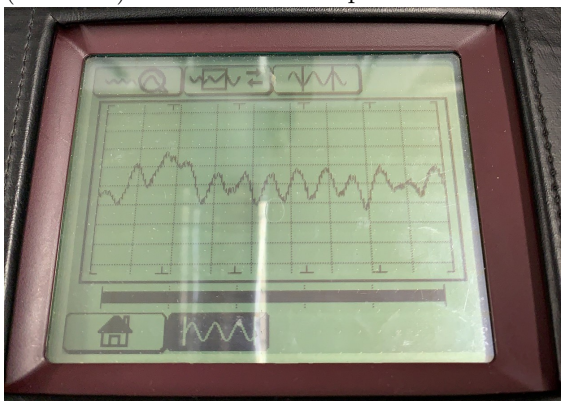

(3D inner) Outer surface graph

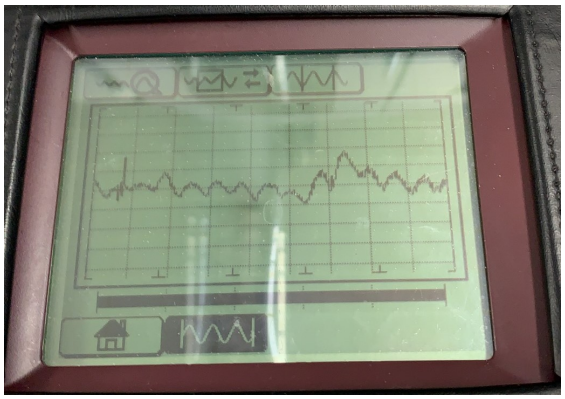

(3D inner) Inner surface graph

3D Outer unpolished

(3D outer untreated) Outer surface sampled

(3D outer untreated) Inner surface sampled

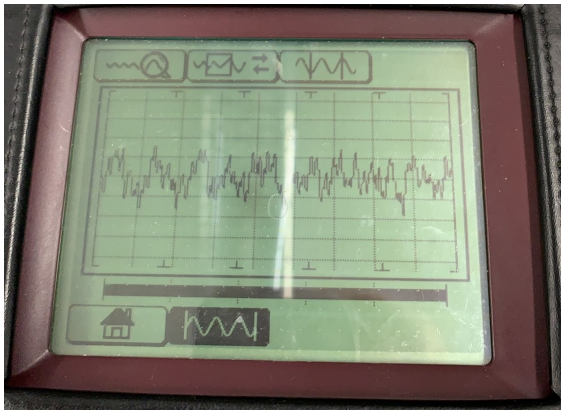

(3D outer untreated) Outer surface graph

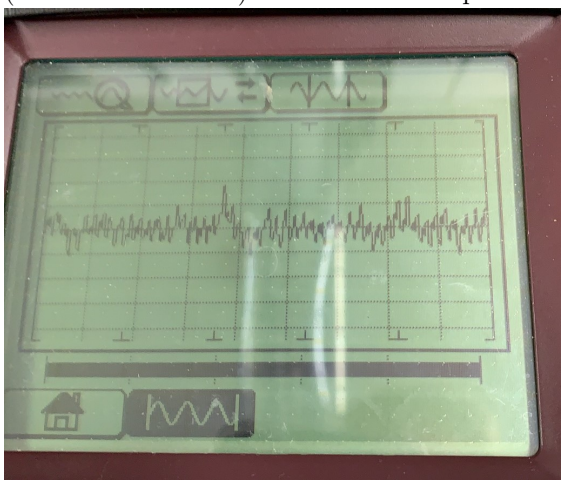

(3D outer untreated) Inner surface graph

3D Inner untreated

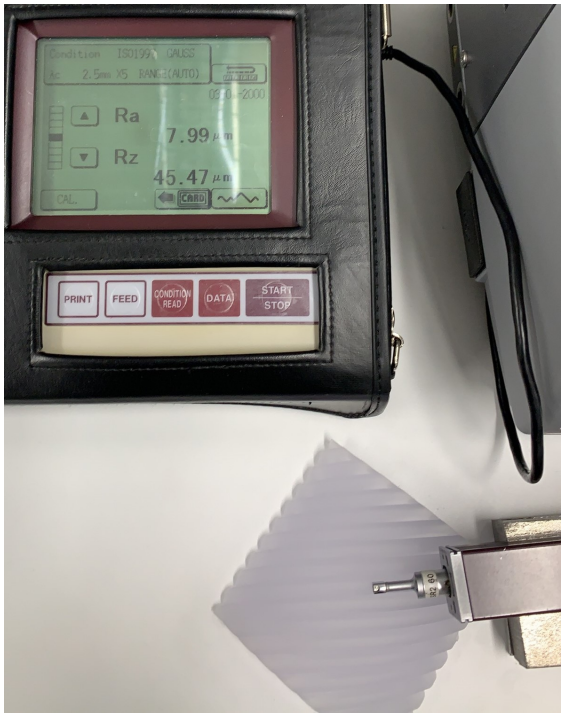

(3D inner untreated) Outer surface sampled

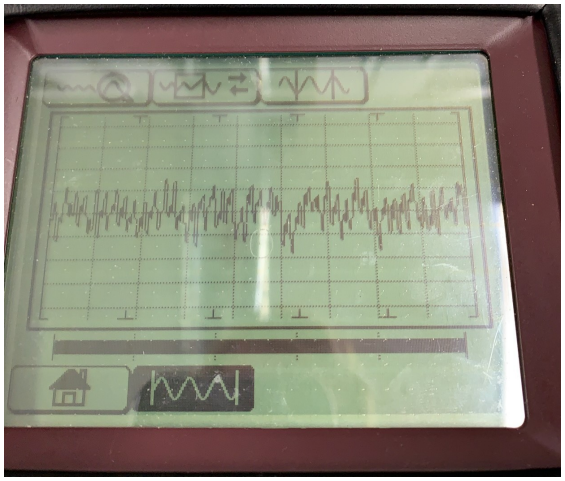

(3D inner untreated) Outer surface graph

Figure 72: Unfortunately the untreated inner lens was to rough to measure with the profilometer, the stylus tip wold stick to creases in the surface.

C Accura Clearvue datasheet

URL: https://www.prototal.no/wp-content/uploads/2022/02/AccuraClearvue_DataSheet.pdf

Accura® ClearVue™

Easy-to-process plastic with best-in-class clarity,
high durability and water resistance for a multitude of applications.

Clear Class

Stereolithography (SLA)

REDEFINING TRANSPARENCY FOR SLA

Utilized in a variety of demanding applications, 3D Systems Accura ClearVue for SLA is the most clear and colorless 3D printing material on the market. Formulated for ease-of-processing, exceptional detail and smooth surface finish, strength, durability and moisture resistance, it simulates the properties and appearance of Polycarbonate and ABS.

This unique combination of clarity, material properties and processing speed makes Accura ClearVue a high performing and cost-effective choice for aesthetic and functional prototypes used to improve product development efficiency of consumer goods, automotive, aerospace and medical components.

Liquid Material

MEASUREMENT	CONDITION	VALUE
Viscosity	@ 30 °C (86 °F)	250 cps
Penetration Depth (Dp)		6.1 mils
Critical Exposure (Ec)		9.5 mJ/cm^2
Color		Clear / Transparent
Liquid Density	@ 25 °C (77 °F)	1.10 g/cm3 | 0.04 lbs/in^3

APPLICATIONS

- Models and prototypes requiring high clarity
  - Lighting and lenses
  - Fluid flow visualization models
  - Transparent assemblies
  - Packaging/bottles
- General purpose prototyping
- Medical models and devices (USP Class VI capable)
- Master patterns for RTV molding
- QuickCast™ patterns for investment casting
- Prototypes of conformal cooling molds
- Snap fits and complex assemblies

BENEFITS

- Best-in-class optical clarity
- Part stability and water tightness
- Applications versatility
- Beautiful transparent parts
- Ease-of-use and fast processing

FEATURES

- Highest clarity and transparency
- USP class VI capable
- Excellent humidity/moisture resistance
- Durable and strong
- High accuracy with exceptional detail and smooth surface finish

3D SYSTEMS®

Accura® ClearVue™

Clear Class

Stereolithography (SLA)

Easy-to-process plastic with best-in-class clarity,
high durability and water resistance for a multitude of applications.

Post-Cured Material

MECHANICAL PROPERTIES		LARGE FRAME SLA PRINTERS		PROJET SLA PRINTERS[1]	
MEASUREMENT	CONDITION	METRIC	U.S.	METRIC	U.S.
Tensile Strength (MPa | PSI)	ASTM D 638	46-53	6700-7700	52	7540
Tensile Modulus (MPa | KSI)	ASTM D 638	2270-2640	329-383	2560	371
Elongation at Break	ASTM D 638	3-15 %		6 %	
Flexural Strength (MPa | PSI)	ASTM D 790	72-84	10400-12200	83	12040
Flexural Modulus (MPa | KSI)	ASTM D 790	1980-2310	287-335	2330	338
Impact Strength (J/m | Ft-lbs/in)	ASTM D 256	40-58	0.7-1.1	46	0.9
Heat Deflection Temperature @ 0.45 MPa (66 PSI) @ 1.82 MPa (264 PSI)	ASTM D 648	 51 °C 50 °C	 124 °F 122 °F	 51 °C 50 °C	 124 °F 122 °F
Coefficient of Thermal Expansion (CTE) (µm/m-°C | µin/in-°F)	ASTM E 831-93 25-50 °C 50-100 °C	 122 155	 68 86	 NA NA	 NA NA
Glass Transition (Tg)	DMA, E"	62 °C	144 °F	70 °C	158 °F
Hardness, Shore D		80		85	
Water Absorption	ASTM D 570-98	0.3 %		0.3 %	
Solid Density (g/cm³ | lbs/in³)	@ 25 °C (77 °F)	1.17	0.042	1.17	0.042

[1] Accura ClearVue was also previously marketed under the VisiJet® SL Clear name for the ProJet 6000 and 7000 printers

OPTICAL PROPERTIES		
MEASUREMENT	CONDITION	VALUE
Haze @ 0.495 mm (0.195 in)	ASTM D1003-13	4.3 %
Luminous Transmittance @ 0.495 mm (0.195 in)	ASTM D1003-13	87.2 %
Diffuse Transmittance @ 0.495 mm (0.195 in)	ASTM D1003-13	3.8 %
Index of Refraction	ASTM D542-14	1.508
L*		95.45
a*		-0.54
b*		1.36

3D SYSTEMS®

www.3dsystems.com

09-20

D Perspex Datasheet

URL: https://www.perspex.co.uk/Perspex/media/General/technical-library/Typical%20Physical%20Properties/Perspex-Acrylic-Typical-Physical-Properties.pdf

TYPICAL PHYSICAL PROPERTIES

PERSPEX® Cast Acrylic Sheet

Property	Test Method	Conditions	Units	Value
Physical				
Relative Density	ISO 1183		g/cm³	1.19
Water Absorption	ISO 62		%	0.2
Mechanical				
Tensile Strength at Yield	ISO 527	5mm/min	MPa	75
Tensile Strength at Break				
Elongation at Yield				
Elongation at Break	ISO 527	5mm/min	%	4
Tensile Modulus of Elasticity				
Flexural Modulus	ISO 178	2mm/min	MPa	3210
Flexural Strength at Yield	ISO 178	2mm/min	MPa	116
Izod Impact Strength	ISO 180/1A	notched	kJm-2	N/A
Charpy Impact Strength	ISO 179	unnotched	kJm-2	12
Impact Falling Weight				
Rockwell Hardness	ISO 2039-2		M Scale	102
Thermal				
Service Temperature			˚C	-40 to 80
Heat Distortion Temperature				
Vicat Softening Temperature	ISO 306		˚C	>110
Coefficient of Thermal Expansion	ASTM D-696		mm/m°C	0.077
Thermal Conductivity				
Specific Heat Capacity				
Optical				
Light Transmission	ASTM D-1003	3mm sheet	%	>92
Refractive Index	ISO 489/A			1.49
Yellowness Index				
Haze				
Electrical				
Dielectric Strength	IEC 243		kV/mm-1	15
Surface Resistivity	IEC 93		Ω m-2	>1014

Other physical properties and values available on request.

Flammability

Standard	Classification
BS 476 Part 7	Class 3
UL 94	HB
NFP 92-307	M4 (without drips)

PERSPEX® is a combustible material and if ignited will continue to burn. However, unlike many other plastic materials, burning PERSPEX® produces very little smoke, an important fire safety benefit.

E Image analysis script

image analysis script,

The code that presented in this document, might not have the exact same parameters as used in the report.

kode:

In [2]:
```
%matplotlib widget

import numpy as np
import matplotlib.pyplot as plt
import cv2
import mplcursors
from mpl_toolkits.axes_grid1 import make_axes_locatable
from PIL import Image
from skimage.draw import polygon
from matplotlib.lines import Line2D
import os
```

click handler og neutral axis

In [3]:
```
# Initialize a list to store the coordinates of the four points
testing = False
if testing:
    clicked_points = [(159, 412), (1080, 519), (1086, 739), (176, 950)]
    print("testmode")
else:
    clicked_points = []


# Function to handle mouse clicks
def click_handler(event, x, y, flags, param):
    if event == cv2.EVENT_LBUTTONDOWN and len(clicked_points) < 4:
        clicked_points.append((x, y))
        cv2.circle(param, (x, y), 5, (0, 255, 0), -1)
        cv2.putText(param, str(len(clicked_points)), (x + 5, y), cv2.FONT_HERSHEY_SIMPLEX, 0.5, (0, 255, 0), 1)
        cv2.imshow("Image", param)
```

```
def find_horizontal_neutral_axis(image):
    if len(image.shape) == 3:
        gray_image = cv2.cvtColor(image, cv2.COLOR_BGR2GRAY)
    else:
        gray_image = image.copy()

    row_sums = np.sum(gray_image, axis=1)
    cumulative_sums = np.cumsum(row_sums)
    neutral_axis_index = np.argmin(np.abs(cumulative_sums - cumulative_sums[-1] / 2))

    clicked_points = []

    return neutral_axis_index
```

perspective transform with mouseclicks

In [4]:
```
def perspective_transform_with_mouse_clicks(image_path, width_mm, height_mm):
    image = cv2.imread(image_path, cv2.IMREAD_UNCHANGED)
    #gamma factor to increase light, to be able to choose the crosshairs precisly
    gamma = 0.2

    # Keep a copy of the original image
    original_image = image.copy()

    # Adjust gamma
    gamma_corrected = np.power(image / 255.0, gamma) * 255.0
    image = np.uint8(gamma_corrected)

    cv2.namedWindow("Image")
    cv2.setMouseCallback("Image", click_handler, image)

    while len(clicked_points) < 4:
        cv2.imshow("Image", image)
        cv2.waitKey(1)

    # Now revert back to the original image
    image = original_image.copy()

    cv2.destroyAllWindows()
    print(f"Clicked coordinates: {clicked_points}, Testing: {testing}")


    #pixel extension to the right in the image
```

```
extend_pixels = 400

# Copy clicked_points
clicked_points_extended = clicked_points.copy()

# Extend top right point
top_vector = np.array(clicked_points[1]) - np.array(clicked_points[0])
top_vector = top_vector / np.linalg.norm(top_vector)
clicked_points_extended[1] = clicked_points[1] + extend_pixels * top_vector

# Extend bottom right point
bottom_vector = np.array(clicked_points[2]) - np.array(clicked_points[3])
bottom_vector = bottom_vector / np.linalg.norm(bottom_vector)
clicked_points_extended[2] = clicked_points[2] + extend_pixels * bottom_vector

# Calculate the reference lengths in pixels
width_ref_length_pixels = np.linalg.norm(np.array(clicked_points_extended[0]) - np.array(clicked_points_extended[1]))
height_ref_length_pixels = np.linalg.norm(np.array(clicked_points_extended[1]) - np.array(clicked_points_extended[2]))


#calculate original length of top vector
width_original_length_pixels = np.linalg.norm(np.array(clicked_points[0]) - np.array(clicked_points[1]))
#calculate original length of right vector
height_original_length_pixels = np.linalg.norm(np.array(clicked_points[1]) - np.array(clicked_points[2]))



# Calculate the DPI for both width and height
width_dpi = width_ref_length_pixels * 25.4 / width_mm
height_dpi = height_ref_length_pixels * 25.4 / height_mm

# Compute the average DPI
avg_dpi = (width_dpi + height_dpi) / 2

#factor width is extended
width_extension_factor = width_ref_length_pixels/width_original_length_pixels
#factor height is inadvertenly extended
height_extension_factor = height_ref_length_pixels/height_original_length_pixels
#print(f"{width_extension_factor}\n{width_ref_length_pixels}\n{width_original_length_pixels}")

 # Convert width and height in millimeters to pixels
width_px = int(width_extension_factor * width_mm * avg_dpi / 25.4)
height_px = int(height_extension_factor * height_mm * avg_dpi / 25.4)


# Define the destination points for the transformed image
```

```
    destination_points = np.float32([[0, 0], [width_px, 0], [width_px, height_px], [0, height_px]])


    # Calculate the perspective transform matrix and apply it
    transform_matrix = cv2.getPerspectiveTransform(np.float32(clicked_points_extended), destination_points)
    transformed_image = cv2.warpPerspective(image, transform_matrix, (width_px, height_px))

    return image, transformed_image
```

In [53]:

vizualize images

In [277…

```
def vizualize_images(input_image, transformed_image,save_path):
    '''
    takes the input image and the transformed images and plots them
    '''


    #lager en linje midt i bildet
    neutral_axis = find_horizontal_neutral_axis(transformed_image)
    visualized_image = transformed_image.copy()
    cv2.line(visualized_image, (0, neutral_axis), (visualized_image.shape[1], neutral_axis), (0, 255, 0), 2)
    # Display the images side by side using matplotlib
    fig, (ax2, ax1) = plt.subplots(1, 2, figsize=(10, 5))


    ax1.imshow(input_image, aspect="equal", cmap='gray')#, norm="linear", vmin=0,vmax=160)

    #ax1.set_title(save_path.split("/")[-1].replace("_"," ").replace("deg","\u00b0")+' input image with points')
    ax1.axis('off')


    ax2.imshow(visualized_image,aspect='equal',cmap='gray')#, norm="linear", vmin=0,vmax=160)
    #ax2.set_title(save_path.split("/")[-1].replace("_"," ").replace("deg","\u00b0")+' transformed with neutral axis')
    ax2.axis('off')

    plt.gcf().savefig(save_path+".png")

    plt.show()
```

remove background

In [6]:
```python
def remove_background(image, threshold=40):
    # Set all values below threshold to zero
    image_no_background = np.where(image < threshold, 0, image)
    # Subtract the threshold from the remaining pixel intensities
    image_no_background = np.where(image_no_background > 0, image_no_background - threshold, 0)

    return image_no_background
```

Out[6]:
```
'\ndef remove_background(image, treshold = 40):\n    #sets all values below treshold to zero\n    removedBackroundImage = np.where(image < treshold, 0, image)\n    return removedBackroundImage\n'
```

plot intensity

In [7]:
```python
def plot_intensity(image,neutral_axis):
    '''
    takes a image, and creates a intesity plot beside it
    '''


    #checks for black/white, and transforms it if not
    if len(image.shape) == 3 and image.shape[2] == 3:
        gray_image = cv2.cvtColor(image, cv2.COLOR_BGR2GRAY)
    else:
        gray_image = image

    accumulated_intensity = np.sum(gray_image, axis=1)

    # Normalize the accumulated intensity to the range [0, 255]
    normalized_intensity = (accumulated_intensity - np.min(accumulated_intensity)) / (np.max(accumulated_intensity) - np.min(accumulated_in
    normalized_intensity = normalized_intensity.astype(np.uint8)

    # Create an empty image with the same height as the original image and a width equal to the maximum intensity value
    intensity_image = np.zeros((image.shape[0], np.max(normalized_intensity)), dtype=np.uint8)

    # Set the intensity values along the x-axis for each row
    for row, value in enumerate(normalized_intensity):
        intensity_image[row, :value] = 255

    # Combine the original image and the intensity image
    combined_image = np.concatenate((gray_image, intensity_image), axis=1)

    return combined_image
```

```
def show_intensity_plot(combined_image,neutral_axis,save_path):
    '''
    shows a image with a given horizontal line
    '''
    # Show the combined image
    plt.figure()
     #adds a horizontal line where the intensity is the same at both sides
    plt.axhline(y=neutral_axis,linewidth=1)
    plt.imshow(combined_image, cmap='gray', aspect='auto')
    plt.xlabel("Row and Intensity")
    plt.ylabel("Column")
    plt.title(save_path.split("/")[-1].replace("_"," ").replace("deg","\u00b0")+f" intensity plot with neutral axis:{neutral_axis}")
    plt.gca().set_aspect('equal')

    plt.gcf().savefig(save_path+"_intensity.png")

    plt.show()
```

show focal energy

In [289…

```
def show_focal_energy(image, neutral_axis,image_height_mm, focal_height_mm, save_path):#,intensity_threshold = 40):
    #sum of intensyties of each row in a picture
    row_sums = [sum(row) for row in image] #list of each rows intensity
    #copy of that sum
    start_sums = row_sums.copy()
    #values for y-axis,  corresponding to the mm size of the square on the paper
    y_heights = np.linspace(image_height_mm,0,len(row_sums))
    #total intensity of the whole image
    total_intensity = sum(row_sums)
    original_intensity = sum(row_sums)

    if (image_height_mm != focal_height_mm):
        #creating the min/max indexes of the intensity list points for the focal tube
        indexes_to_keep = (len(row_sums) * (focal_height_mm/image_height_mm))
        index_to_keep_max = int(neutral_axis + indexes_to_keep//2)
        index_to_keep_min = int(neutral_axis - indexes_to_keep//2)

        #setting all values outside of interest(focal tube) to zero and deleting the values from total intensity
        for i in range(len(row_sums[0:index_to_keep_min])):
            total_intensity -= row_sums[i]
            row_sums[i] = 0
        for j in range(len(row_sums[index_to_keep_max:])):
            total_intensity -= row_sums[j+index_to_keep_max]
            row_sums[j+index_to_keep_max] = 0
```

```
    # Plotting y_heights and row_sums
    plt.figure()
    plt.plot(row_sums, y_heights,)
    plt.plot(start_sums, y_heights)

    #hline for focal size
    try:
        plt.axhline(y=y_heights[index_to_keep_min],linewidth=1,color="tab:red")
    except Exception as e1:
        print(f"An error occurred trying to create min_hline, in 'show focal energy'-function: {e1} \n the hline was set to the first index
        plt.axhline(y=y_heights[0],linewidth=1,color="tab:red")
    try:
        plt.axhline(y=y_heights[index_to_keep_max],linewidth=1,color="tab:red")
    except Exception as e2:
        print(f"An error occurred trying to create max_hline, in 'show focal energy'-function: {e2} \n the hline was set to the last index
        plt.axhline(y=y_heights[-1],linewidth=1,color="tab:red")



    plt.gca().set_aspect('auto')

    plt.ylabel('Y Heights (mm)')
    plt.xlabel('Intensity')
    plt.title(save_path.split("/")[-1].replace("_"," ").replace("deg","\u00b0")+' intensity profile along Y heights')
    custom_lines = [Line2D([0], [0], color='tab:red', lw=2),
                Line2D([0], [0], color='blue', lw=2),
                Line2D([0], [0], color='orange', lw=2)]
    plt.legend(custom_lines, [f'Focal boundaries, height: {focal_height_mm}mm', f'Altered intensity: {total_intensity:.2f}', f'Original int

    plt.gcf().savefig(save_path+"_focal.png")

    plt.show()

    return total_intensity
```

In [8]:

```
def show_focal_energy_multiple(images, neutral_axes, image_height_mm, focal_heights_mm, labels, save_path):
    plotted_focal_lower_tube = False
    plotted_focal_upper_tube = False

    # Making sure that lists have the same length
    assert len(images) == len(neutral_axes) == len(focal_heights_mm) == len(labels),  'Input lists must be of the same length.'

    # Create a figure
```

```
plt.figure()

# Define colors for different plots
colors = ['blue', 'green', 'orange', 'purple']

for (image, neutral_axis, focal_height_mm, label, color) in zip(images, neutral_axes, focal_heights_mm, labels, colors):

    row_sums = [sum(row) for row in image]
    start_sums = row_sums.copy()
    y_heights = np.linspace(image_height_mm, 0, len(row_sums))
    total_intensity = sum(row_sums)
    original_intensity = sum(row_sums)

    if image_height_mm != focal_height_mm:
        indexes_to_keep = (len(row_sums) * (focal_height_mm / image_height_mm))
        index_to_keep_max = int(neutral_axis + indexes_to_keep // 2)
        index_to_keep_min = int(neutral_axis - indexes_to_keep // 2)

        for i in range(len(row_sums[0:index_to_keep_min])):
            total_intensity -= row_sums[i]
            row_sums[i] = 0
        for j in range(len(row_sums[index_to_keep_max:])):
            total_intensity -= row_sums[j + index_to_keep_max]
            row_sums[j + index_to_keep_max] = 0

    # Plot without creating a new figure
    plt.plot(start_sums,y_heights,linestyle='dotted')
    plt.plot(row_sums, y_heights, label=f'{label}: intensity {total_intensity:.2f}')


    # Plot horizontal lines for focal boundaries
    if not plotted_focal_lower_tube:
        try:
            plt.axhline(y=y_heights[index_to_keep_min], linewidth=1, color=color, linestyle='dashed',label="Focal tube")
            plotted_focal_lower_tube = True
        except Exception as e1:
            plt.axhline(y=y_heights[0], linewidth=1, color=color, linestyle='dashed', label="Focal tube")
            plotted_focal_lower_tube = True
    if not plotted_focal_upper_tube:
        try:
            plt.axhline(y=y_heights[index_to_keep_max], linewidth=1, color=color, linestyle='dashed', label="Focal tube")
            plotted_focal_upper_tube = True
        except Exception as e2:
            plt.axhline(y=y_heights[-1], linewidth=1, color=color, linestyle='dashed', label="Focal tube")
            plotted_focal_upper_tube = True
```

```
    plt.gca().set_aspect('auto')

    plt.ylabel('Y Heights (mm)')
    plt.xlabel('Intensity')
    plt.title('Intensity profiles along Y heights')
    plt.legend()

    # Save the figure
    plt.gcf().savefig(save_path + "_focal.png")

    # Show the figure
    plt.show()
```

get focal energy

In [9]:

```
def get_focal_energy(image, neutral_axis,image_height_mm, focal_height_mm):#,intensity_threshold = 40):
    #sum of intensyties of each row in a picture
    row_sums = [sum(row) for row in image] #list of each rows intensity
    #copy of that sum
    start_sums = row_sums.copy()
    #values for y-axis,  corresponding to the mm size of the square on the paper
    y_heights = np.linspace(image_height_mm,0,len(row_sums))
    #total intensity of the whole image
    total_intensity = sum(row_sums)
    original_intensity = sum(row_sums)

    if (image_height_mm != focal_height_mm):
        #creating the min/max indexes of the intensity list points for the focal tube
        indexes_to_keep = (len(row_sums) * (focal_height_mm/image_height_mm))
        index_to_keep_max = int(neutral_axis + indexes_to_keep//2)
        index_to_keep_min = int(neutral_axis - indexes_to_keep//2)

        #setting all values outside of interest(focal tube) to zero and deleting the values from total intensity
        for i in range(len(row_sums[0:index_to_keep_min])):
            total_intensity -= row_sums[i]
            row_sums[i] = 0
        for j in range(len(row_sums[index_to_keep_max:])):
            total_intensity -= row_sums[j+index_to_keep_max]
            row_sums[j+index_to_keep_max] = 0

    return total_intensity, original_intensity
```

flux width plot

In [70]:

```
def flux_width_plot(images, neutral_axes, legend_names, focal_widths, image_height_mm, reference_Flux, save_string):
    plotted_vline = False
    fig, ax = plt.subplots()
    # Loop through each image, neutral axis, and focal width
    for image, neutral_axis, legend_name, focal_width in zip(images, neutral_axes, legend_names, focal_widths):
        # Sum of intensities of each row in the image
        row_sums = np.array([np.sum(row) for row in image])
        # Calculate height of each row in mm
        row_Height_mm = image_height_mm / len(row_sums)

        # Initialize lists to store flux and width values
        flux = []
        width = []
        # Start at the neutral axis
        middle_index = neutral_axis

        flux.append(row_sums[neutral_axis])
        width.append(row_Height_mm)

        for i in range(1, min(neutral_axis, len(row_sums) - neutral_axis)):
            # Adding sum of corresponding row intensities from the neutral axis
            flux.append(flux[i-1] + row_sums[neutral_axis-i] + row_sums[neutral_axis+i])
            width.append(width[i-1] + 2 * row_Height_mm)

        flux_normalized = 100 * (np.array(flux) / reference_Flux)

        # Plot data on the subplot
        ax.plot(width, flux_normalized, label=legend_name)

        # Plot vertical line for focal width
        if not plotted_vline:
            ax.axvline(x=focal_width, color="tab:red", linestyle='dashed')
            plotted_vline = True
        else:
            ax.axvline(x=focal_width, color="tab:red", linestyle='dashed')

    ax.set_xlabel('Width (mm)')
    ax.set_ylabel('Flux % of reference')
    ax.set_title(save_string.split("/")[-1].replace("_", " ").replace("deg", "\u00b0").replace("percent", "%") + ', Flux vs. Width')
    ax.grid(True)
    ax.legend(loc='lower right')
    #fig.savefig(save_string+"_flux.png")
```

```
    for axes in axes_list:
        for line, label in zip(axes.lines, axes.get_legend_handles_labels()[1]):
            ax.plot(line.get_xdata(), line.get_ydata(), label=label)

    plt.show()
    return ax
```

plot multiple axes

In [73]:
```
ax_to_plot = {}
```

In [237…
```
#"name":ax
def add_ax_to_plot(key,ax):
    ax_to_plot[key] = ax
    print("dictionary: ",ax_to_plot)

def plot_all_axis():
    label_list = []

    fig,ax =plt.subplots(figsize=(9,7))
    for key, value in ax_to_plot.items():
        for line, label in zip(value.lines, value.get_legend_handles_labels()[1]):
            linestyle = "solid"
            if key in ["simulation","ref"]:
                linestyle = "dashed"
            if label in label_list:
                ax.plot(line.get_xdata(), line.get_ydata())
            else:
                ax.plot(line.get_xdata(), line.get_ydata(), label=label,linestyle=linestyle)
            label_list.append(label)

    #plot focaltube
    ax.axvline(x=12.45, color="tab:red", linestyle='dotted', label="Focal tube")

    #plot settings
    ax.set_xlabel('Width (mm)')
    ax.set_ylabel('Flux % of reference')
    ax.set_title("Flux / Width, Intensity plot")
    ax.grid(True)

    #sort legend
    handles, labels = ax.get_legend_handles_labels()
    labels, handles = zip(*sorted(zip(labels, handles), key=lambda t: t[0]))
    ax.legend(handles, labels,loc='center left', bbox_to_anchor=(0.6, 0.2))
```

```
    fig.savefig("ImageAnalysis/transmission_gathered")
    ax.grid(True)
    plt.show()
```

output comparison

In [291…

```
loss_factor_simulated = 0.79

def output_comparison(etendue_path,reference_path,save_path,background_etendue,background_reference,legend_name="etendue"):
    squareWidth = 96 #mm
    squareHeight = 60 #mm
    focalTube = 12.45

    etendue_save_path = save_path+"_Etendue"
    reference_save_path = save_path+"_Reference"

    #transformerer bildet
    reference_image, transformed_reference_image = perspective_transform_with_mouse_clicks(reference_path, squareWidth, squareHeight)
    etendue_image, transformed_etendue_image = perspective_transform_with_mouse_clicks(etendue_path, squareWidth, squareHeight)


    #viser input bildet og transformert bilde med nøytralakse
    vizualize_images(etendue_image,transformed_etendue_image,etendue_save_path)
    vizualize_images(reference_image,transformed_reference_image, reference_save_path)


    #fjerner bakgrunn, kan legge in threshpold som 2. argument
    etendue_removed_background = remove_background(transformed_etendue_image,background_etendue)
    reference_removed_background = remove_background(transformed_reference_image,background_reference)

    #neutral axis:
    etendue_neutral_axis = find_horizontal_neutral_axis(etendue_removed_background)
    reference_neutral_axis = find_horizontal_neutral_axis(reference_removed_background)

    # Plot the accumulated intensity of each row in the transformed image
    etendue_intensityplot = plot_intensity(etendue_removed_background, etendue_neutral_axis)
    reference_intensityplot = plot_intensity(reference_removed_background, reference_neutral_axis)

    #neutral axis:
    etendue_neutral_axis = find_horizontal_neutral_axis(etendue_removed_background)
```

```
    reference_neutral_axis = find_horizontal_neutral_axis(reference_removed_background)

    #viser intentsitetsplottet
    show_intensity_plot(etendue_intensityplot,etendue_neutral_axis,etendue_save_path)
    show_intensity_plot(reference_intensityplot,reference_neutral_axis,reference_save_path)

    #calulating flux
    etendue_flux, original_etendue_flux = get_focal_energy(etendue_removed_background, etendue_neutral_axis, squareHeight, focalTube)#show_
    reference_flux, original_reference_flux = get_focal_energy(reference_removed_background, reference_neutral_axis, squareHeight, squareHe

    reference_flux = show_focal_energy(reference_removed_background, reference_neutral_axis, squareHeight, squareHeight,reference_save_path

    #showing focal energy multiple plots
    #show_focal_energy_multiple([etendue_removed_background,reference_removed_background], [etendue_neutral_axis,reference_neutral_axis], s
    #def show_focal_energy_multiple(images, neutral_axes, image_height_mm, focal_heights_mm,labels, save_path):

    transmission = (etendue_flux/reference_flux)*100
    print(f"referece flux = {reference_flux}\n etendue flux = {etendue_flux}\n  transmission = {int(transmission)}%" )

    reference_with_loss = [[x*loss_factor_simulated for x in y] for y in reference_removed_background]



    #flux_width_plot([etendue_removed_background,reference_removed_background,reference_with_loss],[etendue_neutral_axis,reference_neutral_

    #create two ax objects to add to ax:to_plot dict
    '''
    ax = flux_width_plot([etendue_removed_background],[etendue_neutral_axis],[legend_name+", "+str(int(transmission))+"%"], [focalTube], sq
    ax_ref = flux_width_plot([reference_removed_background],[reference_neutral_axis],["Reference"], [focalTube], squareHeight, reference_fl
    ax_ref_loss = flux_width_plot([reference_with_loss],[reference_neutral_axis],["reference fresnel reduced"], [focalTube], squareHeight,
    '''
    #add the  two plots to the dictionary
    #add_ax_to_plot(legend_name,ax)
    #add_ax_to_plot("ref",ax_ref)
```

Virtual model

In [167…

```
def get_x_within_interval(coordinates, y_min, y_max):
    x_values = []
    x_values_total = []
    for coord in coordinates:
        x, y = coord[0], coord[1]
```

```
        x_values_total.append(x)
        if y_min <= y <= y_max:
            x_values.append(x)
    focal_intensity = sum(x_values)
    total_intensity = sum(x_values_total)
    return focal_intensity, total_intensity
```

In [168…

```
def extract_data(path):
    data = []
    with open(path, 'r') as file:
        for line in file:
            line = line.strip()  # Remove leading/trailing whitespace
            if line:  # Skip empty lines
                values = line.split()  # Split the line by whitespace
                data.append([float(value) for value in values])  # Convert values to floats and append to the data list

    # Extract x and y values from the data
    y = [row[0] for row in data]
    x = [row[1] for row in data]

    swapped_data = [[coord[1], coord[0]] for coord in data]

    return x, y, swapped_data
```

In [233…

```
def nice_string(s):
    parts = s.split()

    if len(parts) >= 3:
        s0 = parts[0].ljust(11)
        s1 = parts[1].ljust(6)
        s2 = parts[2].ljust(3)

        formatted_string = s0 + s1 + s2
        return (formatted_string)
    else:
        print("Input string does not contain enough parts.")
        return s
```

In [231…

```
def flux_width_plot_virtual(images, neutral_axes, legend_names, focal_widths, image_height_mm, reference_Flux):
    plotted_vline = False
    fig, ax = plt.subplots()

    # Loop through each image, neutral axis, and focal width
    for image, neutral_axis, legend_name, focal_width in zip(images, neutral_axes, legend_names, focal_widths):
        # Sum of intensities of each row in the image
```

```
        row_sums = np.array([c[0] for c in image])
        # Calculate height of each row in mm
        row_Height_mm = image_height_mm / len(row_sums)

        # Initialize lists to store flux and width values
        flux = []
        width = []
        # Start at the neutral axis
        middle_index = neutral_axis

        flux.append(row_sums[neutral_axis])
        width.append(row_Height_mm)
        print(f"neutral axis: {neutral_axis} len row_sums: {len(row_sums)}")

        for i in range(1, neutral_axis-1):
            # Adding sum of corresponding row intensities from the neutral axis
            flux.append(flux[i-1] + row_sums[neutral_axis-i] + row_sums[neutral_axis+i])
            width.append(width[i-1] + 2 * row_Height_mm)


        flux_normalized = 100 * (np.array(flux) / reference_Flux)

        # Plot data on the subplot
        ax.plot(width, flux_normalized, label=legend_name,linestyle='dotted')

        '''
        # Plot vertical line for focal width
        if not plotted_vline:
            ax.axvline(x=focal_width, color="tab:red", linestyle='dashed', label="Focal tube")
            plotted_vline = True
        else:
            ax.axvline(x=focal_width, color="tab:red", linestyle='dashed')
        '''

    ax.set_xlabel('Width (mm)')
    ax.set_ylabel('Flux % of reference')
    ax.grid(True)
    ax.legend(loc='lower right')
    ax.set_title("0\u00b0 Simulation, transmission 79%, Flux vs. Width")
    plt.savefig(os.getcwd()+"\\"+"zemax_0deg_transmission.png")
    plt.show()
    return ax
```

In [284…

```
focal_height = 12.45
```

```
#file names
etendue_name = "zemax/etendue_histogram.txt"
reference_name = "zemax/reference_histogram.txt"

##paths
etendue_path = os.getcwd()+"\\"+etendue_name
reference_path = os.getcwd()+"\\"+reference_name

x_ete, y_ete, ete_image = extract_data(etendue_path)
x_ref, y_ref, ref_image = extract_data(reference_path)

focal_intensity, total_intensity  = get_x_within_interval(ete_image, -focal_height/2,focal_height/2)
focal_intensity_ref, total_intensity_ref  = get_x_within_interval(ref_image, -focal_height/2,focal_height/2)
print(total_intensity)
print(focal_intensity)
factor = (focal_intensity/total_intensity)*100
print(f"focal flux = {focal_intensity}\n total flux = {total_intensity}\n  transmission = {int(factor)}%" )

# Create the plot
plt.plot(x_ete, y_ete, label = f"Etendue: {int(factor)}% intensity")
plt.plot(x_ref, y_ref, label='Reference')

#focal tube
plt.axhline(focal_height/2, color='b', linestyle='dotted', label='Focal tube')
plt.axhline(-focal_height/2, color='b', linestyle='dotted')

# Add labels and title to the plot
plt.xlabel('relative intensity')
plt.ylabel('Y height [mm]')
plt.title('Intensity profile along Y heights')
plt.legend()

plt.savefig(os.getcwd()+"\\"+"zemax_0deg_focal.png")

# Show the plot
#plt.show()

images = [np.array(ete_image),np.array(ref_image)]
neutral_axes = [len(ete_image)//2,len(ref_image)//2]
legend_names = ["Simulation 0\u00b0, 79%","reference"]
focal_widths = [focal_height,focal_height]
image_height_mm = 60
reference_Flux = total_intensity_ref


#flux_width_plot_virtual(images, neutral_axes, legend_names, focal_widths, image_height_mm, reference_Flux)
```

```
ax = flux_width_plot_virtual([images[0]], [neutral_axes[0]], [legend_names[0]], [focal_widths[0]], image_height_mm, reference_Flux)
add_ax_to_plot("simulation",ax)
```

```
1.4669119230699996
1.42954524
focal flux = 1.42954524
 total flux = 1.4669119230699996
  transmission = 97%
neutral axis: 65 len row_sums: 130
```

Figure

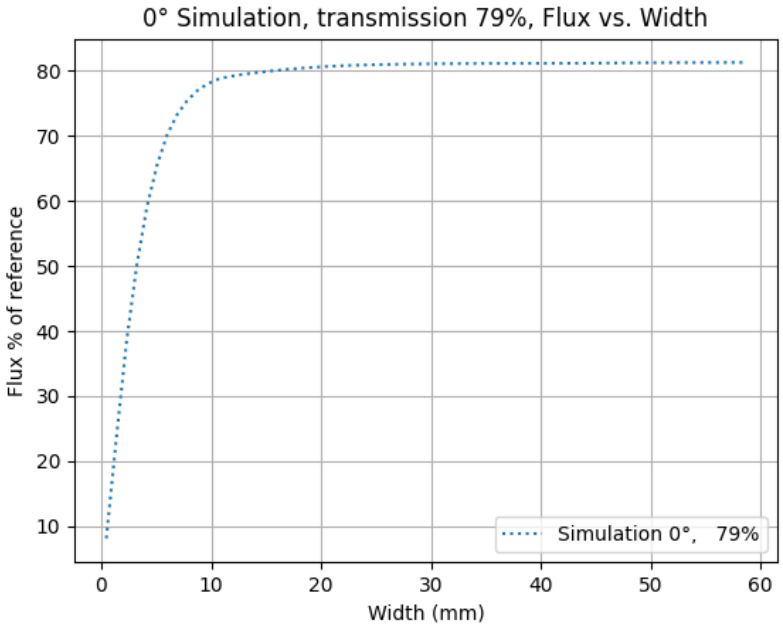

```
dictionary:  {'3D Print 0°': <Axes: title={'center': '0° Etendue, transmission 52%, Flux vs. Width'}, xlabel='Width (mm)', ylabel='Flux % o
f reference'>, '15i 0°': <Axes: title={'center': '0° Etendue, transmission 73%, Flux vs. Width'}, xlabel='Width (mm)', ylabel='Flux % of re
ference'>, '15i 11.75°': <Axes: title={'center': '11.75° Etendue, transmission 67%, Flux vs. Width'}, xlabel='Width (mm)', ylabel='Flux % o
f reference'>, '15i 23.5°': <Axes: title={'center': '23.5° Etendue, transmission 49%, Flux vs. Width'}, xlabel='Width (mm)', ylabel='Flux %
of reference'>, '3D Print 23.5°': <Axes: title={'center': '23.5° Etendue, transmission 39%, Flux vs. Width'}, xlabel='Width (mm)', ylabel
='Flux % of reference'>, '3D Print 11.75°': <Axes: title={'center': '11.75° Etendue, transmission 48%, Flux vs. Width'}, xlabel='Width (m
m)', ylabel='Flux % of reference'>, 'simulation': <Axes: title={'center': '0° Simulation, transmission 79%, Flux vs. Width'}, xlabel='Width
(mm)', ylabel='Flux % of reference'>, 'ref': <Axes: title={'center': ', Flux vs. Width'}, xlabel='Width (mm)', ylabel='Flux % of referenc
e'>}
```

In [203…

```
#del ax_to_plot["ref_loss"]
```

resultater:

In [238…

```
for key in ax_to_plot:
    print(key)
plot_all_axis()
```

```
3D Print 0°
15i 0°
15i 11.75°
15i 23.5°
3D Print 23.5°
3D Print 11.75°
simulation
ref
```

Figure

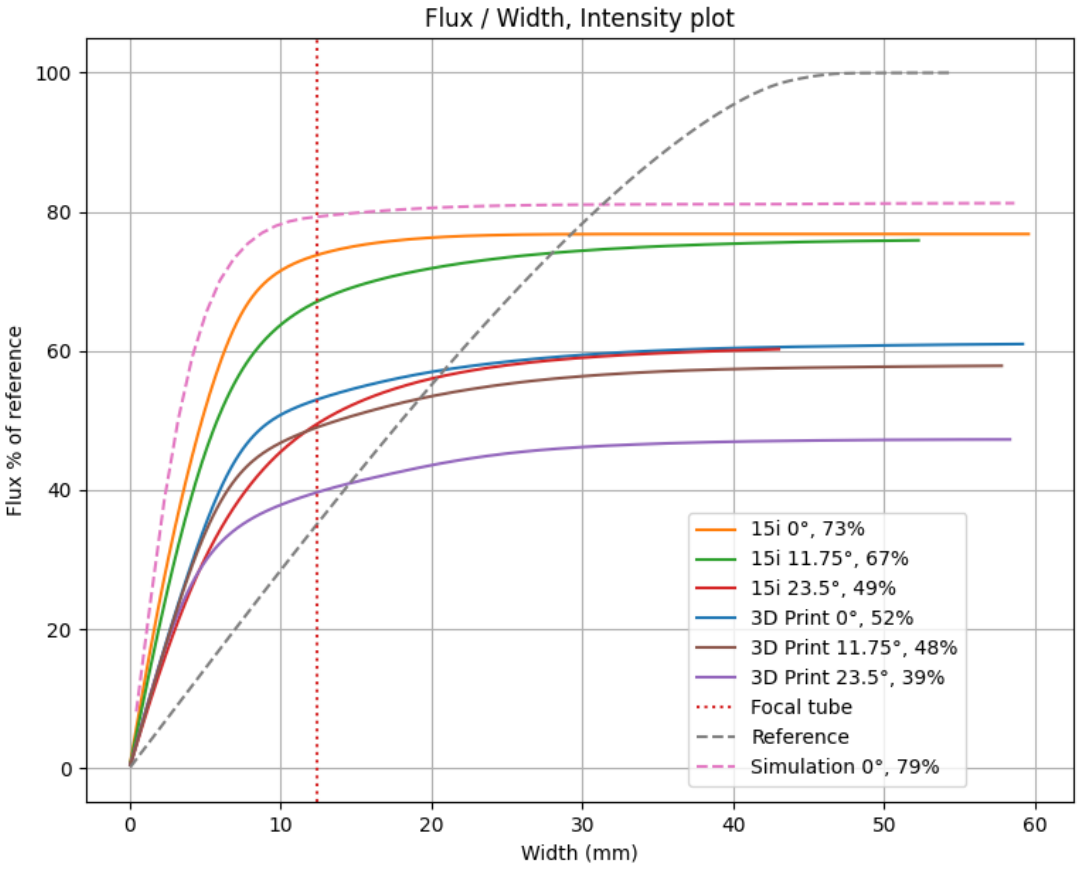

3dprint

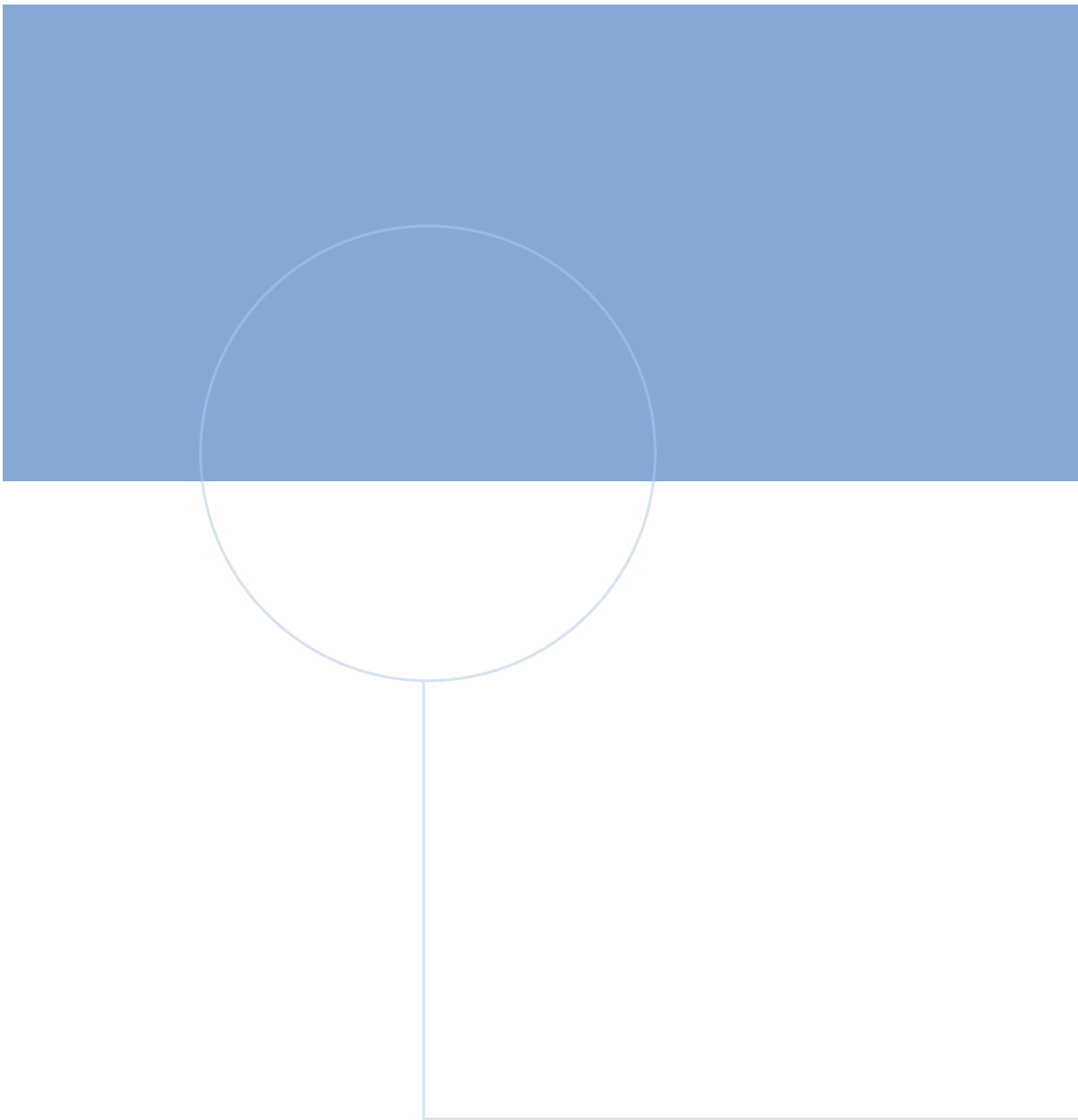

NTNU

Norwegian University of
Science and Technology